COMPARATIVE STUDY OF HOT CORROSION BEHAVIOR OF THERMAL SPRAYED AND MICROWAVE FUSED ALUMINA BASED COATINGS ON BOILER STEELS

Thesis Submitted for the Award of the Degree of

DOCTOR OF PHILOSOPHY

in

Mechanical Engineering

By

Jai Parkash

Registration Number: 42000623

Supervised By

Dr. Harminder Singh Saggu (11530)

Department of Mechanical Engineering

Associate Professor

Lovely Professional University

Co-Supervised By

Dr. Hitesh Vasudev (24804)

Department of Mechanical Engineering

Professor

Lovely Professional University

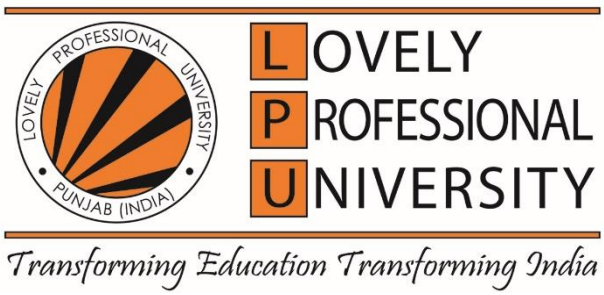

LOVELY PROFESSIONAL UNIVERSITY, PUNJAB

2024

DECLARATION

I, hereby declared that the presented work in the thesis entitled "COMPARATIVE STUDY OF HOT CORROSION BEHAVIOR OF THERMAL SPRAYED AND MICROWAVE FUSED ALUMINA BASED COATINGS ON BOILER STEEL" in fulfilment of degree of **Doctor of Philosophy (Ph.D.)** is outcome of research work carried out by me under the supervision of Dr. Harminder Singh Saggu and Co-Supervisor of Dr. Hitesh Vasudev both working as Associate Professor, in the School of Mechanical Engineering at Lovely Professional University, Punjab, India. In keeping with general practice of reporting scientific observations, due acknowledgements have been made whenever work described here has been based on findings of other investigator. This work has not been submitted in part or full to any other University or Institute for the award of any degree.

Jai Parkash (Research Scholar)

Registration No.: 42000623

School of Mechanical Engineering

Lovely Professional University

Phagwara, Punjab (India)

CERTIFICATE

This is to certify that the work reported in the Ph.D. thesis entitled "COMPARATIVE STUDY OF HOT CORROSION BEHAVIOR OF THERMAL SPRAYED AND MICROWAVE FUSED ALUMINA BASED COATINGS ON BOILER STEEL" submitted in fulfillment of the requirement for the reward of degree of **Doctor of Philosophy (Ph.D.)** in the School of Mechanical Engineering, is a research work carried out by Jai Parkash, Registration No.42000623, is bonafide record of his original work carried out under my supervision and that no part of thesis has been submitted for any other degree, diploma or equivalent course.

Dr. Harminder Singh Saggu (Supervisor)
Associate Professor
Mechanical Engineering Department
Lovely Professional University
Phagwara, Punjab (India)

Dr. Hitesh Vasudev (Co-Supervisor)
Professor
Mechanical Engineering Department
Lovely Professional University
Phagwara, Punjab (India)

ACKNOWLEDGEMENT

First and Foremost, Thank you, Lord, for the blessings you have bestowed on my life. You have provided me with more than I could ever have imagined. You have surrounded me with people who always look out for me. You have given me family and friends who bless me every day with kind words and actions.

I would like to pay my sincere thanks to **Dr. Harminder Singh Saggu** (Supervisor) **and Dr. Hitesh Vasudev** (Co-Supervisor), Associate Professor in School of Mechanical Engineering, Lovely Professional University, for his invaluable guidance and support during the present research work. I wish to express my heartily thanks to **Dr. Amit Bansal**, Assistant Professor in Mechanical Engineering Department, IKGPTU Kapurthala for giving valuable inputs during every phase of my Ph.D. work.

I am thankful to **Mr. Amrinder Mehta**, in-charge of XRD (CIF cell) Lovely Professional University, **Dr. Ravinder Pal Singh,** Professor in Department of Mechanical Engineering, Lovely Professional University and **Mr. Jasleen Bains,** Special Assistant, Bank of India for their continuous support.

I express my profound regards to my parents for their blessings and for being the main source of inspiration to succeed in my endeavors. I would like to express particular thanks to my wife, **Mrs. Rinki Gupta** for her advises, care and continuous motivation she provided me throughout my research work.

I would like to thank everyone who supported me for completing this work successfully and I express my apology that I could not mention everyone individually.

(Jai Parkash)

ABSTRACT

The selection of the boiler steel SA-210 for this particular application is attributed to its utilization in boilers. The primary factors contributing to surface deterioration in boilers are hot corrosion and oxidation processes. The three coatings used to reduce surface damage from heat corrosion and oxidation were Al_2O_3 (AL), Al_20_3 +13% TiO_2 (AL13TI), and Al_2O_3 +40% TiO_2 (AL40TI). To understand the impact of adding TiO_2 to Al_2O_3-based coatings, the coatings were examined for micro-structural assessment. Following flame spraying deposition, the coatings underwent heat treatment using microwave processing. The AL coatings had the highest porosity levels at 2.5% compared to all the other coatings that were developed. While an AL40TI coating had a minimum porosity of 1.5 percent, an AL13TI coating had a porosity level of around 2.1 percent. The microhardness results have shown the 995 HV for AL coating and 790HV and 650HV for AL13TI and AL40TI coatings respectively. The hardness has decreased with increase in addition of TiO_2 in these coatings. The microwave post-treated coatings have shown the porosity values for AL, AL13TI and AL40TI coatings of 2.1%, 1.7% and 1.1%, respectively. Whereas, the microhardness of the post-treated coatings has increased for all developed coatings PT-AL, PT-AL13TI and PT-AL40TI coatings of 1110 HV, 825 HV and 720 HV, respectively.

This research looked at the hot-corrosion and high-temperature oxidation properties of SAE 210 boiler steel, both coated and bare. Coated and uncoated specimens were oxidized cyclically for 50 cycles in an atmosphere of air and molten salt containing a mixture of Na_2SO_4 and 4-60% V_2O_5 at 900ºC. We analyzed the corrosion products using SEM/EDAX, XRD, and thermogravimetric methods. Properties such as coating thickness, constituent distribution, and surface morphology were also examined in

the as coated boiler steel. The investigation revealed that the boiler steel's coating adequately protected the base metal from the oxidation and aggressiveness of the Na_2SO_4-60%V_2O_5 environment. Circular oxidation in air and a molten salt environment with Na_2SO_4-60% V_2O_5 at 900ºC for 50 cycles has shown that the coated boiler steel with the AL40TI post-treatment can resist corrosion at higher temperatures for a longer duration than the untreated SA 210 Grade -I steel.

Table of Contents

List of Figures

List of Tables

CHAPTER 1

INTRODUCTION

Research is a critical component across all domains of society as it enables the ongoing enhancement of any given system. Within the industrial sector, research expedites the most effective utilization of resources, sustainability, and efficiency, and thus the system's economy. Additionally, research in every discipline enhances the quality of life. The research is driven by notions of profound learning, societal responsibility, financial gain, and other such factors.

The effectiveness of machinery is influenced by the critical properties of materials in engineering and technology. The materials selected for machine components are subjected to a variety of working conditions and obstacles. The boiler is a critical component in thermal power plants that is subjected to elevated temperatures in order to convert water into high-pressure steam. Deterioration of engineering system component surfaces at high temperatures imposes an enormous financial burden. In order to mitigate, it is necessary to prevent or postpone their premature failures. Hence, wear-induced high-temperature material degradation poses a significant obstacle in regions characterized by elevated temperatures.

1.1 OPERATION OF THERMAL POWER PLANT

Electric power is a fascinating societal demand due to the fact that it is required to function a variety of electric machines. Electricity is critical to the economy and a fundamental component of contemporary existence. In addition to lighting, refrigeration, heating, and ventilation, electricity is utilized to power machinery, computers, electronic devices, and public transportation systems. Since usable electricity is not naturally occurring, it must be "produced" through the conversion of other forms of energy to electricity (Kumar et al., 2018). Energy generation occurs within power stations, which are alternatively referred to as power plants. In power plants, electromechanical generators are the predominant means by which electricity is produced (Natesan, 1997). While heat engines fueled by combustion or nuclear

fission also contribute, alternative energy sources include the kinetic energy of wind and flowing water. Conventional thermal power plants, alternatively referred to as combustion power plants, function by utilizing energy generated by a steam boiler that is fueled by biomass, coal, natural gas, or heating oil (Natesan et al.). A turbine is energized by the steam, and it powers an alternator to generate electricity.

Coal-fired power plants and power stations are types of thermal power plants that produce electricity through the combustion of coal. Coal-fired power plants are classified as fossil fuel power plants. Typically, pulverized coal is utilized in pulverized coal-fired boilers. Boiler water is converted to steam by the furnace's heat; the steam is then utilized to power generators via turbines (Simms et al., 2004). Consequently, the chemical energy that is contained in coal undergoes a series of conversions, culminating in the production of electrical energy. China provides over 50% of the global coal-fired electricity generation. Sometimes, generating stations are constructed adjacent to a mine, particularly one that processes coal or lignite, both of which are too valuable to be transported over long distances. In such cases, lignite is transported via conveyor belt or massive diesel-electric drive vehicles. A "unit train" is a sizable coal train that can span a distance of 2 kilo-meters. It comprises 130-140 cars, each of which holds approximately 100 tonnes of coal, for a cumulative cargo exceeding 10,000 tonnes. A substantial power plant operating at maximum capacity necessitates a minimum of one coal delivery of this magnitude on a daily basis. Plants may be subjected to as many as three to five trains per day during periods of high power consumption, such as "peak season" during the warmest summer or harshest winter months (depending on the local climate).

A thermal power station, which is a type of coal-fired power station, operates by converting the chemical energy contained in coal through a sequence of processes: mechanical energy, thermal energy, and ultimately electrical energy. In pulverized coal-fired furnaces, pulverized coal is conventionally employed. The combustion of pulverized coal generates steam, which is subsequently converted from boiler water to power generators through turbines. As opposed to thermal power stations that employ alternative fuel types, coal fuels require the indispensable refining and disposal of ash. For units surpassing 200 MW in capacity, is implemented to guarantee redundancy in critical components. In lieu of one reactor, two reactors may

be installed on specific units of around 60 MW. One hundred of the most significant coal power facilities range in high magnitude.

To render unprocessed coal suitable for utilization, it is reduced to particulate dimensions below 5 centimeters. Following this, the coal is transferred from the storage yard to the in-plant storage depots at a maximum velocity of 4,000 tonnes per hour using conveyor belts. Coal mills and pulverizers are both employed in facilities that consume pulverized coal. The mills receive coal from silos and reduce the larger 5 cm portions to particulates resembling talcum powder. Following this, the primary combustion air is incorporated into the resulting mélange, which aids in the coal's transportation to the boiler furnace and preheats it to eliminate any excess moisture. At maximal load, five of the six pulverizers in a 500 MWe facility are capable of supplying the furnace with 250 tonnes of coal per hour. Coal constituted the predominant energy source of 34% in 2020. China accounted for the preponderance of coal production in 2020. There were a total of 2059 gigawatts (GW) of operational coal power on a global scale. Among these, 50 GW were commissioned, 25 GW were under construction (with China hosting the majority of these 25 GW), and 38 GW were retired (primarily in the United States and the European Union). In ascending order of efficacy, coal-fired power stations can be classified into four primary categories.

1.1.1 Operation of Boiler

A substantial thermoelectric facility annually consumes enormous quantities of coal. A pulverizer reduces coal to a fine powder, which is then blown into a boiler, which resembles a furnace, where it is consumed. The generated heat transforms water into steam as it flows through a network of pipelines within the boiler. Figure 1.1 presents a schematic representation of the boiler operation in a thermal power facility that is powered by coal. As the high-pressure steam rotates the turbine's blades, a shaft connects the turbine to a generator. By spinning, the generator generates electricity. Utilizing a boiler to generate vapor at elevated temperatures and pressures. This is explicable by the fact that water's temperature and pressure increase with temperature and pressure; similarly, a boiler utilizes the heat generated by the combustion of fuel to heat water in order to produce steam at high temperature and pressure.

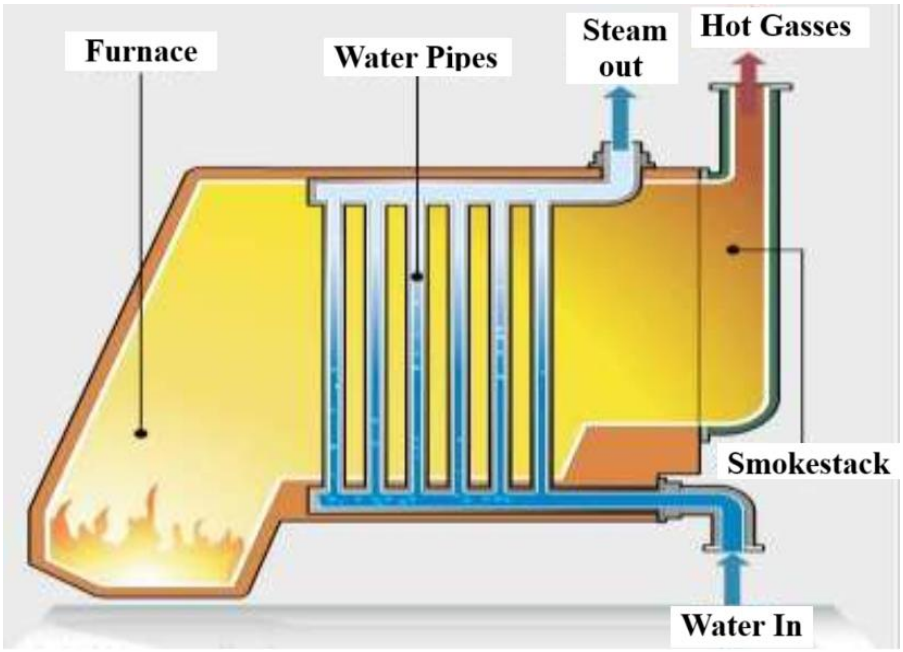

Fig.1.1 Presents a schematic representation of the boiler operation in a thermal power plant powered by coal (https://www.researchgate.net/figure/Water-tube-boilers_fig2_263878729)

This study examines the deterioration of the surface of the furnace, which is exposed to the approximately 900°C high temperature of coal combustion. Deterioration of engineering system component surfaces at high temperatures imposes an enormous financial burden. In order to mitigate these tremendous, it is necessary to prevent or postpone their premature failures. Hence, wear-induced high-temperature material degradation poses a significant obstacle in regions characterized by elevated temperatures.

1.2 DEGRADATION OF THE SURFACE

Particularly, engineering components utilized in a variety of industrial applications must contend with the challenges of high-temperature corrosion and attrition while operating under extreme heat loads. This is especially true for corrosion-resistant and wear-resistant components, as the surface of the component must perform critical functions in aggressive environments (Liu et al., 2017). Consequently, the contact area of the material surface, the operating conditions or environment, and these factors exclusively dictate the material's behaviour. Frequent furnace tube failures are primarily attributed to corrosion and erosion, which serve as diagnostic indicators.

Ash comprises around fifty percent of the coal utilized for electricity generation in India. Among this ash, fifteen percent may comprise abrasive particulates, such as hard quartz, which exacerbate the erosion intensity of the coal (Kumar and Sapra, 2016). Erosion commences at different locations on the tube surface, primarily along the side walls of the tubes. This progressive reduction in tube thickness culminates in the eventual collapse of the tubes. In contrast to associated phenomena like grinding, machining, sliding and abrasive wear, and solid particle erosion, the erodent and the material being eroded have a fleeting period of interaction (Roy, 2006).

Premature tube collapse can be attributed to attrition and localized long-term overheating that occur when the boiler temperature surpasses 700°C and phase changes occur (Husain and Habib, 2005). High temperature oxidation, also referred to as hot corrosion, is a process that begins with the deposition of molten ash on the tubes caused by salt contaminants formed during fuel combustion. This ash dissolves the protective oxide layer, ultimately leading to material degradation (Kamal et al., 2010a; Stringer, 1995). Therefore, the concurrent assault of erosion and oxidation is the primary cause of the calamitous failure of the components installed in a power plant (Matthews et al., 2009; Wang, 1996). Overall, as a result of oxidation and erosion, the power plant will be unable to meet its functional requirements; as a consequence, the power plant will be shut down for an extended period of time, which will not only cause enormous economic loss but also a significant disruption in service provision to society. Therefore, numerous industries have identified oxidation and solid particle erosion as significant concerns (Zhou and Bahadur, 1995; Yang et al., 2012). Due to elevated temperature attrition and corrosion, carbon steel water wall tubes, which were widely utilized in the northern region of India. Carbon steel tubes experience a substantial reduction in yield strength when subjected to temperatures exceed 400°C. (Mohamed and Wilson, 2015). Should the temperature of the metal tube be incrementally increased beyond this threshold, it will undergo plastic deformation followed by rupture. The performance of these functional components is influenced not only by the aggregate properties but also by the properties and characteristics of the surface. This is especially true for wear-prone and corrosion-prone components, given that the surface of such components is heavily influenced by aggressive environments. Researchers have suggested in the literature that coatings consisting of multiple phases are effective in mitigating material degradation

caused by oxidation and other forms of wear. In their study, Bala et al. (2017) conducted erosion-corrosion cyclic investigations in the real boiler environment of the Guru Gobind Singh Super Thermal Power Plant in Punjab (India). The researchers compared uncoated and Ni-based coated specimens located in the central zone of the low temperature super-heater of the Stage-II Boiler. The performance of the coated specimens was found to be superior to that of the uncoated steel.

1.3 OXIDATION

Component degradation in high-temperature oxidation-prone environments. The emergence of fly ash particle-induced high-temperature oxidation and attrition has given rise to boiler tube failure. It is an acknowledged primary contributor to periods of inactivity.

Oxidation is a chemical process characterized by the formation of a metal oxide through a reaction between the oxygen atom and the metal surface (Birks et al., 2006; Rapp, 1984; Reid, 1971). The progression of occurrences that transpire during the oxidation is illustrated in figure 1.2 below.

Fig.1.2 Surface corrosion and scale on a boiler shell are depicted (https://www.watertechusa.com/boiler-blowdown)

Adsorption of O_2 atoms onto the metal's surface subsequently occurs. Following the adsorption of oxygen, metal oxide (MO) begins to accumulate on the metal surface as enclaves, eventually encompassing the entire metal surface, provided that the thermodynamic conditions are met (Deb et al., 1996; Shukla et al., 2012). So long as oxygen remains adsorbed on the surface; this is dependent on the oxygen atom's diffusion capability. Once the oxide layer has fully encircled the metal surface, it endeavors to enlarge in a perpendicular trajectory, as illustrated by the arrows in diagram (c). This expansion causes the oxide layer's thickness to progressively increase. The conduction of electrons (e) and the diffusion of metal ions (M+2) and oxygen ions (O2-) through this oxide layer govern the growth mechanism of the metal oxide. The emission of oxygen may occur as oxygen ions, which have the capability to initiate oxidation on the anodic surface through a reaction with metal ions. On the contrary, the diffusion of metal ions may result in their inclusion in the process of oxide scale formation on the cathode surface (Stringer, 1987; Nicholls, 2000; Meier, 1989). At elevated temperatures, metal oxidation proceeds as follows: (a) oxygen gas (O_2) adsorption, (b) O_2 dissolution, (c) formation of a thin oxide film, (d) expansion of the oxide layer, and (e) apparition of a dense oxide layer.

Overarching reactions that occur include:

To generate M^(+2)+O^(2-), it is possible to remove two electrons from the metal atom, represented as M^(-2e), which leads to the creation of M^(+2). Subsequently, oxygen gains the ability to receive these two electrons as O^(2-). This phenomenon may manifest at the metal's surface in the event of an excess of two electrons. These two electrons are capable of traversing the oxide layer and being assimilated by the adsorbed oxygen. It is crucial to note that the oxide layer facilitates the movement of ions and acts as both a conductor and an electrolyte by facilitating the transfer of electrons between surfaces. Defects manifest as pores, cavities, and minute fractures as a consequence of the ongoing expansion of oxide scale and oxygen diffusion (Kumar et al., 2013; Sadeghi et al., 2019; Oksa et al., 2014). The ongoing dissolution of oxygen leads to the development of pores and macrocracks, which ultimately compromise the functionality of structural elements. In order to prevent surface oxidation, energy conversion and utilization systems employ protective coatings on structural alloys.

It is anticipated that recent developments in high-temperature materials and cooling systems will extend the service life of furnaces and gas turbines by enhancing their creep, fatigue, and strength properties. Extreme caution must be exercised when salts combine in the environment of a gas turbine, as this results in the occurrence of heated corrosion. Rapid consumption of the material occurs as a result of heated corrosion. As a result, the material undergoes degradation, which ultimately results in the untimely malfunction of components (Mahesh et al., 2007). The metallic components of coal gasification power stations are subjected to exceedingly high temperatures and a severe environment (Chawla et al., 2006). A form of oxidation, corrosion occurs when a metal is exposed to oxygen or air at elevated temperatures, devoid of any aqueous solution or water. This type of corrosion is also referred to as dry corrosion. The attributes of the oxide layer that forms on the substrate's surface dictate the rate of oxidation under elevated temperatures (Chen et al., 2001). The oxidation rate of metals and alloys is significantly increased when a thin deposit of fused salt, such as Na_2SO_4, is applied to their surfaces. In heated corrosion, Na_2SO_4 is the predominant salt (Rapp et al., 1986).

1.3.1 Formulation Requirement for Protective Oxides

1. Similar thermal coefficients will characterize metal and oxide. Oxide undergoes stress generation if the two are dissimilar.

2. The absence of oxide evaporation is undesirable; for instance, if V_2O_5 evaporates, it fails to offer any safeguarding to the underlying metal.

3. The plastic deformation capability of oxide should be satisfactory, as brittle oxide will fracture under high-temperature stress.

4. Owing to the low diffusion coefficient, metal ions and oxygen ions will traverse oxide layers more efficiently.

5. There should be a reduced rate of oxide layer formation.

1.4 THERMAL CORROSION

This is the most aggressive method by which metals, alloys, and ceramics degrade, particularly when extremely high temperatures are applied. In India, hot corrosion and erosion is a significant and critical issue in coal-fired power plants. Coal-fired power plants are anticipated to incur losses of around $150 million due to heated corrosion and erosion alone. Coal utilized in power plants in India is of extremely low quality due to the presence of significant quantities of ash, sulphur, carbon, and other impurities. Fly ash, which comprises abrasive mineral particles, erodes the surface of boiler tubes, including water walls and superheater tubes. Concurrently, corrosive compounds accumulate on these surfaces, impeding heat transfer and initiating the corrosion mechanism. Coal sulphur undergoes partial oxidation during combustion, resulting in the formation of SO_3. This SO_3 subsequently reacts with water vapor (H_2O) & (NaCl) contained in the coal to produce Na_2SO_4. An additional trace quantity of elements results in V_2O_5 during coal combustion. The product of this reaction with Na_2SO_4 is $NaVO_3$, which, when exposed to high temperatures, is extremely deleterious to boiler tubes. As a consequence, the material of boiler tubes fails as a consequence of erosion and corrosion combined, leading to significant economic losses. High temperature erosion and corrosion accounted for fifty percent of the eighty-nine failures documented annually (Prakash et al., 2001). As the prevalence of coal-based power generation continues to rise, so too do the losses attributable to erosion and corrosion. As corrosion reduces the boiler's thermal efficacy and raises maintenance and downtime expenses, economic losses also increase. To mitigate these losses, precautions must be taken to prevent the material from failing prematurely. Researchers have employed a range of techniques to accomplish this, including the selection of superalloys, application of corrosion inhibitors, coatings, and cathodic protection. Among all the methods, thermal spray is the most prevalent for protecting materials against corrosion and erosion and extending their useful lives in terms of performance capabilities. Thermal spray provides resistance to heated corrosion by coating any surface with a variety of powders. Additionally, it imparts the necessary surface properties while preserving the metallurgical properties of the parent material.

Thermal spraying is an exceptionally adaptable and versatile method for applying component protection coating materials. Thermal spraying involves the spray of molten coating granules onto the substrate's surface with the intention of enhancing surface properties such as resistance to corrosion and wear (Heath et al., 1997). Plasma spray involves an inert gas, such as nitrogen or hydrogen, is transmitted through the arc at its elevated temperature. By dissociating the gas into ions, plasma is produced. The material is introduced into the plasma, where its high temperature induces a melting reaction. At a high velocity, this molten material is transported by the plasma gas to the surface of the substrate.

Fig.1.3 Depicts corrosion on boiler steel (https://feedwater.co.uk/boiler-corrosion-prevention-to-stop-deposit-formation/)

1.5 COATINGS

A coating is a substance that is utilized to cover the substrate, which is the surface of an object. The application of the coating may serve a functional, aesthetic, or both purposes.

Surface coatings are essential in surface engineering for enhancing material properties such as wear resistance, corrosion protection, and thermal stability (Goh,

C.Y., et al., 2019). Methods like physical vapor deposition (PVD), chemical vapor deposition (CVD), and thermal spray coatings are widely used to improve the durability of components in industries such as aerospace and automotive (Abbasi, S., et al., 2019). These coatings extend the lifespan of components by forming a protective layer, reducing degradation in harsh environments. Recent advancements focus on multifunctional coatings that offer combined mechanical and chemical benefits, addressing both performance and environmental demands (Guney, M., et al., 2020). Utilizing coatings as liquids, gases, or solids, for instance. Powdered finishes. Coatings are utilized for a wide variety of purposes and applications. A primary function of coatings is to safeguard metals against corrosion. The preservation of structures, apparatus, and equipment falls under this purpose. For the characterization of coatings, destructive and non-destructive evaluation (NDE) techniques are abundant. Performing microscopy on a mounted cross-section of the coating and its substrate is the prevailing destructive technique. Material characterization is performed to examine the chemical composition of a thin surface layer, which is measured in nanometers. The utilization of energy dispersive X-ray spectrometry in conjunction with scanning electron microscopy (SEM-EDX, or SEM-EDS) enables the visualization of surface texture and the investigation of its fundamental chemical composition.

1.6 CORRECTION OF BOILER STEELS UNDER HEAT AND PREVENTATIVE MEASURES

Boiler and thermal power plant equipment is susceptible to a diverse range of failures that involve at least one mechanism. A review of the relevant literature revealed that scalding is one of the leading causes of steam boiler failure. A survey of 413 investigations conducted over a twelve-year period by a single laboratory revealed that overheating was the primary most prevalent factors, accounting for 21.5% or 89 failures, subsequent to overheating.

The remaining 13.3% of failures can be attributed to improper or defective materials (Metals Handbook, 1975). At elevated temperatures, metallic components in coal gasification facilities are subjected to an extremely hostile and severe corrosion environment. The corrosive properties of oxygen, carbon, and sulphur, which are found in the abrasive gaseous environment at high temperatures, accelerate the

material's degradation and cause it to fail before it reaches the end of its useful life (Chawla et al., 2006).

1.6.1 Preventive Precautions

Completing the issue of corrosion and the subsequent losses it causes is an unattainable goal. However, by implementing optimal corrosion control and prevention strategies, we can reduce maintenance expenses by 25 to 30 percent (Priyantha et al., 2003). Suggested several preventive measures to address the issue of hot corrosion in harsh environments, including the selection of suitable alloys and protective coatings (Heath et al., 1997). A fundamental categorization of corrosion prevention techniques is illustrated in figure 1.4 below.

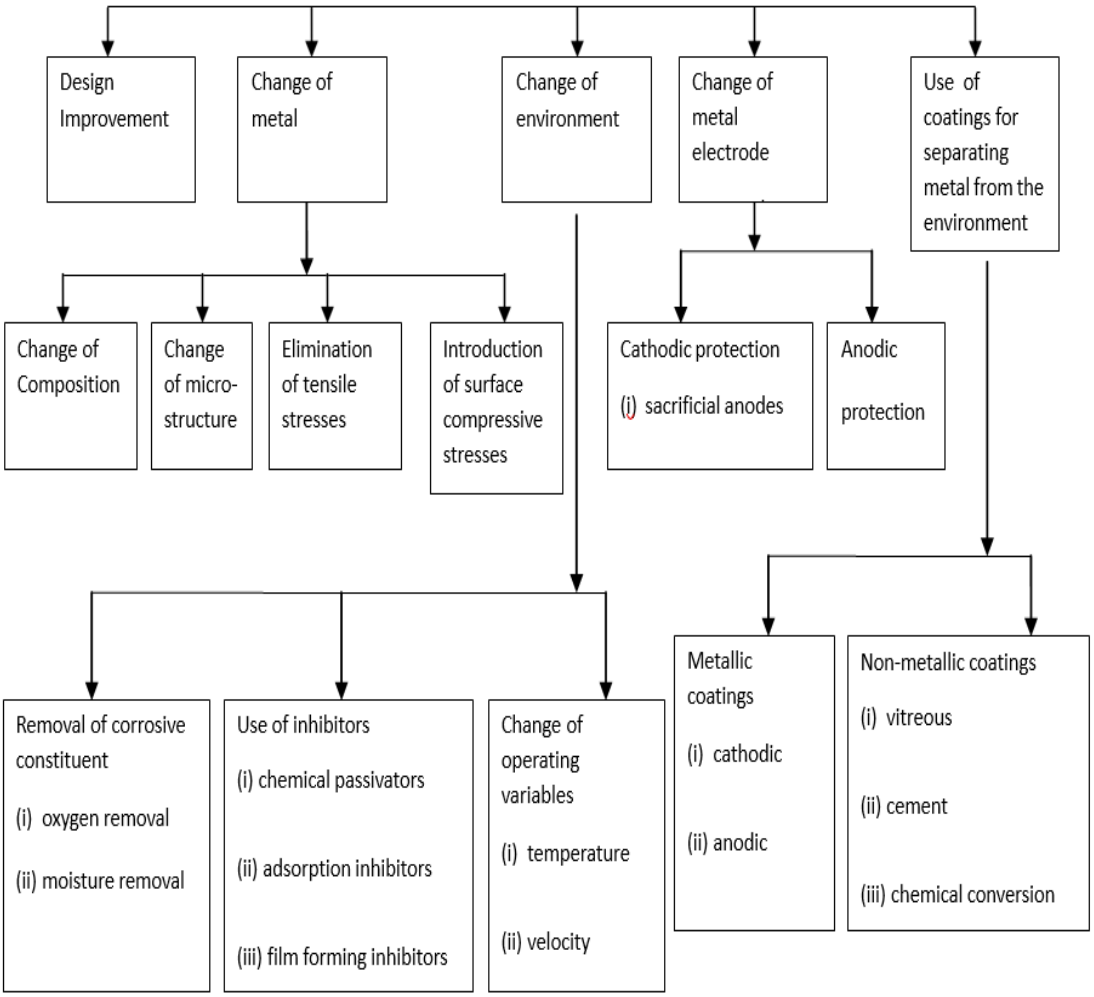

Fig.1.4 Methods of preventing corrosion are categorized (Chawla et al., 2006)

To protect a metal effectively against corrosion in an aggressive environment, it is critical to choose techniques and materials that are optimal and compatible. In numerous corrosive environments, the introduction of inhibitors such as pyridines, quinolines, and pyrimidines has effectively impeded metal corrosion. However, one drawback of inhibitors is that their effectiveness is somewhat compromised by solubility or thermal instability issues when exposed to concentrated salt solutions and high temperatures (Priyantha et al., 2003).

The selection of materials must be meticulous and optimal in order to prevent corrosion in extremely harsh environments. Nickel-based superalloys have demonstrated favourable mechanical characteristics and exceptional resistance to corrosion at elevated temperatures; consequently, numerous heated components are constructed from nickel-based alloys. However, alloys continue to be susceptible to corrosion as a result of their operation in extremely severe environments and at extremely high temperatures.

The appropriate choice of material is determined by several factors, including mechanical and fabrication properties, cost, weight, and physical properties. These considerations restrict the range of material options available, and none of the potential materials are completely impervious to the corrosive environment they will be exposed to during operation.

Therefore, it is optimal for a protective coating to completely isolate the substrate material from the corrosive environment. If this objective can be fulfilled, then the only factor that requires consideration is the contact between the coating and the corrosive environment.

1.7 COATING METHODS

To attain distinct functionalities of coatings, such as resistance to corrosion and abrasion, electrical or thermal insulation, various coating methods are employed. The techniques that are frequently utilized are illustrated in Table 1.1. Hardfacing is of the utmost importance in metallic categories from the perspective of this research field.

Table 1.1 Various methods of coating (Mohamed et al, 2021)

S. No.	Coating Method	Remarks
1	Thermal Spraying	Thermal spraying involves melting a material and spraying it onto a substrate. Methods include plasma spraying, High-Velocity Oxygen Fuel (HVOF), and flame spraying. Materials like ceramics, metals, and polymers can be applied to enhance wear resistance, corrosion resistance, and thermal insulation. Thermal spraying is commonly used in turbine blades, boiler tubes, and automotive parts
2	Physical Vapor Deposition (PVD)	PVD is a process in which materials are vaporized in a vacuum environment and then deposited onto a surface to form a thin film. This method is often used for wear-resistant coatings, such as titanium nitride (TiN) or aluminum oxide (Al_2O_3), and provides high hardness and excellent adhesion. PVD is widely used in tools, aerospace, and electronics
3	Chemical Vapor Deposition (CVD)	In CVD, volatile precursors react on a heated substrate to form a solid material coating. CVD produces coatings with excellent uniformity and is commonly used for coating materials like silicon carbide (SiC) and titanium carbide (TiC) on components that require high-temperature stability and wear resistance. It's popular in semiconductor, aerospace, and cutting tool applications.
4	Electroplating	In electroplating, a metallic coating is deposited onto a surface using an electrical current. This method is commonly used to improve corrosion resistance or for decorative purposes, using metals like chromium, nickel, and gold. It is widely applied in automotive, jewelry, and electronics industries
5	Anodizing	Anodizing is an electrochemical process that converts the surface of a metal, usually aluminum, into an oxide

		layer. This oxide layer enhances corrosion resistance, wear resistance, and can be dyed for aesthetic purposes. It is commonly used in aerospace, automotive, and consumer goods
6	Powder Coating	Powder coating involves applying a dry powder to a surface and curing it with heat to form a solid, protective layer. It provides excellent corrosion resistance, wear resistance, and is commonly used in automotive, appliances, and outdoor structures
7	Hot-Dip Galvanizing	In hot-dip galvanizing, steel or iron is dipped into molten zinc, forming a protective layer of zinc oxide. This process is primarily used for corrosion protection in outdoor structures, such as bridges, pipes, and construction materials. Each method has its own advantages and is selected based on the specific requirements of the application, such as environmental exposure, mechanical stresses, and desired material properties.

1.7.1 Various Methods of Thermal Spray Coatings

In the field of surface engineering technology, thermal spraying has become an indispensable instrument. Through thermal spraying, a substance is molten into droplets, which are then sprayed at an extremely high rate of speed onto the surface of a substrate using a spray cannon in order to deposit a coating layer. Prior to applying the actual coating layer, the majority of thermal spray processes necessitate surface preparation for optimal coating adhesion, such as abrasive blasting or the application of a bond coat (Budinski, 1998).

In addition to possessing the ability to apply coatings that exhibit exceptional resistance to wear, thermal spraying is also limited in its ability to spray a broad

spectrum of materials (Heath et al., 1997). Figure 1.7 illustrates the schematic representation of a thermal spray process (Stokes, 2000).

Table 1.2 Various methods of thermal spray coatings

S. No.	Coating Method	Remarks
1	Plasma Spraying	In plasma spraying, a high-temperature plasma arc is used to melt the coating material, which is then sprayed onto the surface. This method can apply a wide range of materials, including ceramics, metals, and composites. Plasma spraying is ideal for applications requiring high melting point materials like zirconia, and it's used in aerospace, biomedical implants, and thermal barrier coatings.
2	High-Velocity Oxy-Fuel (HVOF)	HVOF uses a high-speed combustion process to melt the material and propel it toward the substrate at supersonic speeds. This method produces dense and well-adhered coatings, particularly for wear resistance, corrosion protection, and oxidation resistance. HVOF is commonly used for turbine blades, pump components, and engine parts.
3	Flame Spraying	In flame spraying, a fuel gas (such as acetylene) is used to melt the coating material, which is then sprayed onto the surface. It is a more economical method than plasma or HVOF spraying and is used for coatings that require lower precision. Flame spraying is often used in applications such as corrosion protection for steel pipes or adding wear resistance to mechanical components.
4	Cold Spraying	Cold spraying involves accelerating solid powder particles at high speeds without melting them. The particles bond to the surface through high kinetic energy. This method is beneficial for materials that degrade at high temperatures, such as aluminum, copper, and titanium. Cold spraying is used in

		applications that require minimal thermal degradation of materials, like electronic components and aerospace coatings.
5	Detonation Spraying	In detonation spraying, a controlled detonation of a fuel-oxygen mixture occurs in a barrel, propelling the coating material toward the substrate at high speeds. This produces dense and high-quality coatings, particularly for wear and corrosion resistance. Detonation spraying is used for components like engine parts and high-wear industrial machinery.
6	Wire Arc Spraying	Wire arc spraying uses two electrically conductive wires as feedstock. An electric arc melts the wire material, and compressed air is used to spray the molten particles onto the surface. This method is often used for anti-corrosion coatings on large steel structures, such as bridges and marine equipment
7	Suspension and Solution Precursor Plasma Spraying	These methods involve spraying suspensions or solutions of fine particles or precursors, producing nanostructured coatings with unique properties. They are typically used in applications requiring precise microstructures, such as fuel cells and thermal barrier coatings.

1.7.2 Materials & Application

1. In situations where a lower quality can be tolerated and a cost-effective thermal spray application is desired, flame spraying is commonly employed. Spraying the bulk of components by hand is the norm.

2. Protection against corrosion of structures and components.

3. Reclaim deteriorated shafts, specifically bearing regions, by incorporating bronze alloys or stainless steel.

4. The generated surface coatings are porous, allowing lubricants to be absorbed and thereby improving the bearing's performance.

The boiler steel SA 210 was chosen for the current study on account of its suitability for use in furnaces. In boilers, heated corrosion and oxidation serve as the primary indicators of surface deterioration. Three coatings—Al_2O_3, Al_20_3 +13% TiO_2, and Al_2O_3 +40% TiO_2—were employed to reduce the surface protection against heated corrosion and oxidation. These coatings are referred to as AL, AL13TI, and AL40TI, respectively. Subsequent to being deposited via flame spraying, these coatings underwent microwave processing to apply heat treatment.

CHAPTER 2
REVIEW OF LITERATURE

A literature review is intended to establish a foundation of knowledge on the subject. It identifies research gaps, inconsistencies in prior investigations, and unanswered inquiries that remain unresolved in the field of study. Furthermore, it investigates the need for further research in the relevant discipline. The most recent chapter provides a literature review concerning the mechanism and salt chemistry associated with heated corrosion and high-temperature oxidation of boiler steels. This literature review additionally examines various preventive measures employed to avert heated corrosion, encompassing diverse coating techniques, with particular emphasis on the function of plasma.

2.1 STEELS OPTED FOR BOILER CONSTRUCTION

The atmosphere inside coal-fired furnaces is complex, consisting of a wide range of operating conditions that are specific to the system, thermodynamic activity of corrodants, and at times, depositions of different chemistries that are both particulate-laden and contain them.

The materials utilized in the construction of various boiler components are also classified in a broad manner. For instance, water walls are constructed from carbon steel and low alloy steel, while steam superheaters and reheaters are constructed from austentic alloys. For sulfidizing conditions, reheaters employ high chromium alumina alloys containing iron (Natesan, 1993).

2.2 MATERIAL DEGRADATION AT HIGH TEMPERATURES

An significant drawback associated with metallic materials is that their properties degrade as a result of their interaction with the environment in which they are utilized. As a result, the metallic components experience untimely failure. The closure of the facility gives rise to economic losses, environmental contamination, and potential

risks to human life. Environmental degradation results in significant annual direct losses of natural resources, such as metals (Chatterjee et al., 2001).

Material degradation is an exceedingly critical concern in numerous high-tech sectors. Corrosion significantly impairs or destroys components of gas turbines. This not only leads to increased maintenance costs but also reduces overall efficiency (Khanna, 2002).

2.2.1 Oxidation

Dry corrosion is another term for oxidation. Regarding the composition of the oxide layer that forms, the oxidation rate varies. Certain oxidations are detrimental, whereas the formation of an oxide layer is advantageous. For instance, alloys often depend on oxidation reactions to generate protective oxide layers that withstand corrosion attacks in severe environments. The formation of an oxide scale is the culmination of a series of stages (Khanna, 2002).

2.2.2 Corrosion in Heat

The acceleration of hot corrosion, an oxidation reaction, is exacerbated by the existence of salt contaminants including Na_2SO_4, V_2O_5, and NaCl. These contaminants chemically react with the substrate to produce a molten deposit, which in turn damages the protective surface oxides (Eliaz et al., 2002).

The boiler steel is subjected to an extremely corrosive environment at temperatures above ambient. As the temperature rises, the material's deterioration caused by reaction with the severe environment multiplies by a significant amount (Khana, 2002).

2.3 HOT CORROSION MECHANISM

The process of hot corrosion can be categorized into two distinct stages: initiation and propagation. The heated corrosion process typically necessitates the existence of liquid sodium sulphate on the metal surface, with a melting point of 884˚C. As the

protective oxide scale dissolves through a fundamental flux mechanism, the corrosion rate is typically low during the initiation stage, which is the initial phase of heated corrosion. In the course of propagation, the protective oxide scale undergoes complete destruction and is incapable of reforming. As a result, the alloy is exposed to sulphidation via invert diffusion of sulphur, which significantly accelerates the rate of corrosion (Natesan, 1993). Hot corrosion takes place at elevated temperatures and is initiated either when the deposit is initially in the form of a liquid or when a reaction between the deposit and the environment transforms it into a solid state

2.3.1 High Temperature Hot Corrosion (HTHC)

Corrosion at elevated temperatures predominantly transpires (Hancock, 1987). By means of the deposition of fused alkali metal compounds on the substrate's surface, this form of hot corrosion spreads. A chemical reaction cycle occurs during HTHC. Na_2SO_4 is the predominant salt in HTHC owing to its exceptional thermodynamic stability. Vanadium, lead, chlorides, and phosphorous, among other impurities found in fuel or air, are capable of combining with Na_2SO_4 to produce a compound with a reduced melting point. This characteristic effectively expands the scope of the attack. For instance, the combination of Na_2SO_4, produces an extremely hostile environment (Tiwari, 1997).

2.3.2 Low Temperatures Hot Corrosion (LTHC)

LTHC primarily develops, which is significantly Na_2SO_4 (884˚C) (Nicholls, 2000). This process primarily takes place in the eutectic phase of sodium sulphates and base metal sulphates; consequently, it takes place at a reduced temperature (Natesan, 1993). Pit formations are indicative of a non-uniform attack in the reaction product. In close proximity to the alloy-scale interface, LTHC induces negligible sulphate formation, and the alloy substrate experiences minimal Cr or Al depletion (Rapp and Zhang, 1996).

In this case, a SO_3 partial pressure is necessary to stabilize the formed base metal sulphate. These sulphates then react with sulphates of alkali metals to produce

eutectics.. The Na_2SO_4-$CoSO_4$ eutectic with 540˚C, which inhibits the development of protective oxides. Localized pitting is the consequence of LTHC.

2.4 CHEMISTRY OF SALTS

Accelerated corrosion is a thermal phenomenon that manifests on the heating surfaces of re-heaters and superheaters located within the furnaces of a power station. This occurs as a result of the ash deposition generated during the coal combustion process within the furnace. Compounds such as sodium, sulphur, and vanadium are present in the ashes as Na_2SO_4-V_2O_5 complexes and vanadium sodium composites. Residual oils utilized as boiler fuel.

Certain compositions of these compounds have a lower metallic surface temperature due to their low melting point (480 to 510 degrees Celsius). They increase the rate of corrosion as they transform into a liquid state . A sufficient quantity of potassium and sodium are volatilized flame as coal is burned in furnaces powered by coal.

The sulphur emitted during coal combustion reacts with oxygen to produce SO_2 and a trace quantity of SO_3. Further reaction of this SO_2 and SO_3 with volatile alkalies produces Na_2SO_4 vapours, which condense on the surface of the pendant super-heater and re-heater tubes in the boiler, along with fly ash. This results in the rapid occurrence of localized corrosion, which is accompanied by sulphidation (Beltran and Shores, 1972; Rapp et al., 1981).

2.4.1 Process of Salt Formation

It is not feasible to completely and economically eliminate sulphur particles from fuel oil or coal, nor can the formation of SO_2 during combustion be prevented (Nelson et al., 1959). During the combustion of coal or fuel oil, sulphur produces SO_2, which is subsequently partially oxidized to SO_3, and water vapours at the temperature of combustion produce Na_2SO_4 as a byproduct as explained in equation 2.1.

$$2HCl + SO_3 + H_2O \text{ produces } Na_2SO_4 \text{ (g)} \qquad (2.1)$$

At a reduced temperature, Na_2SO_4 reacts with SO_3 to produce sodium pyrosulphate $Na_2S_2O_7$, as explained in equation 2.2, which possesses a melting point of 401˚C.

$$SO_3 + Na_2SO_4 \text{ produces } Na_2S_2O_7 \quad (2.2)$$

Fuel oils contain a trace quantity of vanadium, which combustion produces V_2O_5. This substance subsequently reacts with $Na2SO_4$ to produce sodium vanadate, which have a highly corrosive nature presented in equation 2.3.

$$x\ Na_2SO_4 + V_2O_5 \rightarrow (Na_2O)xV_2O_5 + x\ SO_3 \quad (2.3)$$

Metals and alloys are consequently subjected to a range of corrosive agents, including molten ions such as Na_2SO_4, sodium vanadate, and NACl, as well as oxidizing agents like O_2, SO_2, and SO_3 (Khanna and Jha, 1998).

2.4.2 Na_2SO_4-V_2O_5 Salt Chemistry

Combustion by products condensation, such as molten vanadate-sulphate deposits, is accompanied by highly corrosive substances that penetrate high-temperature components within the combustion system (Natesan, 1976). The researchers have conducted a thermochemical test with S, Na, and N. On the gas turbine's surface, they discovered that Na_2SO_4, $Na_2V_2O_6$, and V_2O_5 were the most prevalent salt species. Both oil-fired and coal-fired furnaces produced the identical outcome.

According to the findings of (Barbooti et al., 1988), the salt precipitate most frequently observed on boiler superheaters, which possesses a comparatively low melting point of 550˚C. According to Tiwari, 1997, a eutectic phase V_2O_5 and Na_2SO_4 mixture in a 60:40 ratio that has a low melting point (550 C).

The reaction rate between the salts is dependent on the molar ratio of V_2O_5 to Na_2SO_4 and temperature (600–1300 degrees Celsius). (Kolta et al., 1972) investigated the kinetics of this Na_2SO_4 and V_2O_5 reaction. Upon undertaking further investigation, the author ascertained that an extension of 30 minutes in the reaction time led to an eventual cessation of the reaction rate, culminating in its complete cessation. This

phenomenon is caused by meta-vanadate and pyro-vanadate, respectively, upon decomposition at elevated temperatures.

(Seiersten and Kofstad, 1966) conducted thermogravimetric investigations at temperatures 650˚C to 800˚C to examine the concurrent corrosion induced by sulphate and vandate. The corrosion results were identical when samples coated with sodium vanadate were initially subjected to O_2 + 4%SO_2 and uncoated samples were exposed to pure oxygen. However, following an incubation period, it was observed that the duration decreased as the temperature increased and a sufficient quantity of SO_3 and Na_2SO_4 on the metal's surface. As a result of the f molten $NiSO_4$-Na_2SO_4 and a trace quantity of vanadate, sulphate-induced hot corrosion ensues. This occurred as a result of sodium sulphate formation under high sulphur trioxide pressure.

2.5 ESSENTIAL COATINGS: PURPOSE AND CHOICE

A surface engineering term for a material layer deposited onto a substrate for the surface properties and provide protection against corrosion and abrasion is "coating." A coating is a substance that is applied onto the surface of another substance using an optimally compatible technique in order to achieve the desired aesthetic or technical characteristics. Coatings may be artificially deposited, applied naturally, or synthetically (Burakowski and Wierzchon, 1998). Coating is a technique of surface modification. In thermal power facilities boilers to increase the corrosion resistance of inexpensive alloys. Additionally, coating is more cost-effective than employing costly corrosion-resistant alloys. When applied to low-grade alloy steel, a coating can provide exceptional resistance to corrosion. Comparable to the properties exhibited by high-priced superalloys (Priyantha et al., 2003). By safeguarding against corrosion and abrasion, the material to be utilized to its fullest capacity.

Corrosive environment causes components of superheaters and re-heaters experience catastrophic material failure; therefore, documented the application of protective coatings to these components.

The following are a summary of the primary benefits of coatings by Heath et al., 1997:

1. Coating enables the selection of an alloy with greater flexibility and facilitates the optimization of resistance to corrosion, particle attrition, and specific environments.

2. A functionally graded or multilayered coating system may be utilized; for instance, a ceramic protective coating employs an adhesion bond coat.

3. Unique alloys and microstructures can be produced through the application of thermal spray technology, which is unattainable with wrought material. Particular alloys, such as continuously graded composites, feature microstructures that resemble amorphous phases resistant to corrosion.

4. The cost of coating is considerably diminished in comparison to the costly bulk material that is highly alloyed. As of late, thermal spray coatings have gained popularity due to their excellent performance-to-cost ratio.

5. Coating is advantageous due to the ability to restore components and apply it on-site. This results in decreased maintenance expenses and repair time for components.

2.6 RECENT RESEARCHES CONCERNING THE RESISTANCE OF THERMAL SPRAY COATINGS TO HOT CORROSION AND OXIDATION

An investigation carried out by Kaur and Prakash (2012) utilized the HVOF spray method to apply a Cr_3C_2-NiCr coating to SAE-347H boiler steel. The HVOF-spray Cr_3C_2-NiCr coating maintained its adhesion effectively under the specified conditions.

Bala and Prakash (2011) investigated the thermal corrosion characteristics of Ni-20Cr were coated using the cold spray (CS) technique. In order to ascertain the rate of heated corrosion, the weight change of the specimens subsequent to each cycle was quantified.

In 2011, Kaushal et al. conducted a comparative analysis of the heated corrosion efficacy of detonation and HVOF techniques. In order to conduct experiments, Ni-20Cr coatings were implemented on T-22 steel. The researchers observed that HVOF-sprayed coatings exhibited enhanced resistance to thermal corrosion when subjected to elevated temperatures. On the contrary, coatings that were deposited using a detonation cannon demonstrated oxide scale spalling upon exposure to environments that contained molten salt.
In their 2011 study, Bala and Prakash compared HVOF and CS methods utilizing a comparable coating composition (Ni-20Cr) but in real-world environments. In actual conditions, HVOF was discovered to be more effective than cold spray.

(Chatha et al., 2013) investigated alloy coating in the superheater zone for a duration of 1500 hours through high temperature experiments conducted at 900ºC. As a consequence of the scale-bound Cr_2O_3, it was determined that Ni-20 Cr-coated steel exhibits superior performance to the bare substrate.

Kaur et al. (2012) utilized HVOF to develop a Cr_3C_2-25NiCr coating on bare steel in order to compare its efficacy in the harsh conditions, no scale spallation was observed in the coating following exposure, and it remained intact under all tested conditions.

(Mishra et al., 2013). Plasma-spraying is a prevalent method for applying coats in order to prevent oxidation, corrosion, and erosion-induced surface degradation. The PS technique was utilized to deposit NiCrAlY coatings on steels.

In their study, Hussain et al. (2014) examined four distinct alloy compositions based on Ni and Fe. These alloys were deposited using the PS process and subsequently subjected to real power plant conditions for one thousand hours at 650°C beneath a coal ash deposit. The Ni-Cr coating exhibited superior performance compared to the other alloys (in that order: NiCr > FeCrAl > Alloy625 > NiCrAlY).

On the superni-75 superalloy substrate, $75Cr_3C_2$–25(Ni–20Cr) coatings were developed by Singh et al. in 2015. At 900 °C, the derived coatings were evaluated in environments containing Na_2SO_4–10%NaCl and a real medical waste incinerator. The microstructure produced by cold spray coating was rigid, dense, and possessed a

reduced number of pores, all of which were crucial in preventing corrosive species from penetrating the substrate.

Kumar et al. (2018) applied CS-deposited nano Ni-20Cr coatings (powder sizes 42 nm and 57 nm) to SA-516 and T-22 boiler steels. Investigating the high-temperature erosion-corrosion behavior of nanostructured coatings is the primary objective of this research. This can be ascribed to the microhardness of the coating increasing in comparison to conventional powders as the particle size decreases.

By utilizing the PS technique, Ni-20Cr coatings were deposited (Mishra and Prakash, 2015). and examined under real-world furnace conditions. The superior attrition resistance was observed on superfer 800-H, as determined by the Ni-20Cr coating, in comparison to the oxides of Cr_2O_3, Al_2O_3, and SiO_2.

Praveen et al. (2015) experiments were conducted at 450˚C. As indicated by the results, coated specimens demonstrated a significantly higher resistance to attrition when compared to untreated samples. The increased resistance to attrition noted at an impact angle of 30˚ may be ascribed to the shielding and pinning characteristics of alumina particles. The attrition resistance of coatings is two and a half times that of the substrate.

Singh et al. (2016) deposited Cr_3C_2-25(Ni-20Cr) and Ni-20Cr coatings onto T-91 boiler steel via the HVOF method. Fifty cycles of heated corrosion investigation were carried out in an environment containing molten salt at a temperature of 900ºC. With regard to performance, Cr_3C_2-25(Ni-20Cr) exhibits an edge over its substitute. The unprotective Fe_2O_3 scale contributed to a greater increase in the weight gain of the uncoated substrate.

By employing the HVOF method, a 75Cr_3C_2-25NiCr coating was applied to T-91 boiler steel (Chatha et al., 2016). 1500 hours at 900 degrees Celsius were used to assess the high-temperature performance of uncoated and coated materials. A total of 15 cycles were implemented, wherein each cycle consisted of one hour of refrigeration followed by 100 hours of operation. The corrosion resistance of the 75Cr_3C_2-25NiCr coating, which was coated with HVOF, is noteworthy. Furthermore,

it has not experienced any internal oxidation attack, providing confirmation that the oxide scale remains intact.

Mishra et al. (2017) conducted a cyclic investigation wherein superalloys composed of Ni and Fe bases were plasma-sprayed with Ni_3Al powder. The Ni_3Al coating was found to experience partial oxidation under actual conditions; nevertheless, it maintained its integrity for a duration of 1000 hours of exposure and continued to serve as a barrier against erosion and corrosion.

In their experimental study, Singh et al. (2017) compared the cyclic high temperature oxidation characteristics of a substrate coated with NiCrAlY with those of an uncoated substrate. A total of fifty cyclic oxidation cycles were performed at 900°C. Each cycle in a silicon carbide tube furnace consists of twenty minutes of air cooling subsequent to an hour of heating. The NiCrAlY coating demonstrated improved oxidation resistance at high temperatures . These oxides effectively hindered the rate of corrosion.

The erosion behavior of a Cr_3C_2-NiCr coating was investigated by Zhang et al. (2017) across three distinct temperature ranges: 400, 500, and 600˚C. The findings indicated that the coating might exhibit greater suitability when exposed to relatively high temperatures. The erosion rate of volume in composite coatings exhibits a negative correlation with the elevation of erosion temperature. This may be associated with the protection against oxidation and plastic deformation that occurs at elevated temperatures.

In 2018, Premkumar et al. investigated the performance of nanocomposites as coatings. SA 210 Gr C was coated. Erosion experiments were conducted at 450˚C and impact angles of 30, 60, and 90˚. The advantage of the nanocomposite over conventional and uncoated substrates in terms of erosion resistance was attributed to the protective barrier function of the Cr_2O_3 layer, which impedes the ingress of erodent particles. Additionally, the nanocomposite's reduced porosity was identified as the cause of its low erosion rates. The erosion rate was found to be greater at oblique angles for all materials exhibiting ductile behavior. Furthermore, at a dismal impact angle of 30˚, both conventional and nanocomposite coatings exhibit erosion

resistance that is 7.5 times and 3.5 times greater, respectively, than that of an uncoated substrate.

Manikandan (2018) investigated the resistance of Cr_3C_2-25% NiCr coated on alloy X22CrMoV12-1 to high-temperature corrosion at 600°C. Uncoated substrates corrode at a rapid rate. Conversely, the corrosion resistance of a coated substrate is improved through the formation of Ni_2O and $NiCr_2O_4$ in both molten salt and oxygen environments.

Swaminathan et al. in 2019 have performed Experiments on oxidation were performed at 900°C for fifty hours in air. A range of characterization techniques (TEM, SEM, EDX, SAED, and FIB) were employed to analyse coatings both prior to and subsequent to oxidation experiments. The absence of flaking and spalling caused by scale in the coating subsequent to exposure was noted by the authors. Resistance to high-temperature oxidation was achieved through the combination of a nano-sized chromium oxide nanolayer and a nano-structured matrix. Furthermore, the nickel metallic granules are encircled by nanoscale Cr_2O_3 precipitates, which function as grain pinning entities.

Vasudev et al. (2019) scrutinized the effectiveness of high-temperature oxidation and attrition on a naked or coated cast iron sample. The resistance of alloy-718 to oxidation and attrition is reportedly greater than that of a cast iron substrate, as reported by the authors. A stronger resistance to erosion is associated with increased microhardness and the deposition of durable and protective oxides on the exposed surface, such as Al_2O_3 and Cr_2O_3.

In 2019, Praveen and Arjunan utilized the HVOF technique to deposit two weight compositions of nano-Al_2O_3 with NiCrSiB: 1.4% and 0.17 percent. The authors documented that the incorporation of 1.4wt% nano-Al_2O_3 resulted in an increase in micro hardness from 576 to 748Hv, leading to an enhancement in erosion resistance.

Reddy et al. (2019) investigated the corrosion behavior of Ni_3Ti and Ni_3Ti+(Cr_3C_2+20NiCr) coatings subjected to high temperatures via HVOF spraying. The surfaces of the specimens were treated with 40% V_2O_5 and 60% Na_2SO_4 to hasten

the corrosion process. Fifty cycles were performed on each specimen at a temperature of 650ºC. The rate of corrosion was quantified as weight gain per unit area. According to reports, coated specimens experience a reduction in weight gain in comparison to exposed substrates.

Vasudev et al. (2020) Post-processing restored porosity and microcracks, which the authors deemed to be indicative of a substantial enhancement in microstructure results in the healing of pores attributed to the material movement that occurs during microwave processing. Additionally, there was an enhancement in microhardness, fracture toughness, and surface irregularity.

Additionally, Daram and Banjongprasert (2020) investigated the impact of post-treatments on the corrosion performance and microstructure of NiCrMoAlY alloy coatings. The authors reached the conclusion that thermal treatment leads to a reduction in pores, which subsequently enhances the resistance to corrosion.

Using the HVOF spray method, composite coatings of IN718-Al_2O_3 Vasudev et al., 2020. A correlation can be established between enhanced oxidation of composite coatings and the development of stable and protective phases, including Al_2O_3, $NiCr_2O_4$, and Cr_2O_3.

The erosion efficacy of Cr_3C_2-NiCr-based coatings deposited via plasma spraying on an SS-304 L substrate was investigated by Dhzurinskiy et al. in 2021. The developed coating has a dense microstructure devoid of microcracks and pores, in addition to possessing exceptional hardness and durability. Developed coatings with elevated values of fracture toughness and hardness will exhibit enhanced resistance to erosion.

The erosion behavior and mechanical properties of NiAl-20 wt% Bi_2O_3 coatings sprayed with atomspheric plasma while modulating the Cr_2O_3 content were examined by Sun et al. in 2021. The results indicated that the incorporation of Cr_2O_3 significantly enhanced the mechanical strength of the coatings while maintaining their plasticity. Furthermore, the wear characteristics of the coatings are enhanced by the high hardness and resistance to plastic deformation exhibited by Cr_2O_3.

Thermal barrier coatings containing varying amounts of TiO2 were applied onto 6061 aluminum alloy using plasma spraying techniques.

Jia at al., 2014 investigated that there is a phase transformation occurring in all of the feedstock powders during the spray process. Due to the differences in thermal conductivity, melting point, and brittleness between TiO_2 and Al_2O_3, TiO_2 is able to disperse easily. This dispersion of TiO_2 helps to seal holes, release stress, and reduce cracks.

Michalak et al, 2021 have explored how the amount of TiO_2 developed through atmospheric plasma spraying (APS). We examine the impact of different TiO_2 content levels on the resulting characteristics of Al_2O_3, Al_2O_3+3 wt% TiO_2, Al_2O_3+13 wt% TiO_2, and Al_2O_3 +40 wt% TiO_2 coatings. The study focused on analyzing the phase composition, morphology, microstructure, and mechanical and tribological performance of the coatings. It was found that an increased amount of TiO_2 caused a change in the phases, resulting in the creation of intermediary Al_2TiO_5 and Al_2-xTi_1-xO_5 phases. It was demonstrated that the higher concentration of TiO_2 led to a decrease in the micro-hardness of the coatings. This was attributed to phases, which in turn affected the coatings' tribological performance. The Al_2O_3 +13 wt% TiO_2 coating had the lowest volumetric wear.

The selection of 900°C as a testing temperature in studies of boiler steels is primarily due to its relevance to operational conditions in high-temperature environments, particularly in coal-fired boilers. At this temperature, materials are exposed to aggressive corrosive agents, such as alkali salts and sulfur compounds, which significantly accelerate oxidation and degradation (Singh, G., et al., 2018). Research indicates that testing at 900°C effectively simulates real-world scenarios, allowing for a comprehensive evaluation of the performance and durability of protective coatings (Eklund, J., et al., 2019; Cheng, J., et al., 2019). Furthermore, studies have shown that various coating materials, including NiCrAlY and AlCrN, exhibit different corrosion resistance characteristics at this temperature, providing valuable insights into their effectiveness (Sundaresan, C., et al., 2021). Consequently, 900°C serves as a standardized condition for assessing the protective capabilities of coatings

against hot corrosion and oxidation, facilitating comparisons across different studies and coating technologies (Goyal, L., et al., 2017).

In the case of boiler applications, TiO_2 is often added to Al_2O_3 coatings primarily for its ability to enhance the toughness, thermal stability and oxidation resistance at high temperatures. Boilers operate under harsh environments that involve high temperatures, oxidative atmospheres, and exposure to corrosive elements like sulphur compounds. While Al_2O_3 itself has excellent wear resistance and high melting point, it tends to be brittle and may not perform as well in environments requiring greater toughness and resistance to cracking. By adding TiO_2, the composite material gains flexibility and reduced brittleness, while still maintaining high wear and corrosion resistance. TiO_2 also improves the coating's adherence to the substrate and enhances the overall oxidation resistance at high temperatures, making the Al_2O_3-TiO_2 composite ideal for industrial applications like gas turbines and boilers (Mohamed et. al., 2021). However, when it comes to enhancing corrosion resistance specifically, there are alternatives that may provide superior performance compared to TiO_2. For instance, zirconium nitride (ZrN) offers better corrosion resistance, particularly in aggressive environments. ZrN has excellent chemical inertness and provides superior protection against oxidation at elevated temperatures. It also has better resistance to certain corrosive chemicals and is widely used in the aerospace and automotive industries (Duran, A., et al., 2020). While TiO_2 is suitable for improving the toughness and oxidation resistance of Al_2O_3 coatings, ZrN or even chromium nitride (CrN) could be better alternatives for applications where extreme corrosion resistance is required. ZrN coatings, in particular, provide a dense barrier against corrosive agents, outperforming TiO_2 in specific corrosive environments (Zhao, Y., et al., 2022).

2.7 RESEARCH GAPS

Limited research has been conducted on the investigation of thermal spray coatings for alumina-based coatings and their microwave post-processing, according to the available literature. As the post-processing of flame-sprayed coatings is still in the developmental phase, it has been chosen as the subject of the current study.

1. Comparative studies of the heated corrosion performance of Al_2O_3-based coatings on ASTM-SA210 grade A1 boiler steel are not well documented in the literature.

2. The Al_2O_3-based coatings have been tried for high-temperature applications of hot-corrosion and oxidation in literature. The plasma spray technique was applied to deposit the Al_2O_3-based coatings. The performance of the coatings was evaluated and found that the use of plasma spray leads to the degradation of the coatings due to excessive temperature. Therefore, there is need to retain the phases present in the coatings and other technique with low temperature can be applied.

3. The literature presents the work where the material composition was varied other than the standard compositions such as Al_2O_3, Al_2O_3-13TiO_2, and Al_2O_3-40TiO_2 and found that if the titania content is varied, it effects the phase stability of the material at high-temperature applications.

4. The coatings can be further heat-treated to improve its performance in corrosion applications. The various methods other than conventional heat-treatments can be applied due to the restriction of use of these treatments.

5. Ceramic coatings offer resistant properties to extreme temperatures. The mechanical and microstructural properties of Al_2O_3-based coatings in the face of heated corrosion must be investigated.

6. Base material has been chosen following an examination of the literature review, previous research, and prospective studies that are practical in real-world scenarios and have the potential to benefit society. As the substrate, ASTM-SA210 grade A1 furnace steel has been chosen.

7. Furthermore, the Flame spray thermal spray technique has been selected for the present work as it offers the finest, hardest coatings.

8. Very few studies have been conducted regarding the microwave post-processing of alumina-based coatings. As a result, post-processing has been incorporated into the present research.

2.8 TREATMENT AFTER HEATING

In accordance with the literature, microwave hybrid heating [MHH] has been chosen as the post-processing method for developed coatings in the current proposed research. The developed coatings are subjected to microwave processing in this step.

2.9 PROPOSED FORMULATION OF THE PROBLEM

The primary criterion for choosing this material was its wide application in the production of furnace tubes. This substance is utilized extensively in power facilities.

At temperatures as high as 900°C, the failure of boiler tubes was attributed to two primary factors: (a) corrosion, which occurred when salt contaminants generated during fuel combustion began to accumulate as molten ash on the tubes; and (b) the dissolution of the protective oxide layer, which precipitated material degradation. and (b) as a result of bed coil tube erosion caused by the abrasive characteristics of ash particles.

Additionally, scholarly research has revealed that over time, any aggressive environment will cause a material to gradually lose its surface integrity. In order to improve the material's surface properties, some form of protection must be placed at the interface between two bodies in contact.

The objective of this study is to investigate the application of alumina-based coatings (specifically Al_2O_3, Al_2O_3-13TiO_2, and Al_2O_3-40TiO_2) as a preventive measure against surface failures. ASTM-SA210 GrA1 has been implemented as a substrate material owing to its extensive application in boiler tubing fabrication.

2.10 RESEARCH OBJECTIVES:

The present work has been planned in order to fulfill following objectives:

1. To develop Al_2O_3-based ceramic coatings on ASTM-SA210 grade A1 boiler steel through flame spray thermal spray coating technique.

2. Microwave post-processing of flame sprayed Al_2O_3-based coatings using Microwave Hybrid Heating technique.

3. To examine the as-sprayed and microwave post-treated Al_2O_3-based ceramic coatings for comparison in terms of mechanical and micro-structural characteristics.

4. To compare the hot corrosion performance of as-sprayed and microwave post-processed coatings at 900°C for 50 cycles.

5. To compare the oxidation performance of as-sprayed and microwave post-processed coatings at 900°C for 50 cycles.

CHAPTER 3
EXPERIMENTAL PROCEDURE

The experimental procedures and techniques utilized for the deposition of coatings and their subsequent characterization are detailed in this chapter. Additionally, the apparatus and other instruments utilized in this investigation have been described in detail.

3.1 PROCEDURE OF EXPERIMENT

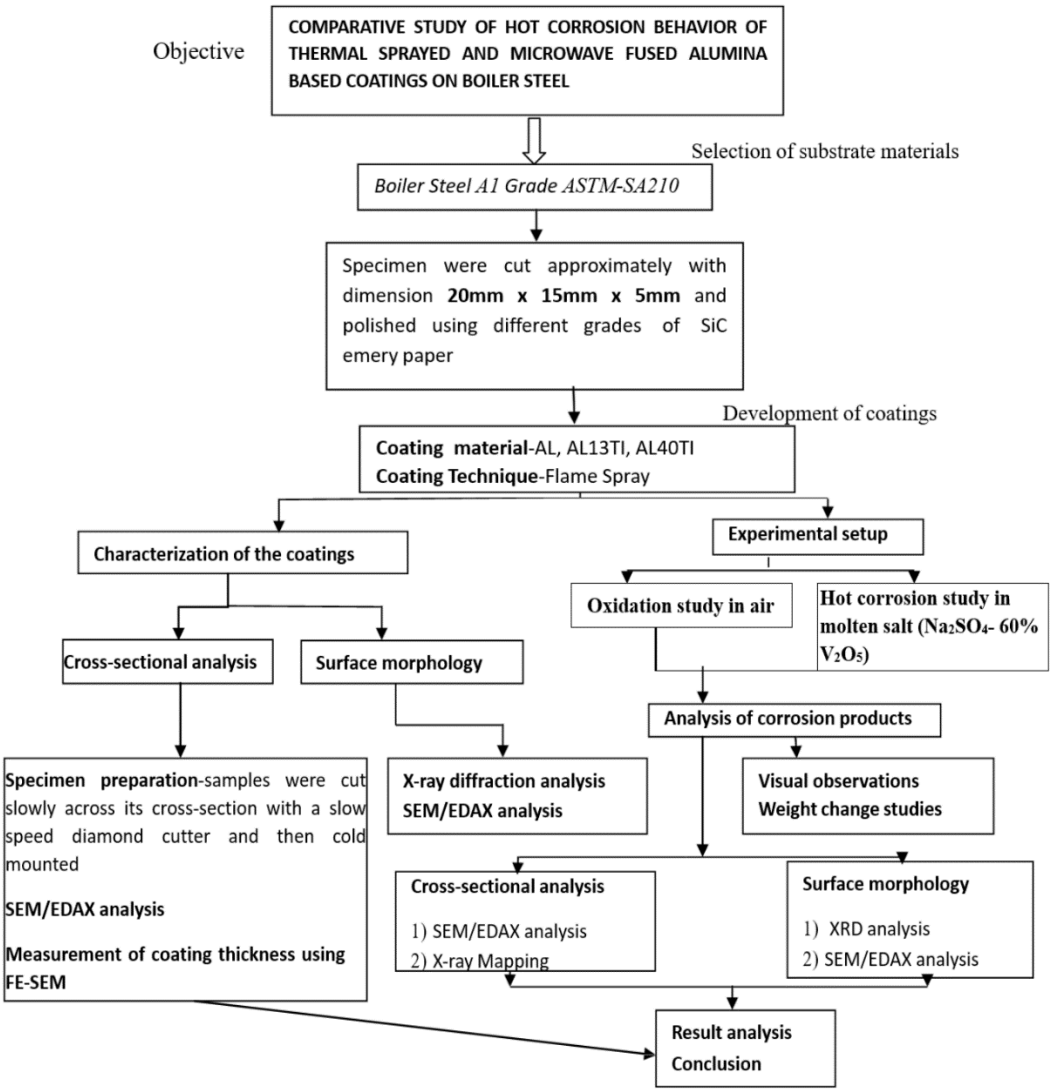

Fig.3.1 Flowchart illustrating the current work's methodology

3.2 THE PROCESS OF SUBSTRATE MATERIAL SELECTION

Mishra Dhatu Nigham Ltd, Hyderabad (India), and Cheema Boilers were consulted prior to the selection of the prospective materials for the research. An Fe-based superalloy comprising two varieties of boiler steel substrate materials, specifically "ASTM-SA210-Gr A-1 (Gr A-1)" and Midhani Grade Superfer 800H. have been chosen as the substrate materials for the current investigation.

In the chemical industry, the chosen superalloy is extensively utilized in steam boilers, furnace equipment, and piping; in fertilizer facilities, it is applied to baffle plates and tubes. Certain boiler steels are employed as materials for boiler tubes in power facilities located in Northern India. Gr A-1 exhibits a diverse array of utility profiles within boilers, most notably in the fabrication of their water walls. The tube form of the boiler steels was obtained from Cheema Boilers, Ropar, India. The rolled sheet form of the superalloy was obtained from Mishra Dhatu Nigham Ltd., Hyderabad.

3.3 THE PROCESS OF DETERMINING CHEMICAL COMPOSITIONS

The ASTM-SA210 grade A1 boiler steel, which is extensively utilized in the production of boiler tubes, has been employed as a substrate material.

The optical emission spectrometer (Thermo Jarrel Ash, TJA181/81, U.S.A.) was utilized to ascertain the precise chemical composition of these alloys. The analytical results, both nominal and actual, for these steels are detailed in Chapter 4 of the current investigation.

3.4 MATERIALS PREPARATION FOR SUBSTRATES

The specimens were meticulously prepared by hand, ensuring that no structural modifications occurred. Samples measuring around 20mm x 20mm x 5mm were extracted from the alloy tubes, which contained the furnace steels, and the rolled sheet, which contained the superalloy. The specimens underwent a polishing process utilizing SiC emery papers with grain sizes of 220, 400, and 600, followed by 1/0, 2/0, 3/0, and 4/0 grades. The specimens are illustrated in Figure 3.2.

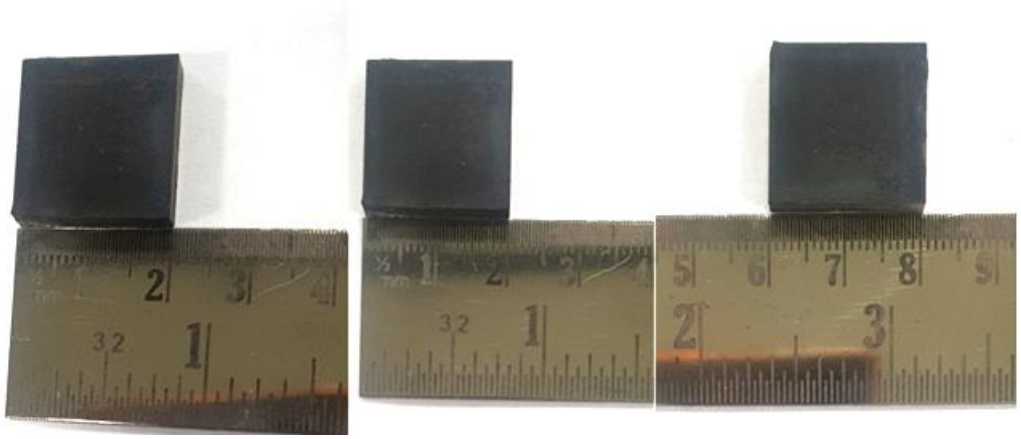

Fig.3.2 Cutting of samples prior to deposition of coatings.

3.5 MICROSTRUCTURAL ELEMENTS OF SUBSTRATE MATERIALS

A single example of each alloy was subjected to polishing with emery papers of different grain sizes. A cloth polishing wheel machine was then utilized to achieve mirror polishing with a suspension of 1μm levigated alumina powder. The Zeiss Axiovert 200 MAT Inverted Optical Microscopes were utilized to capture optical micrographs (X 200) of the substrates. These micrographs are detailed in Chapter 4 of the current investigation.

3.6 ACQUISITION OF POWDERS

Three powders specifically Al_2O_3, Al_2O_3-13TiO_2, and Al_2O_3-40TiO_2 were used in the current research work for deposition of coatings.

Table 3.1 Designation system used for powders in the current work.

S.No	Powder Used	Designation System
1	Al_2O_3	AL
2	Al_2O_3-13TiO_2	AL13TI
3	Al_2O_3-40TiO_2	AL40TI

The designation system used for these three powders was AL, AL13TI, and AL40TI, respectively. These powders were produced by H.C. Starck of Germany and available

for commercial purchase were chosen. The granules were supplied by Shree Sai Metal Coating, located in Noida, India. In order to further validate the average particle size.

3.7 DEVELOPMENT OF COATINGS

The formulation of a coating is a critical component in achieving the desired outcome and meeting the specifications of the intended application site. The phases comprised of the costing development process are detailed below. The logic of combining aluminium oxide (Al_2O_3) with titanium oxide (TiO_2) hinges on enhancing the performance characteristics of composite materials, particularly in high-temperature and corrosive environments. Al_2O_3 is known for its hardness, wear resistance, and thermal stability, making it suitable for various industrial applications. Incorporating TiO_2 not only improves toughness and flexibility but also enhances thermal stability **(**Mohamed, M., & Zaki, F., 2021; Duran, A., et al., 2020). The percentage of TiO_2 included in the composite is critical, as it directly influences the material's mechanical and thermal properties. At lower concentrations, such as 13% TiO_2, the composite retains the hardness and wear resistance of Al_2O_3 while gaining some toughness from TiO_2. This balance makes the material particularly suitable for applications where high abrasion resistance is essential **(**Radhakrishnan, P., et al., 2019; Feng, J., et al., 2018**)**. In contrast, a higher percentage, like 40% TiO_2, significantly alters the composite's characteristics, enhancing its flexibility and resistance to thermal shock. This is particularly advantageous in environments subjected to rapid temperature changes, allowing the material to withstand mechanical stresses without failure (Zhao, Y., et al., 2022; Goyal, L., et al., 2017). Furthermore, the integration of TiO_2 with Al_2O_3 has been shown to enhance corrosion resistance, which is crucial for the longevity of materials used in aggressive environments **(**Eklund, J., et al., 2019; Singh, G., et al., 2018**)**. Therefore, the careful selection of TiO_2 percentages is fundamental in tailoring material properties to meet specific engineering requirements, thus advancing the development of high-performance coatings and ceramics (Krishnan, A., & Gupta, A., 2020; Kim, K., et al., 2020). This strategic approach not only facilitates enhanced material performance but also supports innovations in various applications ranging from aerospace to energy production.

3.7.1 Coatings' Feedstock Materials

For the application of the top coat, powdered AL, AL13TI, and AL40TI alloys were chosen as the coating substance. For the bond coat, NiCrAlY in powder form was selected. The granules were supplied by Spraymet Surface Technologies, located in Bangalore, India.

In order to further validate the average particle size and composition of the coating granules, the Institute Instrumentation Centre, I.I.T. Roorkee performed SEM/EDAX and XRD analyses.

All coating powders' chemical compositions and particle sizes are detailed in Chapter 4 of the present investigation. It is worth noting that the selection of these coating particles for coating deposition on the substrates was based on the scarcity of literature examining the characterization and high temperature corrosion of the coated substrates.

3.7.2 Coating Preparation

Substrate coatings were applied utilizing Flame Spray apparatus, which operates on a thermal spray process (shown in Figure 3.3). After being cleansed and degreased, the test specimens were shot blasted. Before the coatings were flame-sprayed onto the specimens, alumina (grit 60) grit bombarded. The application of the coating was performed by Shree Sai Metal Coating, a commercial enterprise located in Noida, India.

Table 3.2 The process parameters utilized in coating deposition.

Torch	CastoDy8000
Nozzle	SSM 30
Acetylene pressure	0.7 bar
O_2 pressure	4.0 bar
Compressed air pressure	300 bar

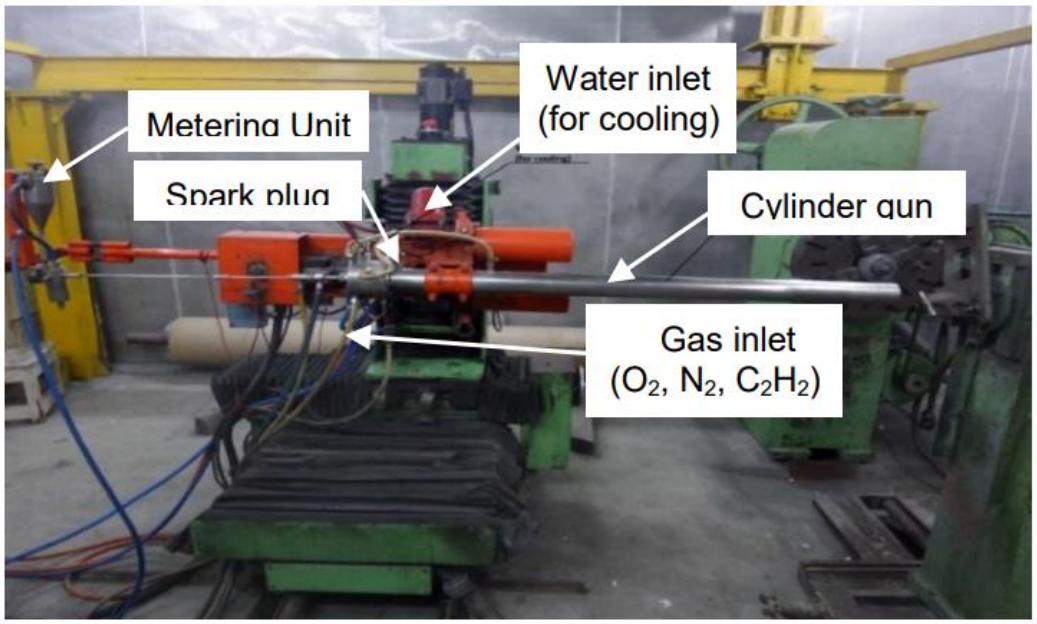

Fig.3.3 Illustrates a schematic representation of the flame discharge apparatus.

Figure 3.4 illustrates the flame spray coatings in their as-sprayed state. The alumina compounds comprised a layered white coating. In contrast, AL13TI and AL40TI coatings have exhibited a sombre visual characteristic.

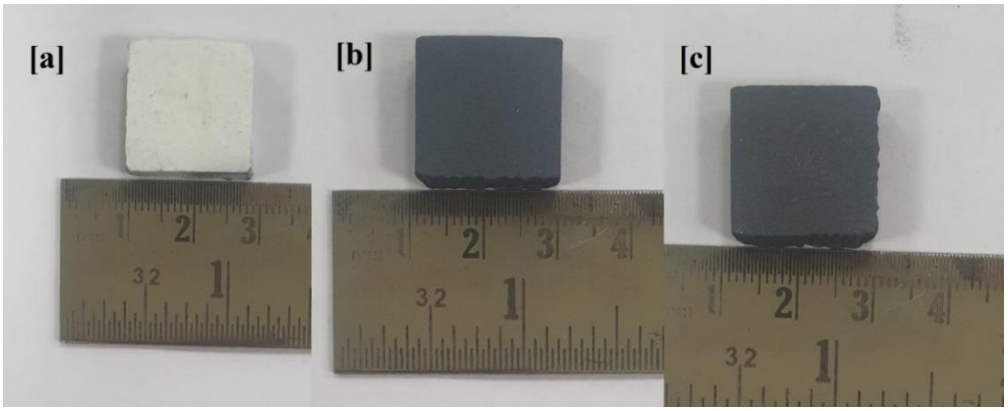

Fig. 3.4. (a): AL coating samples; (b): AL13TI; and (c): AL40TI coatings sprayed with a flame.

3.8 PROPERTIES ASSOCIATED WITH COATINGS

3.8.1 Preparation of a Specimen

At Guru Nanak Dev Engineering College in Ludhiana, India, the cross-sections of the as-coated specimens were meticulously cut using a slow speed diamond cutter

(Buehler's Precision Diamond Saw, Model ISOMET 1000, manufactured in USA). Following the procedure, the specimens were coated with cold epoxy using plastic rings and a cold setting resin and hardener in a 1:1 ratio, which was supplied by Kishore Scientific in Delhi.

Following that, the specimens underwent a meticulous manual polishing procedure utilizing emery papers of varying grain sizes, accompanied by different grades.

Ultimately, the specimens underwent refining using a cloth polishing wheel machine and a suspension of 0.05 μm alumina powder and 0.3 μm diamond paste.

The use of distilled water and a suspension of diamond material for fine polishing reduces the likelihood of smearing or pull-out. After performing a thorough cleansing with running water, the specimens were dried in heated air to eliminate any residual moisture.

3.8.2 Determination of Thickness of Coating

Every effort was exerted to ensure that the coatings had an even thickness. The thickness of a subset of the uncoated specimens was assessed subsequent to cross-sectional sectioning and cold mounting of the specimens (as detailed in Section 3.8.1). The researchers utilized an EDAX attachment (Oxford, UK) on a Field Emission Scanning Electron Microscope (FE-SEM) (FEI ZEISS; at IIT Roorkee, Roorkee) in order to acquire backscattered electron (BSE) images.

Using BSE images, the average coating thickness was calculated. In Chapter 4 of the current investigation, the mean thickness of the coatings, calculated by averaging five measurements for each coating, is presented.

3.8.3 Analysis by X-ray diffraction (XRD)

The as-coated specimens underwent XRD analysis in order to discern the different phases that were present on their surfaces. The d' values are immediately displayed on the diffraction pattern by the diffractometer that is interfaced with the Bruker DIFFRACplus X-Ray diffraction software. The 'd' values were subsequently employed in conjunction with JCPDS data sheets to distinguish between different phases.

3.8.4 Analysis By Energy Dispersive X-Ray (Edax) And Scanning Electron Microscopy (Sem)

3.8.4.1 Analysis of Surface Morphology and EDAX

At the point or area of interest, the SEM and EDAX Genesis software provides an indication of the elemental compositions (in weight percent). While the composition of the coatings may not precisely match specific locations on the surfaces as-sprayed, it is still valuable to comprehend how the coatings acquire their desired compositions. The examination of the coated specimens via SEM/EDAX is detailed in Chapter 4 of the current research.

3.8.4.2 Analysis by cross-sectional means (X-ray mapping)

In order to perform a cross-sectional analysis of the various elements found in the coatings, the specimens were mounted and polished following the steps outlined in Section 3.8.1 after being cut along the cross-section. The samples were analyzed using X-ray mapping on a field emission scanning electron microscope (FEI; as previously stated). In order to obtain images, the microscope utilized two modes. X-ray mapping was utilized in conjunction with FE-SEM imaging to acquire elemental composition and surface morphology data, respectively, at various locations within the coating. In order to enhance conductivity, the specimen was sandwiched between samples and the fragment using silver paste. Subsequently, gold was applied to the coating to enable elemental X-ray mapping analysis of the various elements present. There are three distinct regions in the chosen area: the substrate, the coating, and an epoxy region. X-ray mappings were acquired for every element present in both the substrate and the coatings; however, only those mappings that provide evidence of the presence of a specific element are reported.

3.9 LABORATORY INVESTIGATIONS OF HIGH TEMPERATURE OXIDATION AND HOT CORROSION

3.9.1 Experimental Environment

The investigation into high-temperature oxidation and heated corrosion was conducted in a silicon carbide tube furnace for 50 cycles at 900°C. Every cycle comprised subjecting the specimen to a silicon carbide tube furnace for one hour, after which it was allowed to settle for twenty minutes at ambient temperature. The procedure involving 1 hour heating and 20 minutes cooling during hot corrosion and oxidation testing of thermal spray coatings deposited on boiler steels is commonly followed in various research studies. This method is based on practices outlined in standards such as ASTM G54 and ASTM G116. A cyclic study was conducted for a total of 50 cycles, as this time frame is deemed sufficient to attain the constant state of oxidation for the majority of the substances (Ul-Hamid et al., 2003; Bala et al., 2009). A point of comparison was established between uncoated and as-coated specimens in the experiments. Following this, the samples were dried and washed to eliminate any moisture. Following this, the sample's dimensions were determined utilizing a digital vernier calliper. After obtaining measurements for each dimension at three distinct locations, the mean value was calculated. Initial placement of the sample occurred in an Alumina (Al_2O_3) boat. For three to four hours, the vessels were preheated in a furnace set to one thousand degrees Celsius to ensure that their weight remained constant throughout the corrosion study. In order to conduct the experiment, individual samples were placed in the boat, and subsequently, the combined weight of the samples and the boat was determined. The boats were subsequently inserted into the furnace containing the samples at a temperature of 900ºC. The samples remained inside the furnace at 900ºC for one hour before being removed along with the boats to allow them to settle in air for twenty minutes at room temperature. The weights of the samples and the boat were determined subsequent to chilling using a digital weight balance. The scale that was assembled and subsequently descended into the canoe was also utilized to quantify the change in weight. In order to ascertain the reproducibility of the experiments, two cases of the experiments were replicated.

3.9.2 Studies of Oxidation in Air

As described in section 3.8.1, oxidation experiments at 900°C were conducted on all three bare alloys (mirror polished) and coated alloys in a laboratory silicon tube furnace for a maximum of 50 cycles.

3.9.3 Investigations of Hot Corrosion in Molten Salt (Na_2SO_4 - 60%V_2O_5)

For research purposes, mirror polished and uncoated specimens were prepared, following the methodology outlined in section 3.8.1After that, the specimens were heated to 250°C in an oven, and a salt solution made of Na_2SO_4-60%V_2O_5 dissolved in distilled water was carefully applied to all six surfaces of the polished specimens using a delicate camel hair brush. The compound Na_2SO_4 was obtained from S.D. Both V_2O_5 and Fine-Champ Limited, which are both headquartered in Mumbai, were acquired from Loba Chemie Pvt., Mumbai, Ltd.
Maintaining the salt coating concentration between 3.0 and 5.0 mg/cm2 was possible. After three hours of drying at 100°C in an oven, both the alumina vessels and the salt-coated specimens were measured in weight before being subjected to thermal corrosion experiments. In accordance with the methodology outlined in Section 3.7.1, heated corrosion was applied to both the uncoated and salt-coated specimens in a laboratory furnace at 900°C for 50 cycles.

3.10 EVALUATION OF CORROSION-INDUCED PRODUCTS

A comprehensive analysis was conducted on each specimen that underwent oxidation and heated corrosion testing in order to characterize the corrosion products. Utilizing a variety of analytical techniques, including XRD, SEM/EDAX, and X-ray mapping, the surface and cross-section of the corroded specimens were examined.

3.10.1 Visual Inspection

The specimens underwent visual inspection following the conclusion of each cycle in the laboratory (each cycle consisted of 1 hour of heating followed by 20 minutes of cooling). This inspection aimed to detect any alterations in color, sheen, adherence-

spalling tendency, fissure formation in the coatings or oxide scales, and so forth. Once the samples had undergone fifty cycles of laboratory testing, they were inspected and macrographs were taken. The macrographs provide visibility into the physical conditions of the exposed specimens, including any discernible signs of disintegration of the coating, color changes, spallation, or surface fissures.

3.10.2 Studies on Weight Change

In order to determine the kinetics of heated corrosion and oxidation, the weight change values at the conclusion of each cycle were measured. The weight change data for each specimen was graphed against the number of cycles, and the graphs are presented in the following chapters. The spalled scale, if present, was incorporated during the weight change measurement for oxidation studies conducted in air and hot corrosion studies conducted in a molten salt environment.

3.10.3 Analysis by X-ray diffraction (XRD)

In order to identify the different phases present in the oxide scales of specimens that have undergone 50 cycles of oxidation and corrosion in the laboratory, the X-ray diffractometer was utilized in accordance with the procedure outlined earlier.

3.10.4 Evaluation by SEM/EDAX

3.10.4.1 Morphology of the Face

The samples was analyzed provided comprehensive information regarding the apparatus and methodology utilized in this investigation.

3.10.4.2 X-ray mapping analysis (cross-sectional analysis)

In order to gain insight into the process by which elements, oxides, and different phases form throughout the cross-section of samples was utilized to conduct X-ray mapping analysis, as discussed. Three regions comprise the selected area: substrate, scale, and an epoxy region. Although X-ray mappings were acquired for every element of the substrate and the scale, only those mappings that demonstrate the presence of a particular element are discussed in the following chapters.

3.11 POST-PROCESSING MICROWAVE HYBRID HEATING OF FLAME SPRAYED COATING

The flame spray coatings in their as-sprayed state underwent post-processing utilizing an industrial microwave. The experimental configuration utilized to post-process the AL-based coatings via microwave exposure is depicted in the schematic diagram presented in figure 3.5. The superficial epidermis depth of the as-sprayed deposits causes them to reflect microwave radiation at ambient temperature. To operationalize the principles of MHH, an Enerzi Microwave Systems-manufactured boron carbide (BC) susceptor was employed.

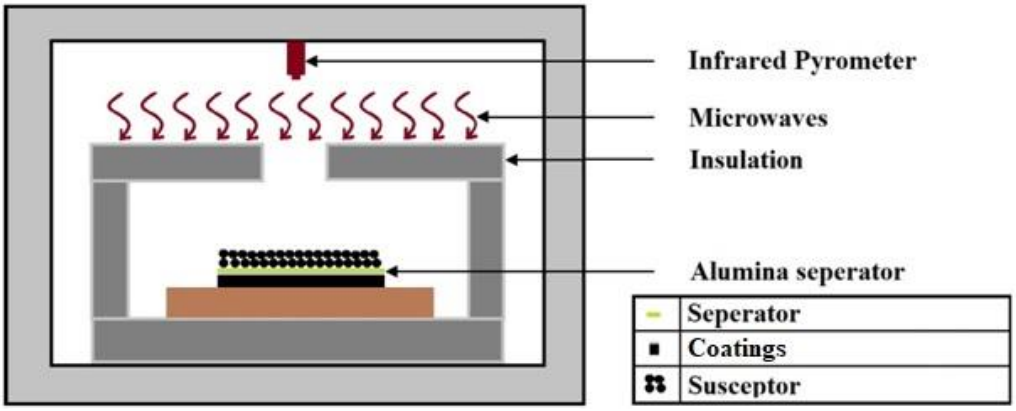

Fig.3.5 Diagrammatic depiction of microwave hybrid heating

The coatings undergo post-processing through the utilization of a microwave furnace, which is illustrated in Figure 3.6. A water chiller is incorporated into this apparatus to facilitate the chilling of the magnetron of the microwave. It is possible to utilize an inert gas cylinder, which is employed to establish an inert environment throughout the coating processing phase to prevent any reaction [oxidation] between the coating and the surrounding environment. In the following section, the initial outcomes of the post-processing will be presented.

3.12 POROSITY AND MICROHARDNESS ANALYSIS

An analysis was conducted on the micro-porosity of the coatings, both in their as-sprayed and heat-treated states. This evaluation involved the use of image processing software, specifically ImageJ, to analyze SEM micrographs taken from the top

surface of the deposited coatings. The present work reports the average of ten readings. In the present work, a load of 200gms was applied with a dwell period of 15s.

Fig.3.6. Utilization of a microwave furnace to process flame-sprayed coatings post-spray.

CHAPTER 4
RESULTS AND DISCUSSIONS

Within this chapter, an evaluation was conducted on the performance of the boiler steel substrate "ASTM-SA210- Gr A-1 (Gr A-1)" both uncoated and coated with AL, AL13TI, and AL40TI via flame spray thermal process. The assessment involved subjecting the sample to various heating conditions, including heating in the presence of air and heating in an aggressive environment consisting of molten salt Na_2SO_4-60%V_2O_5 at 900˚C under cyclic conditions. The examination of the surface topography and analysis of the weight change of the samples were conducted using thermogravimetric data. Following cyclic heating, the final products were analyzed by means of SEM, EDAX, and XRD.

The findings that were acquired are elaborated upon in this segment.

4.1 FINDINGS

4.1.1 Microstructure and Chemical Composition of Substrate Steel

Table 4.1 details the chemical composition of this boiler steel.

Table 4.1 Chemical composition of ASTM-SA210 grade A1

Element	**C**	**Si**	**Mn**	**S**	**P**	**Mo**	**Cr**	**Fe**
Wt.%	0.27	0.1	0.93	0.058	0.048	-	-	Balance

4.1.2 Descriptive Features of Powders

As a coating material, powdered AL, AL13TI, and AL40TI alloys produced by H.C. Starck of Germany and available for commercial purchase were chosen. The granules were supplied by Shree Sai Metal Coating, located in Noida, India. In order to further validate the average particle size and composition of the coating granules, SEM/EDAX and XRD analyses were performed (Mahesh et al., 2008). As shown in Fig.4.1 (a), the AL powder has an angular morphology and an average particle size of 40–50µm.

The EDS that is in correspondence with the SEM [Fig.4.1(a)] is illustrated in Fig. 4.1 (b). Figure 1 illustrates the XRD spectrum of aluminum oxide particles. 4.2. The peaks corresponding to the α-Al_2O_3 have been found in the XRD pattern of the powder. The peaks observed in this XRD reflector are associated with the JCPDS reference code 00-001-1243, which also represents the alumina peaks (Bai et al., 2004).

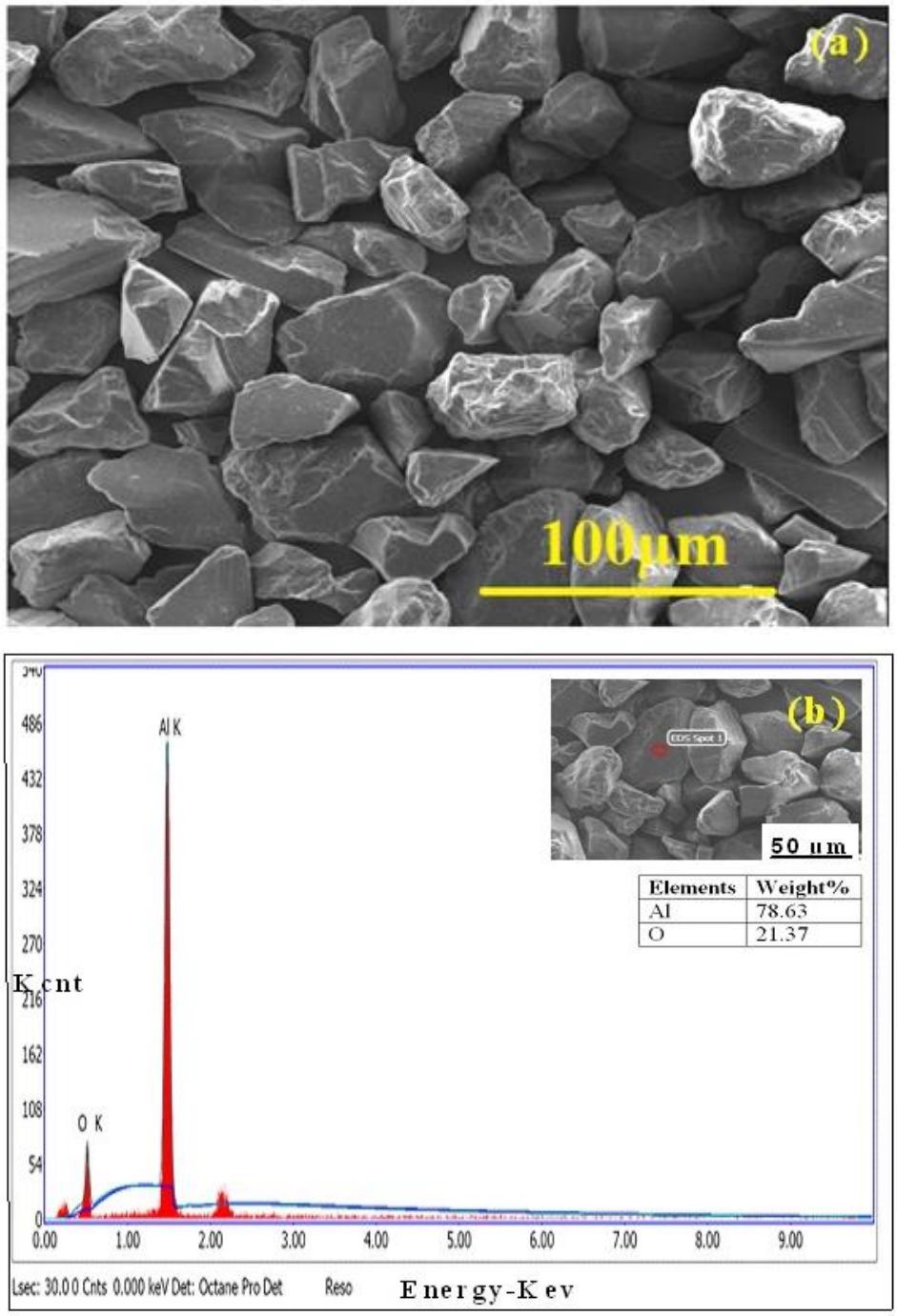

Fig.4.1 (a): An electron micrograph of AL powder; (b): AL powder's EDS spectrum.

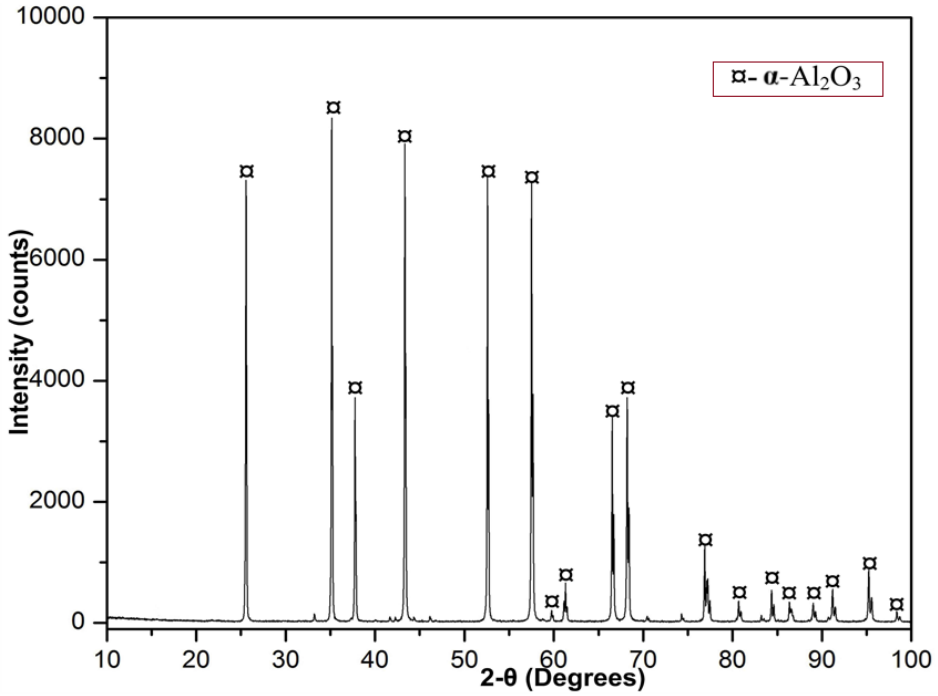

Fig. 4.2 The XRD pattern of AL powder

The irregular morphology of the particles of Al and Ti is evident from the figure. 4.3 (a). The EDAX evaluation of the coating powder is illustrated in Figure. 4.3 (b). The presence of Al, Ti, and O is confirmed by the analysis; the element with the highest peak is Al. The EDAX analysis was corroborated by XRD, as illustrated in Figure. 4.4. The EDAX analysis reveals that the material exhibits an even distribution of Al and Ti (Harsha et al., 2008; Sidhu et al., 2005; Zafar and Sharma, 2017). As illustrated in the figure, the principal phases identified by XRD analysis of the coating powder are AL and TI.

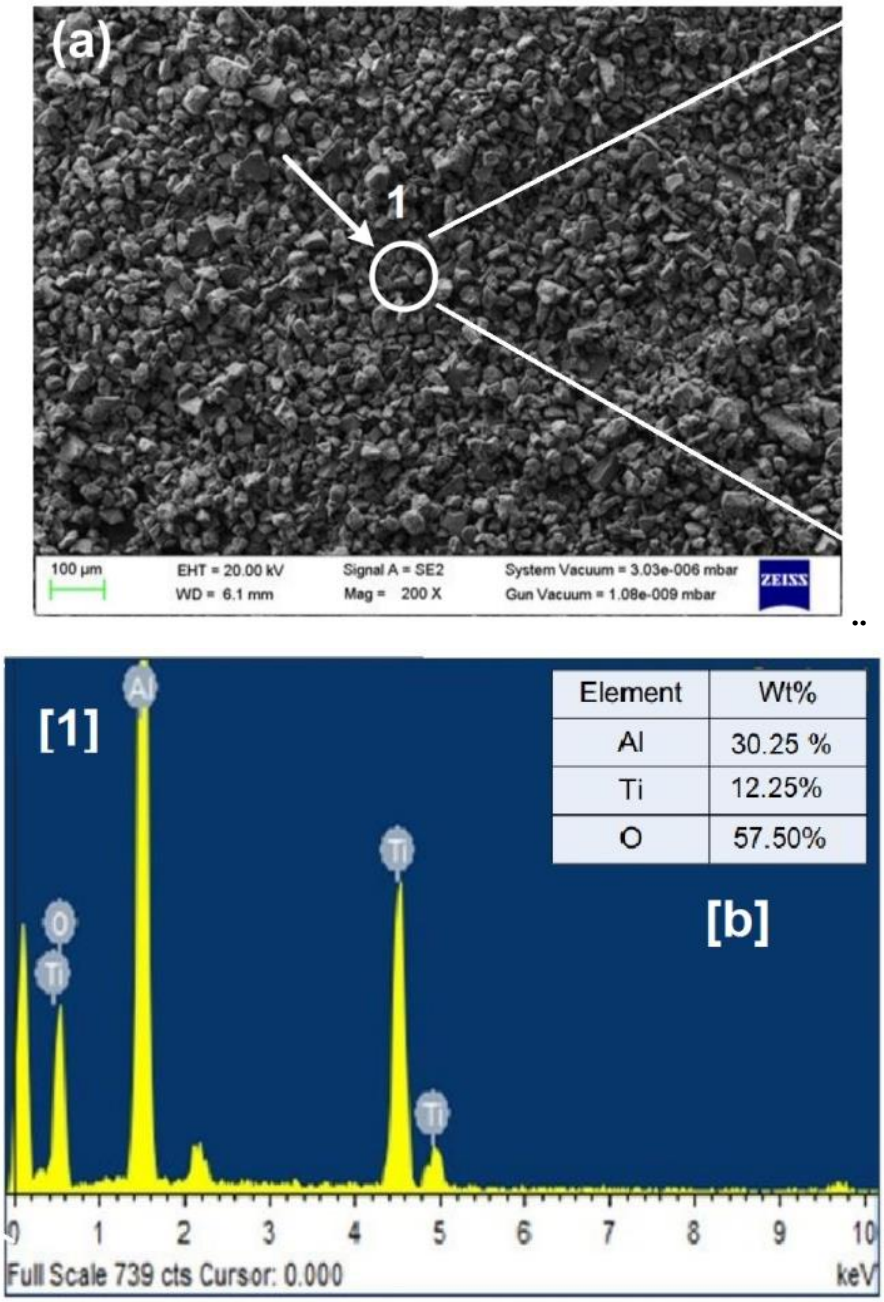

Fig.4.3 (a) SEM micrograph of AL13TI powder and (b) the EDS spectrum of AL13TI powder.

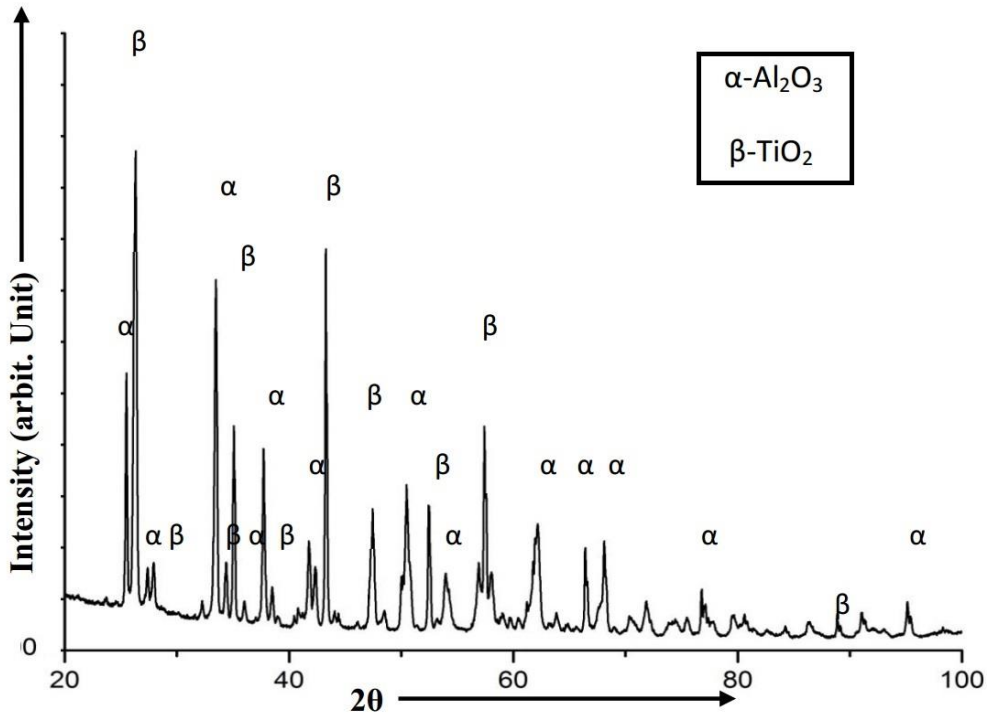

Fig.4.4 The XRD pattern of AL13TI material

The AL40TI powder exhibited irregularly shaped particles of Ti and Al, as depicted in Fig. 4.5 (a) & (b). The EDAX evaluation of the coating powder is illustrated in Figure. 4.5 (c). The presence of Al, Ti, and O is confirmed by the analysis; the element with the highest peak is Al (Kaur et al., 2012; Somasundaram et al., 2015; Bhatia et al., 2015). The EDAX analysis was corroborated by XRD, as illustrated in Figure. 4.6. The EDAX analysis reveals that the material exhibits an even distribution of Al and Ti (Somasundaram et al., 2016; Mangla et al., 2017; Cunha et al., 2017). As illustrated in above fig.4.4, the principal phases identified by XRD analysis of the coating powder are Al_2O_3 and TiO_2.

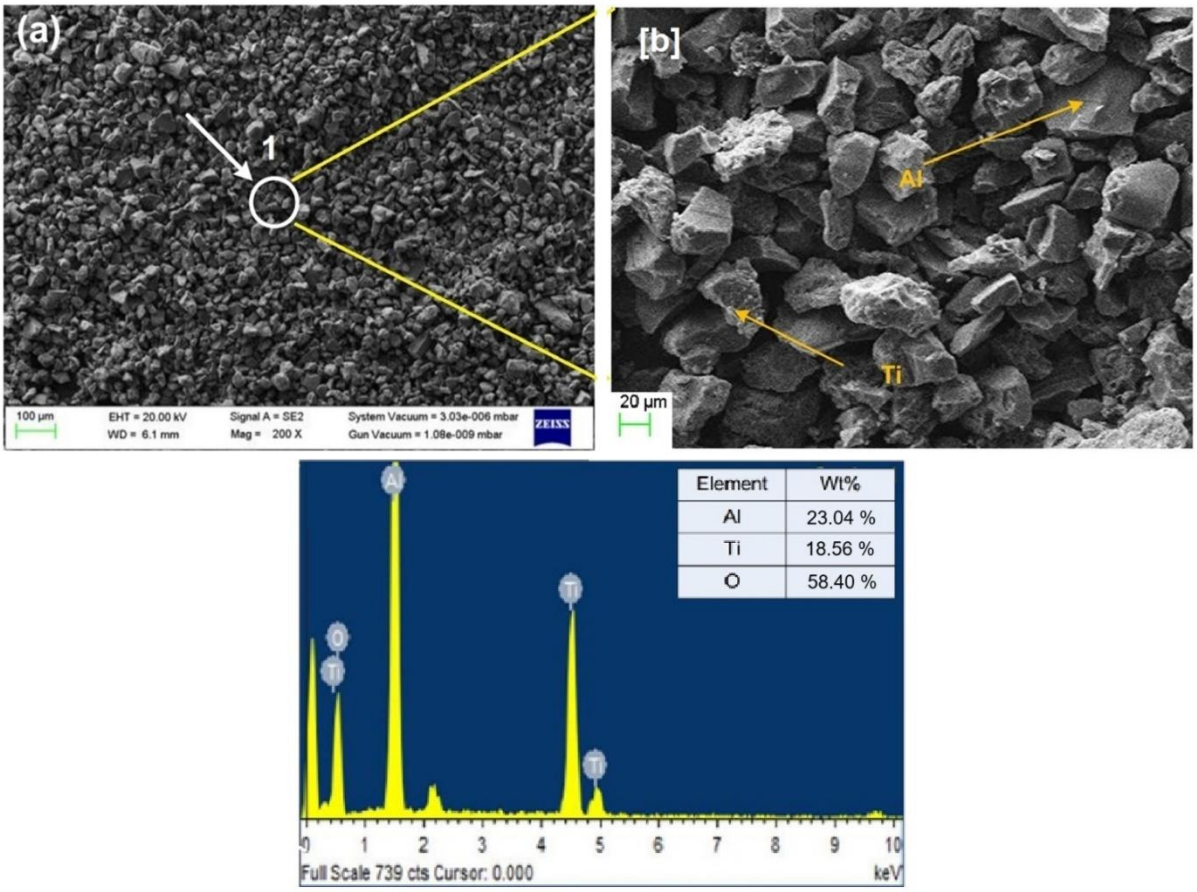

Fig.4.5 (a&b) SEM micrograph of AL40TI powder and, (c) EDS of powder.

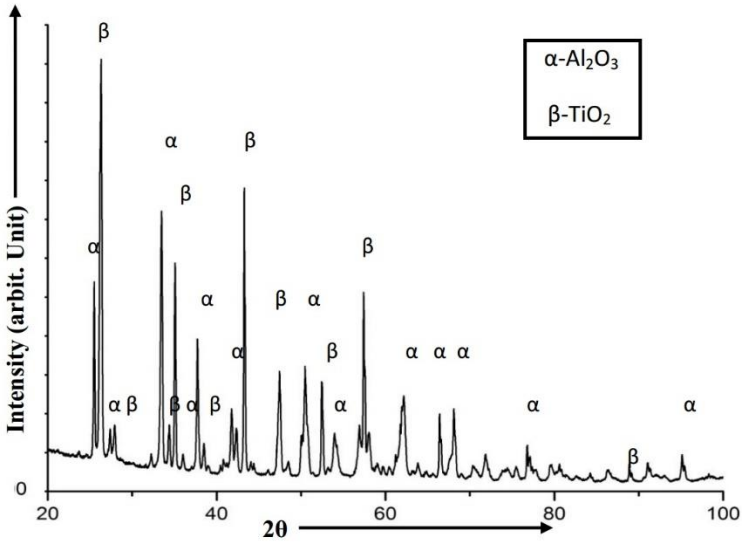

Fig.4.6 XRD pattern of AL40TI powder.

4.1.3 Details of the Coatings

As shown in Fig.4.7 (a), the SEM image reveals the formation of a splat-by-splat lamellar structure in each coating, with partially melted regions and un-melted particulates (Fig.4.7 (b)) in the ceramic coating (Kumar et al., 2018; Reddy et al., 2019). As compatible, the coating layer is connected to the substratum material.

The EDS pattern of the AL coating corresponding to point 1 as illustrated in 4.7 (c). An evident observation is the substantial abundance of Al and O within the as-sprayed coating. The anisotropic mechanical properties of flame-sprayed coatings are a result of the droplet structure and directional solidification, which supports the findings of AL (Houdková et al., 2018; Manikandan, 2018; Sreenivasulu and Manikandan, 2018; Česánek et al., 2018).

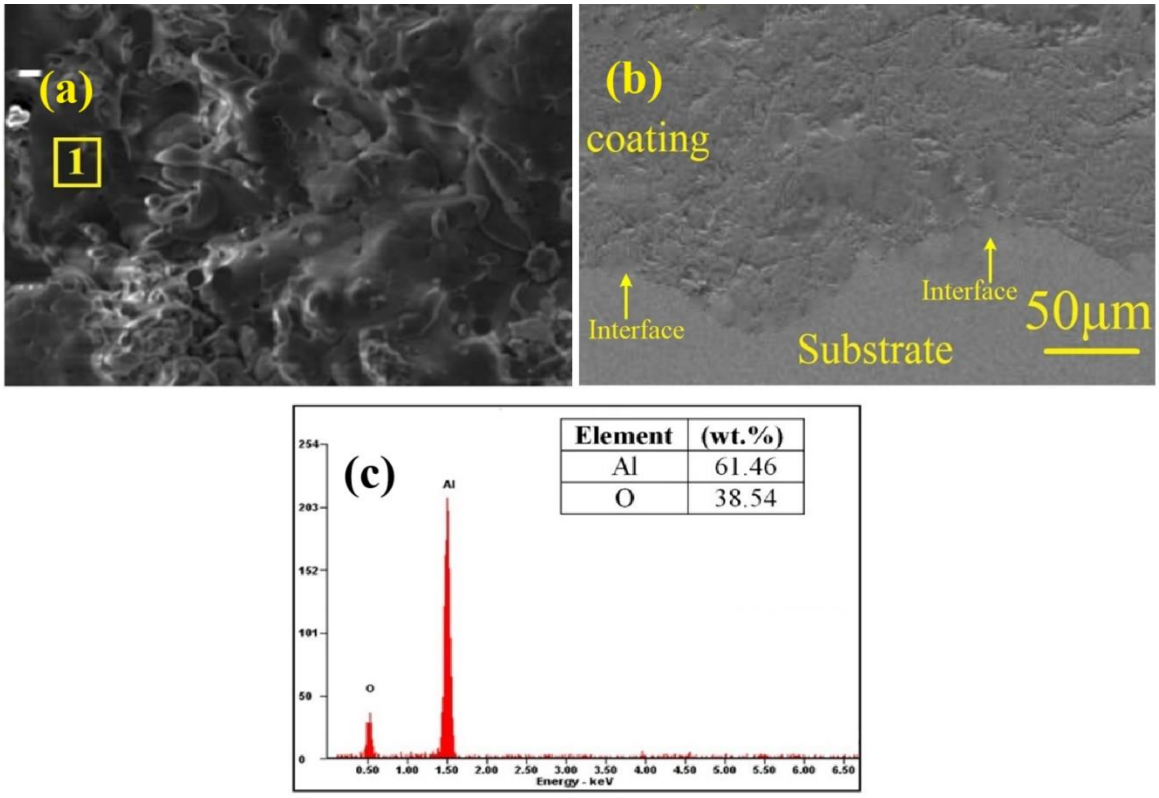

Fig.4.7 (a) Surface morphology of Al_2O_3 coating, and (b) Cross-section OF Al_2O_3 coating and, (c)EDS spectrum.

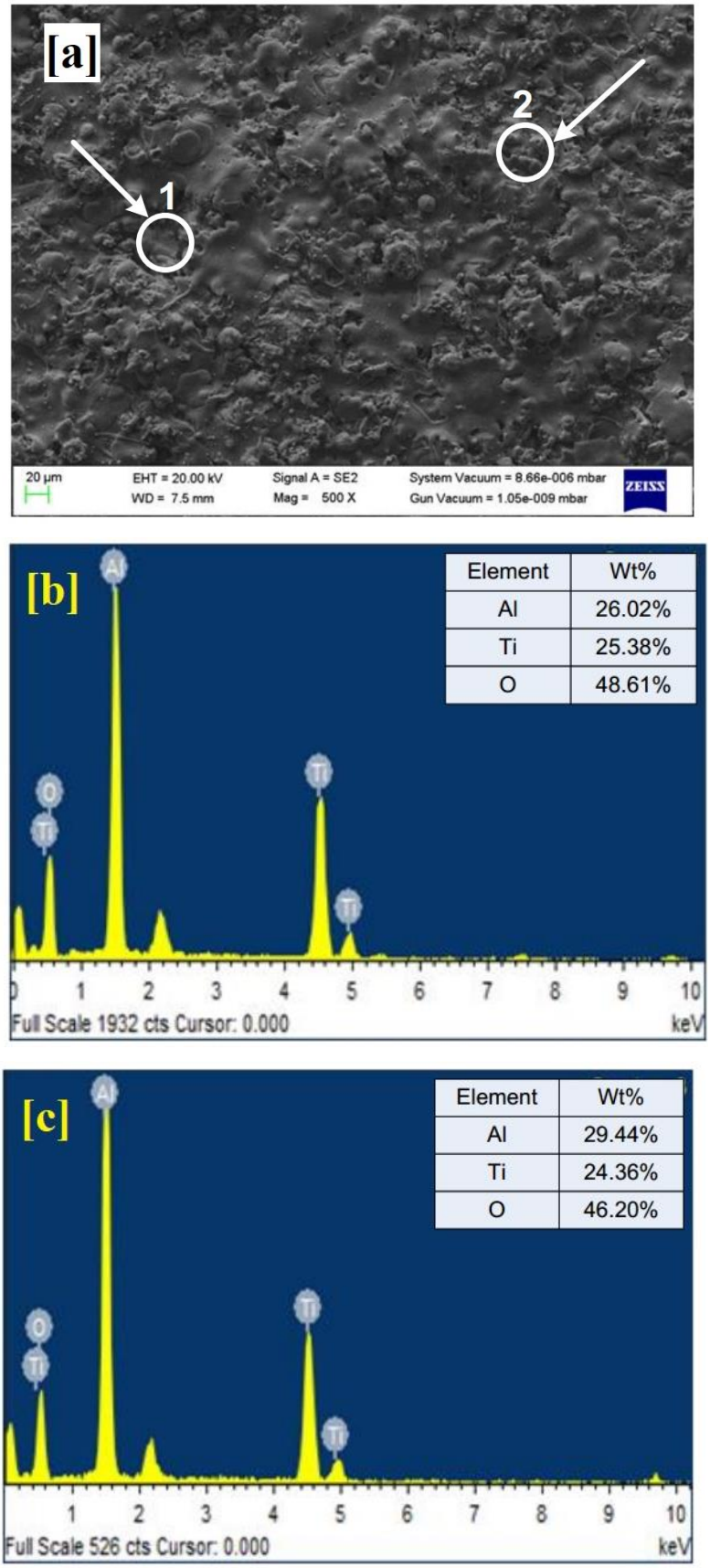

Fig.4.8 (a) The surface morphology of the AL13TI coating; (b) the EDS associated with point 1; and (c) the EDS associated with point 2.

The micrograph depicts a dense and uniform coating, as illustrated in Figure 4.8 (a). Dark spots, as well as globules composed of molten and unmolten powder particles, indicate that the coating is porous (Price et al., 1992; Chatha et al., 2016; Somasundaram et al., 2016). The presence of Al and Ti as the principal elements is confirmed by EDAX analysis, as illustrated in Figure 4.8 (b) and (c).

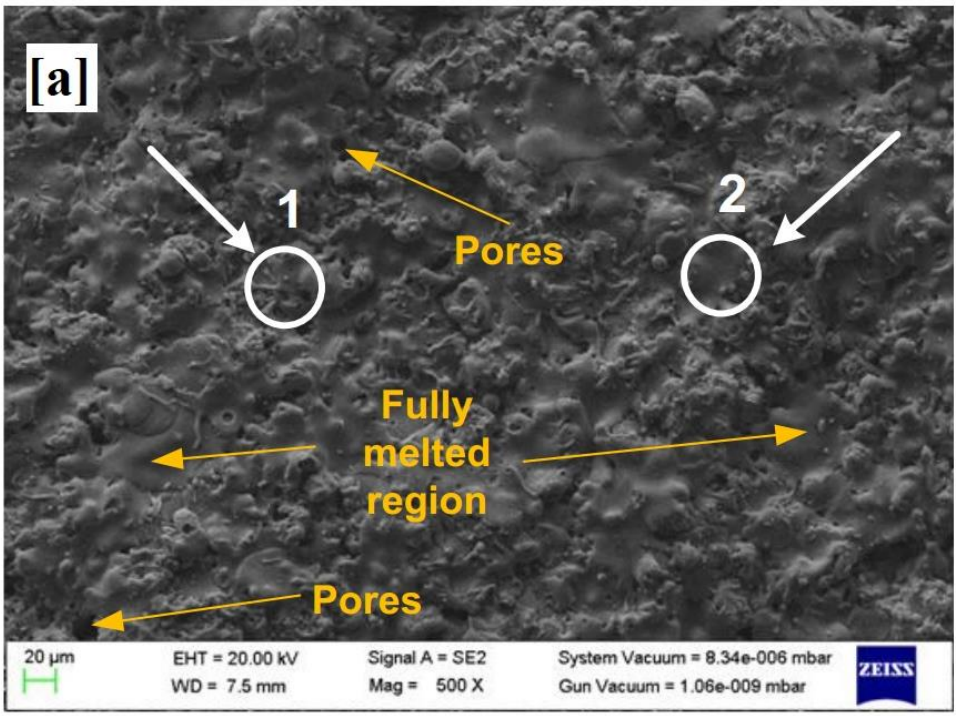

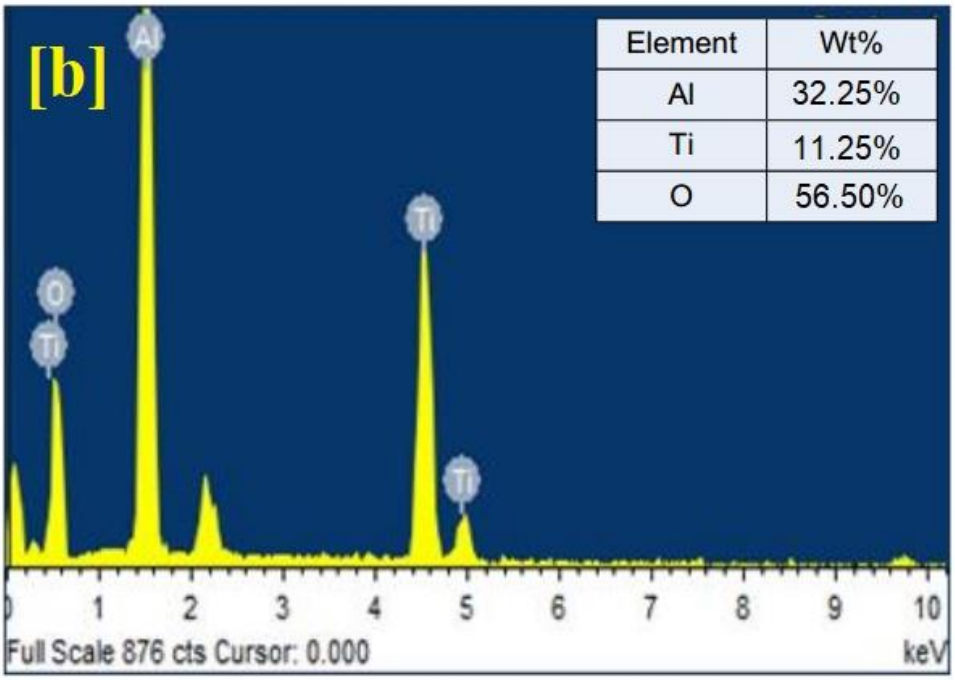

Cont'd next page..

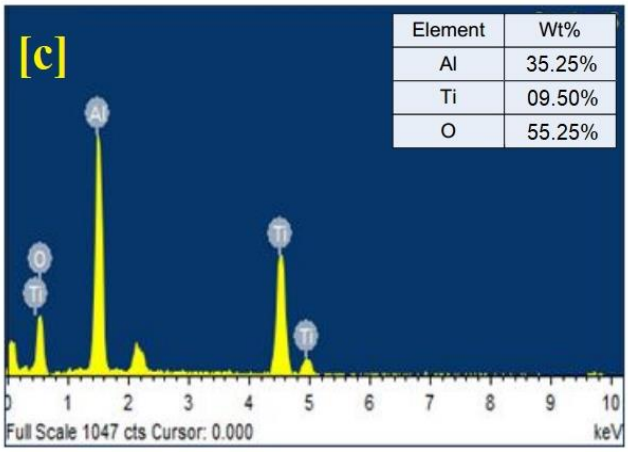

Fig.4.9. (a) Surface morphology of the AL40TI coating; (b) EDS associated with point 1; and (c) EDS associated with point 2

As shown in Fig.4.9 (a), the micrograph of the AL40TI coating reveals a dense and uniform coating. Dark spots, as well as globules composed of molten and unmolten powder particles, indicate that the coating is porous (Mangla et al., 2017; Cunha et al., 2017). EDAX analysis verifies that Al and Ti are the predominant elements in Fig. (b) and (c) of 4.9.

Consider the figure below. Respective XRD patterns of AL, AL13TI, and AL40TI coatings are shown in 4.10 (a), (b), and (c).

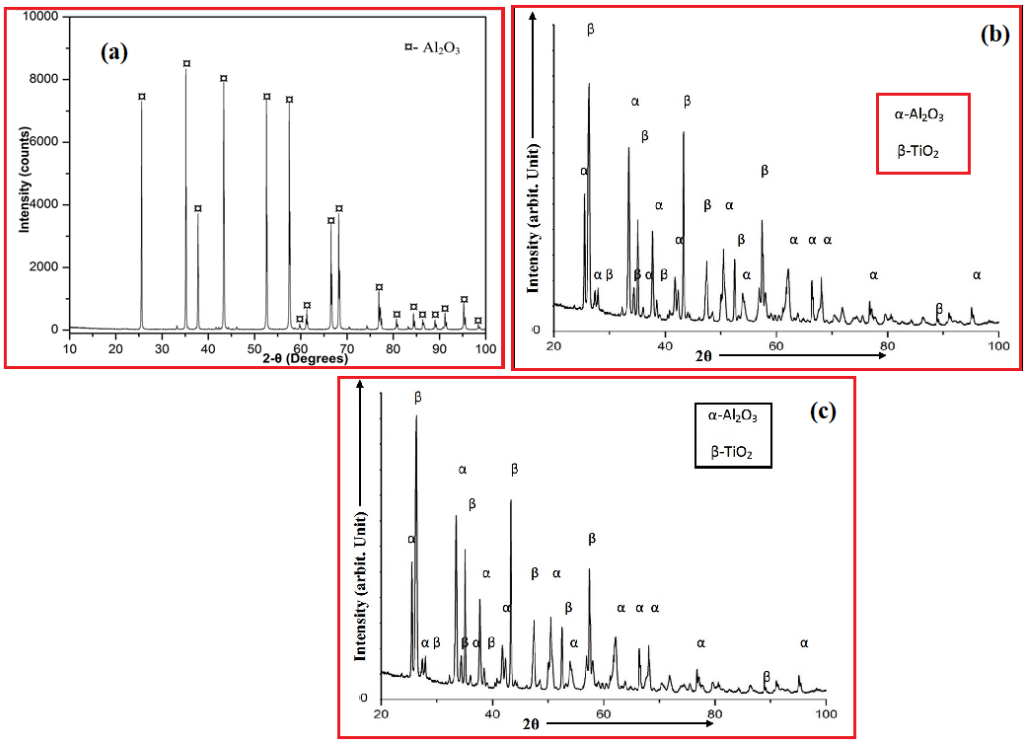

Fig.4.10 The XRD patterns of AL coating (a), AL13TI coating (b), and AL40TI coating (c) is shown respectively

The cross-sectional SEM images of AL coating, AL13TI coating, and AL40TI coating are illustrated in Figure. 4.11. It has been demonstrated that the coatings adhere well to the surface (Praveen and Arjunan, 2019). The figure illustrates three distinct zones: the substrate region, the coating region, and the epoxy region (Brar et al., 2017). Additionally, the coating exhibits the characteristic spatter formation that traverses its cross-section. The aforementioned are the customary attributes of thermally applied coatings. The coatings are applied in a series of passes, with each pass being approximately equivalent in size to the average powder particulate size (He et al., 2001; Bai et al., 2004; Chatha et al., 2013; Chatha et al., 2012). Hence, the current study necessitated approximately six approaches to deposit the developed coatings, which spanned a distance of 200-300µm. Additionally, the EDS was performed on the coating region, and this analysis illustrated the elements present in the different coatings (Gond et al., 2010; Goyal et al., 2018; Dent et al., 2000). Various coatings' EDS values are illustrated in Fig. 4.12. In contrast to the AL13TI and AL40TI coatings, which have Al, O, and Ti as elements, the AL coating has Al and O as elements. The coating with the highest Ti content was AL40TI, as illustrated in Fig. 4.12 (c).

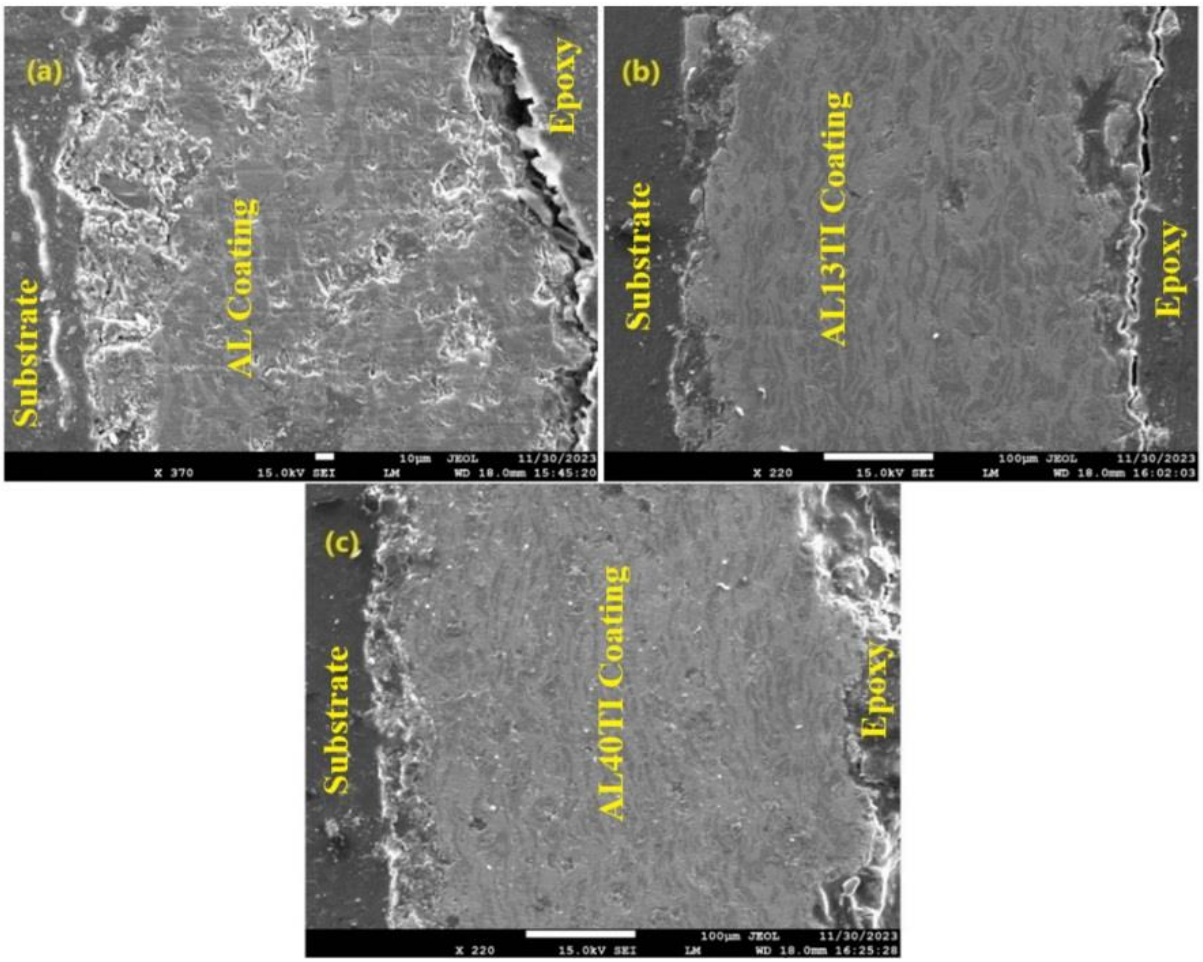

Fig.4.11 Cross-sectional SEM images of the following coatings: (a) AL, (b) AL13TI, and (c) AL40TI.

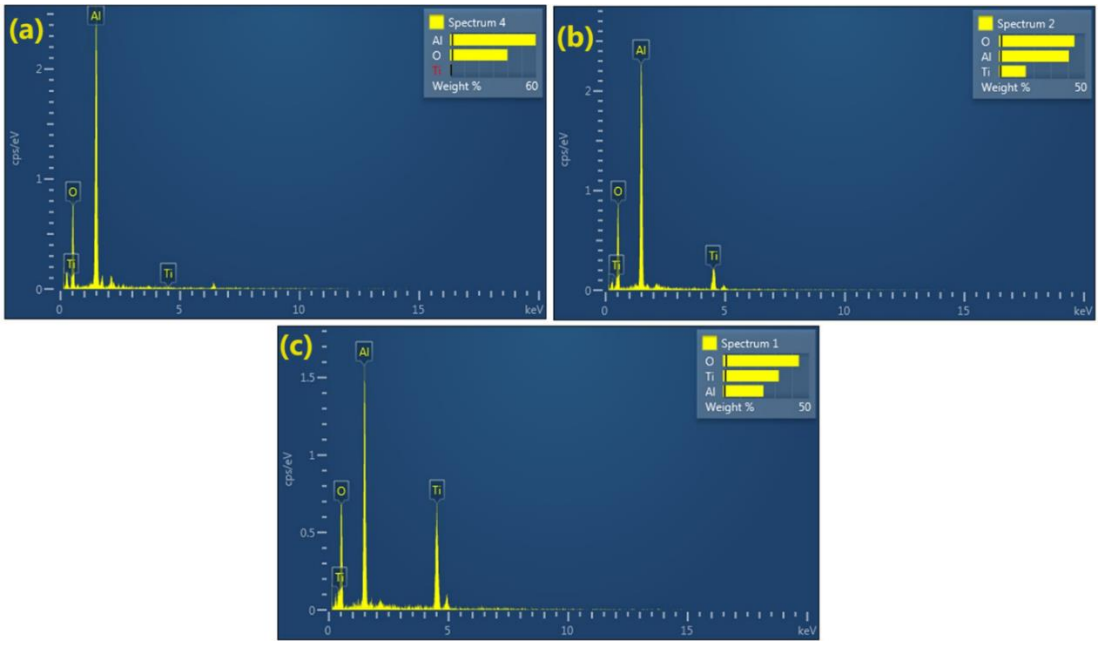

Fig.4.12. displays the EDS measurements of the coating regions of (a) AL, (b) AL13TI, and (c) AL40TI

4.1.4 Application of microwave hybrid heating for post-processing of flame-sprayed coating

The flame spray coatings in their as-sprayed state underwent post-processing utilizing an industrial microwave. Fig.3.5 depicts the schematic representation of the experimental configuration employed to process coatings via microwave exposure. As a result of their shallow epidermis depth, the as-sprayed deposits reflect microwave radiation at room temperature (Fryburg et al., 1984; Goyala et al., 2016; Heath et al., 1997). In order to implement the tenets of MHH, a boron carbide (BC) susceptor manufactured by Enerzi Microwave Systems was utilized. The coatings undergo post-processing through the utilization of a microwave furnace, which is illustrated in Figure 3.6. A water chiller is incorporated into this apparatus to facilitate the chilling of the magnetron of the microwave. It is possible to utilize an inert gas cylinder, which is employed to establish an inert environment throughout the coating processing phase to prevent any reaction [oxidation] between the coating and the surrounding environment (Kumar et al., 2020; Kumar et al., 2018).

The scanning electron microscope (SEM) image of the AL coating after treatment is shown in Figure 4.13 (a), whereas Fig. The matching energy-dispersive X-ray spectroscopy (EDS) mapping is illustrated in 4.13 (b). The as-sprayed coating demonstrates a noticeable abundance of Al and O atoms, distributed uniformly. The scanning electron microscope (SEM) image provides insights into regions where melting has partially transpired, in addition to the presence of undamaged particles that remain on the surface. The micrograph demonstrates a uniform and condensed coating. The porosity of the coating is distinguished by the existence of dark regions and globules that comprise a combination of molten and unmolten powder particles.

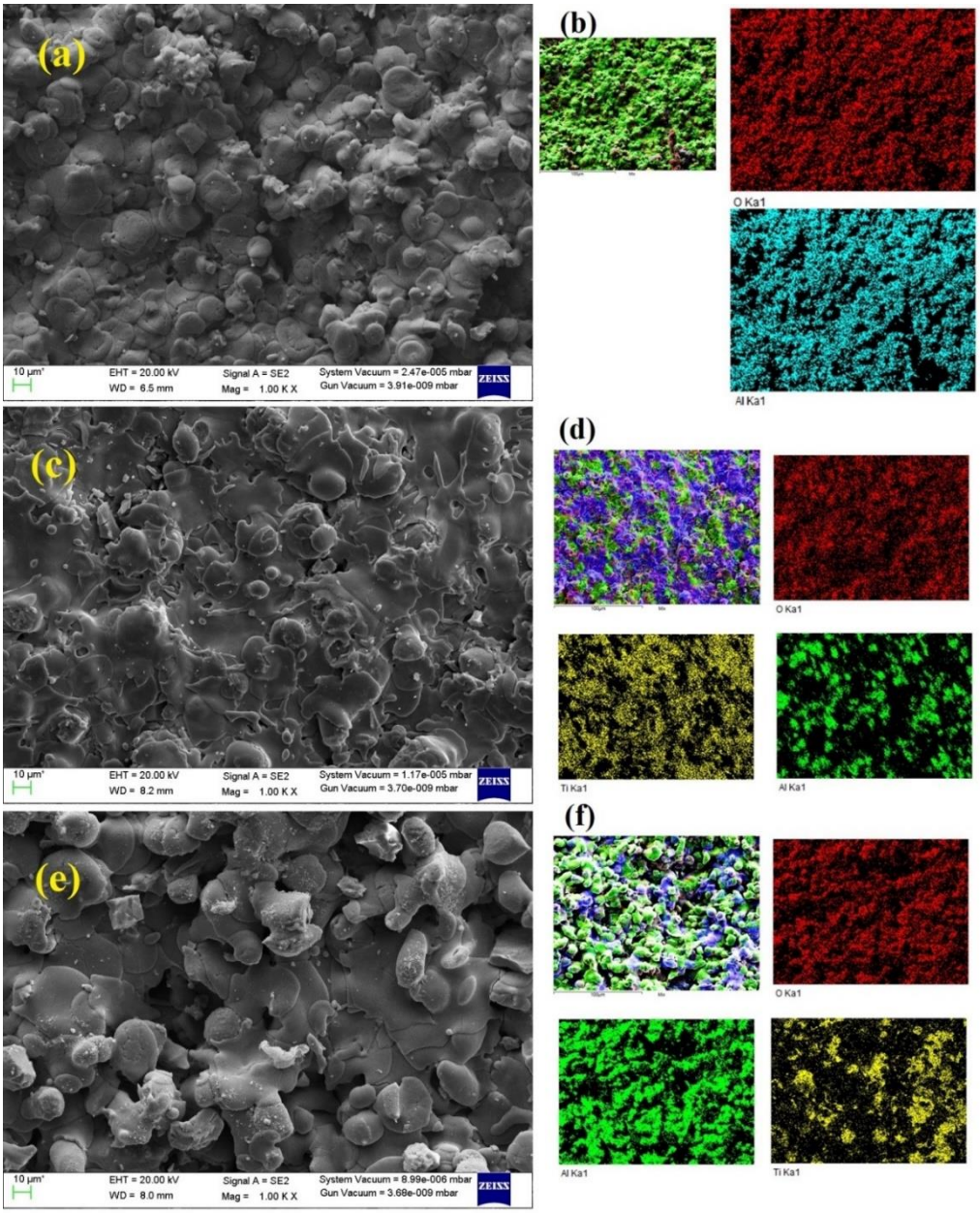

Fig.4.13 (a) Surface morphology of post-treated AL, (b) AL13TI, and (c) AL40TI coatings.

A micrograph of the post-treated AL13TI coating, depicted in Figure 4.13 (c), reveals that it is dense and uniform. As illustrated in Figure 4.13 (d), EDS mapping provides confirmation that the principal elements present on the coating's surface are Al, O, and Ti. One key differentiating factor between the AL and AL13TI is the presence or absence of a molten region. The incorporation of TiO_2 into AL13TI has resulted in a reduction in its melting point. Consequently, there has been a reduction in the porosity level of the coating. The AL40TI that has been post-treated demonstrates the same attributes as illustrated in Figure 4.13 (e), in addition to the EDS mapping that is

presented in Figure 4.13 (f). The deposited coatings underwent a porosity investigation, and the conclusive findings were calculated by averaging ten readings. The XRD patterns of the different coatings are illustrated in Figure 4.14, where the accentuated peaks in comparison to the flame-sprayed coatings are evident.

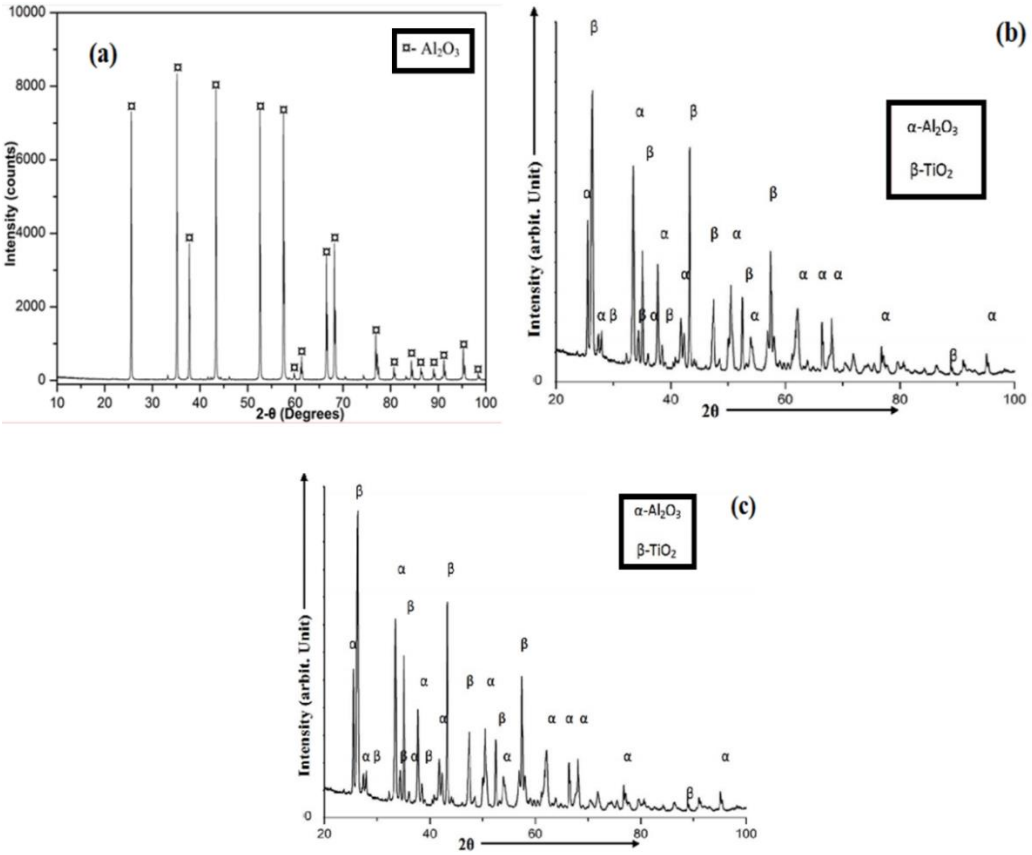

Fig.4.14 (a) XRD patterns of PT-AL coatings; (b) PT-AL13TI; and (c) PT-AL40TI.

A cross-sectional scanning electron micrograph (SEM) of the PT-AL, PT-AL13TI, and PT-AL40TI coatings is illustrated in Figure 4.15. Three distinct zones are depicted in the figure: the substrate region, the coating region, and the epoxy region. In addition, the coating exhibits a discernible spatter formation that is evident throughout its cross-section. The cross-section has provided insight into the coating's refined structure. The coatings undergo healing as a result of the microwave refining. The process of microstructure healing entails the clogging of porosity sites that were created by flame sprinkling. Crack formation and open porosity zones occur due to the abrupt transition from high temperature to room temperature and the excessive heat generated during flame misting (Mangla et al., 2017; Nielsen et al.; Natesan, 1997). The aforementioned outcome can be attributed to the inadequate incubation

period of thermal sprinkling, which is necessary for microstructure refinement (Prakash et al., 2001). The subsequent attributes delineate coatings that are applied through the process of thermal sprinkling. The application of the coatings consists of a sequential process involving the spraying of multiple layers. Every successive layer is applied in a manner that precisely corresponds to the mean size of the powder particulates (Mahesh et al., 2008; Rapp and Zhang, 1994). The thickness of the coatings produced in this investigation ranged from 200 to 300 µm. In order to accomplish this, around six passes were necessary.

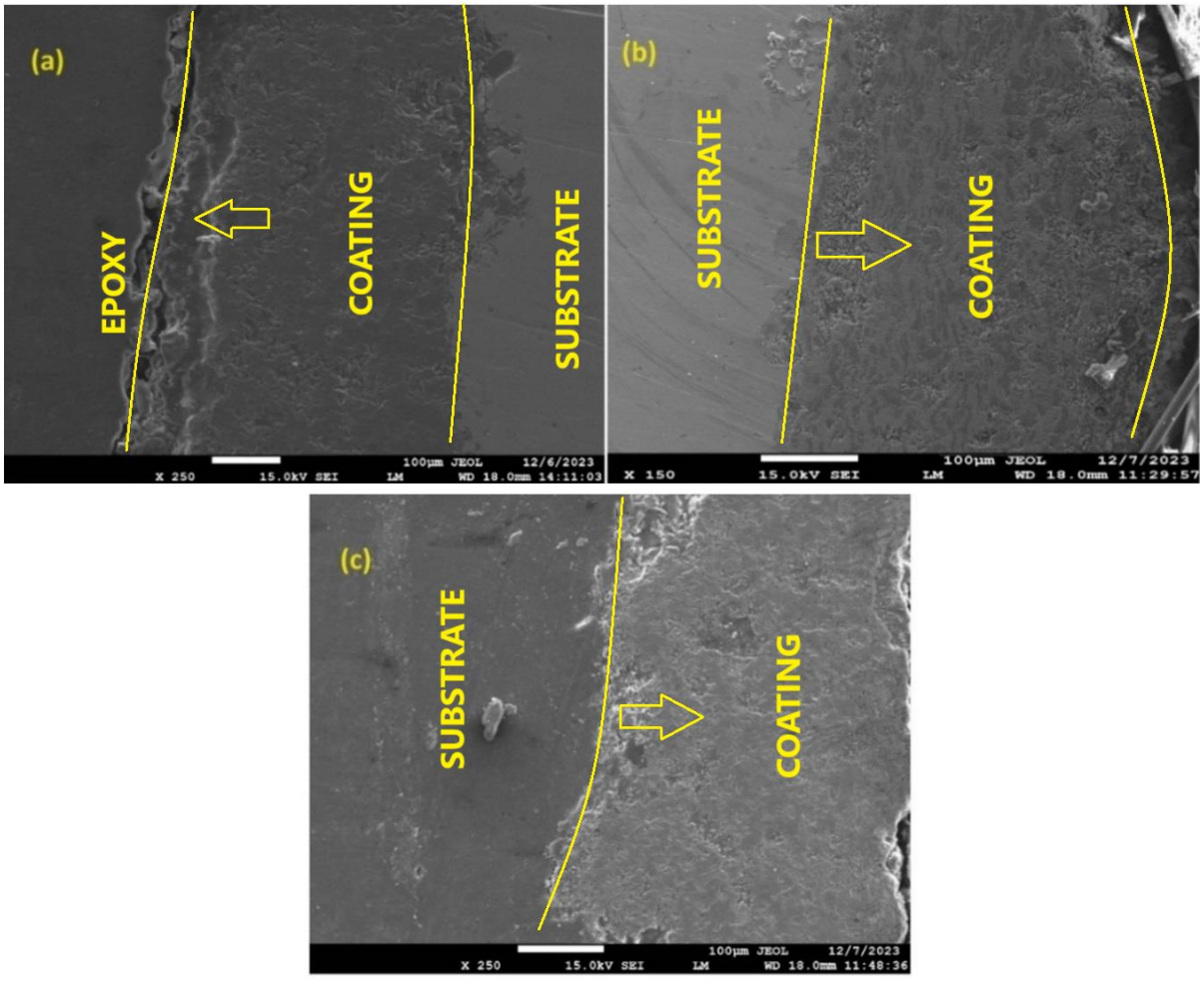

Fig.4.15 The SEM of Cross-sectional of (a) AL (b) AL13TI and (c) AL40TI coatings for post-treated samples.

Due to the compacting effect of incoming splats strikes, the previously deposited splats are typically compressed. The top surface of the Al_2O_3 coatings had the highest porosity and a microstructure that was not uniform. Meanwhile, the microstructure observed in the microwave post-processing reveals a dense and uniform composition

throughout the cross-section of the coatings, as depicted in the cross-sectioned figures. When exposed to microwaves, the coatings interact with the radiation, resulting in the melting of splats at high temperatures. This process leads to the healing of pores. At high temperatures, the splats undergo melting and effectively conceal the surface imperfections found in the as-sprayed coatings. The slight change in peaks suggests that there is lattice straining occurring in the post-processed coatings, resulting in the densification of the porous as-sprayed deposits.

Microwave post processing helps decrease the porosity level of thermal spray coatings by employing various mechanisms. It improves the microhardness, reduces porosity, and enhances the microstructure through changes induced by irradiation. Through the process, the coatings are created with microwave-fused properties, showcasing a strong bond, a uniform structure, and minimal porosity when compared to standard coatings. Microstructural changes lead to improved material properties, including a reduction in porosity and an enhancement in microhardness of the irradiated coatings.

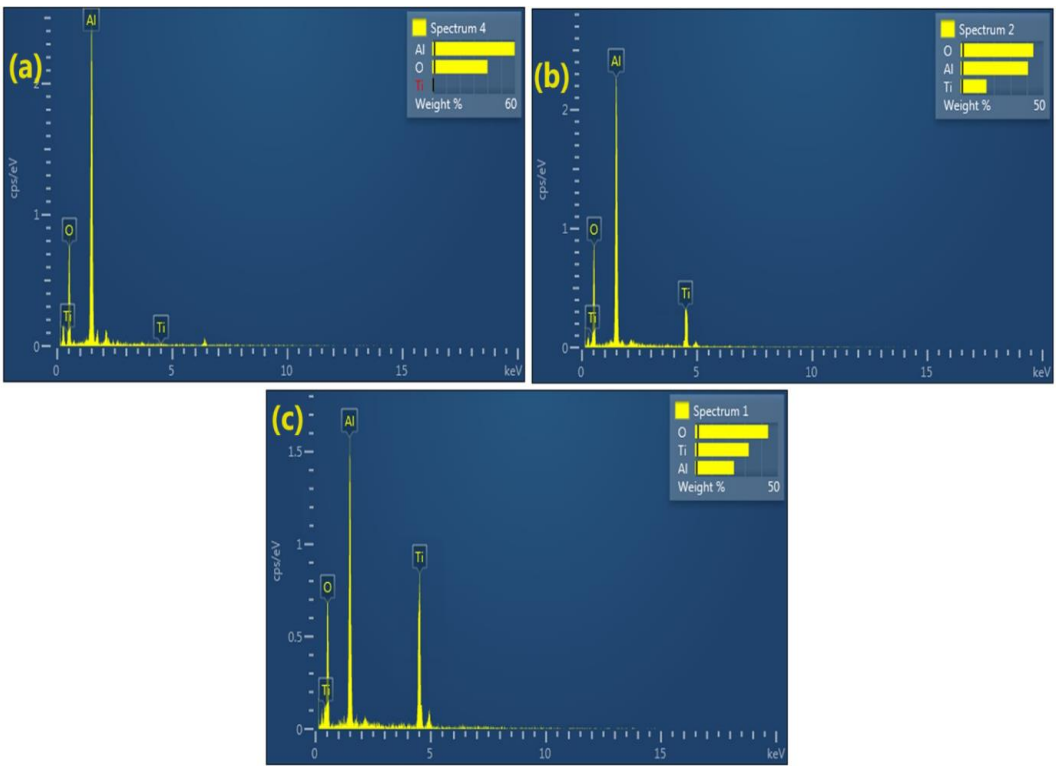

Fig.4.16 EDS analysis of coatings that had been post-treated is represented with (a) AL, (b) AL13TI, and (c) AL40TI.

Furthermore, an EDS analysis was conducted on the coating region, yielding valuable information regarding the elements present in the various coatings. The EDS values corresponding to various coatings are depicted in Figure 4.16. Conversely, the AL coating has demonstrated the presence of Al and O in isolation as separate elements, whereas the AL13TI and AL40TI coatings have exhibited a diverse array of elements, which includes Al, O, and Ti. According to the findings presented in Figure 4.16 (c), the AL40TI coating contained the greatest amount of titanium.

Table 4.2 displays the porosity and microhardness measurements of the coatings in their as-sprayed and post-treated states. It was determined that AL coatings had the maximum porosity levels of all developed coatings, at 2.5%. In contrast, the AL40TI coating maintained a minimum porosity level of 1.5%, whereas the AL13TI coating displayed an approximate porosity level of 2.1%. The results of the microhardness analysis indicate that the AL coating has a microhardness value of 995 HV, whereas the AL13TI and AL40TI coatings have respective microhardness values of 790 HV and 650 HV. A reduction in the hardness of these coatings has been observed as a consequence of the augmented TiO_2 content. Following microwave post-treatment, the porosity values of the AL, AL13TI, and AL40TI coatings were determined to be 2.1%, 1.7%, and 1.1%, respectively. The rapid and uniform heating provided by microwave hybrid heating leads to enhanced sintering of the sprayed coatings. This method promotes diffusion and densification at the particle boundaries, effectively reducing voids and increasing the coating's density. The microwave energy penetrates deep into the material, ensuring consistent temperature distribution, which aids in closing pores and minimizing cracks that may have formed during the flame spraying process. As a result, microwave hybrid heating decreases the porosity content, enhancing the mechanical properties and wear resistance of the coatings. Microwave absorption by the ceramic materials increases internal heat generation, causing localized melting and sintering. Densification occurs due to grain boundary diffusion, filling the voids left during the initial spraying. Rapid heating and cooling minimize grain growth, improving the microstructure and reducing porosity.

On the contrary, the microhardness of the coatings that underwent treatment exhibited an upward trend across all generated coatings. This includes AL, AL13TI, and AL40TI coatings, which possess microhardness values of 1110 HV, 825 HV, and 720 HV, respectively, as illustrated in Table 4.2.

Table 4.2 The values of Porosity and Microhardness for as-sprayed and post-treated coatings

Coating Composition	Porosity (as-sprayed & Post Treated Coating) wt.%	Microhardness (as-sprayed) $HV_{0.2}$
AL	2.5	995
AL13TI	2.1	790
AL40TI	1.5	650
PT-AL	2.1	1110
PT-AL13TI	1.7	825
PT-AL40TI	1.1	720

4.2 SUMMARY

This chapter provides a comprehensive analysis of the behavior of a critical furnace steel substrate, ASTM-SA210-Gr A-1 (Gr A-1), across a range of conditions. Following an initial assessment of the substrate in its uncoated state, it is subsequently evaluated following the application of AL, AL13TI, and AL40TI coatings using the flame spray thermal process. The chemical composition of the ASTM-SA210 grade A1 substrate is detailed in the Results Section. The predominant elements are carbon, silicon, manganese, sulfur, phosphorus, and iron. Mintage amounts of molybdenum and chromium are also present. The data that has been provided serves as a fundamental component for the subsequent evaluations. Commercially available AL, AL13TI, and AL40TI alloys are analyzed so as to characterize the coating particulates. The analysis of these particles through the utilization of SEM/EDAX and XRD provides crucial insights into their composition and structure. Angular morphology and the mean particle size of AL powder are delineated. Analyses by EDAX and XRD similarly aid in the characterization of AL13TI and AL40TI powders, which comprise Al and Ti particles of irregular shape. Placing emphasis on achieving elemental uniformity in the granules forms the fundamental basis for subsequent evaluations of the coatings. Detailed SEM micrographs, EDS spectra, and XRD patterns are presented with annotations for each coating, namely AL, AL13TI, and AL40TI. The visual depictions facilitate a more nuanced understanding of the coating structures, thus confirming the presence of the elements Al, Ti, and O. As evidence of the coatings' compatibility with the substrate, their density, consistency, and distinct particulate formations are observed.

The utilization of Microwave Hybrid Heating (MHH) as a post-treatment method for the flame-sprayed coatings is a critical element of the investigation. By employing an industrial microwave furnace, a boron carbide (BC) susceptor is incorporated into this post-treatment. The experimental configuration utilized in this post-processing procedure is illustrated in the schematic diagram. The justification for employing MHH is explicated: the restricted skin depth of as-sprayed deposits at room temperature necessitates a method to circumvent this limitation. The profound impact of microwave exposure is effectively demonstrated by employing SEM images, EDS mapping, and XRD patterns to depict the results of the treatment process. The post-treatment coatings exhibit improved structural integrity, reduced porosity, and enhanced microhardness. The presence of Al, O, and Ti elements is confirmed by EDS mapping, which emphasizes the successful assimilation of these elements during the post-treatment stage.

The cross-sectional scanning electron microscopy (SEM) analysis provides a more thorough understanding of the coatings' structure through the identification of three distinct zones: the coating region, the substrate region, and the epoxy region. The detection of distinctive droplet formations throughout the cross-section serves as an indication of thermally deposited coatings. A comprehensive analysis is conducted on the complexities associated with coating recovery through microwave processing, focusing specifically on the void-filled areas that result from flame sprinkling. Post-treatment is required to refine the microstructure as a result of fissure formation and open porosity sites brought about by the excessive heat and rapid cooling that ensue after flame spraying. Comprehensive analyses are presented regarding the porosity and microhardness measurements of coatings in their as-sprayed and post-treated states. The impact of composition on the aforementioned properties is clearly observed in the AL coating, which exhibits significantly higher levels of microhardness and porosity when compared to the AL13TI and AL40TI coatings. There is evidence to suggest that the application of TiO_2 to coatings results in a decrease in hardness. Post-treatment with MHH results in a reduction in porosity and an increase in microhardness for all coatings, which signifies an enhancement in structural integrity.

CHAPTER 5
OXIDATION AND HOT COROSSION STUDIES

5.1 THE STUDY OF SAMPLES UNDER OXIDATION

An isothermal oxidation study encompassing 50 cycles was conducted at a temperature of 900 °C on both uncoated and coated samples within a silicon-carbide box furnace. The specimen is subjected to a 900°C tube furnace heating for one hour (Make: Carbolite Gero, RHF-1400), followed by a 20-minute cooling period at ambient temperature. Cyclical loading was applied to the examples in order to generate testing conditions that closely resembled real-life scenarios. This will aid in the practical resolution of the corrosion issue. The furnace was initially adjusted to 900°C with the assistance of a platinum-rhodium thermometer and a temperature gauge capable of indicating fluctuations of no more than 5°C (Sidhu and Prakash, 2006). The untreated samples were polished to a mirror finish using alumina paste and a wheel cloth prior to the oxidation investigation. Following this, the sample was desiccated to eliminate any remaining moisture after being cleansed with an ultrasonic cleaner. After that, the surface area of both the untreated and coated specimens was determined using an automated Vernier calliper. Following three measurements of each region, the mean value of those three readings was calculated. The specimen was initially placed in an Al_2O_3 canoe. To remove moisture, the vessels were heated to 1000 degrees Celsius for three to four hours. Following that, these vessels were inserted into the section of the 900°C furnace containing the samples (Singh et al., 2017). At 900°C, the samples were heated in the furnace for one hour. Following this, both the samples and the boat were removed and allowed to cool for twenty minutes at ambient temperature in the air. Following the cooling of the samples and the vessel, their combined mass was approximated utilizing a digital scale with a precision of 0.01mg. (Make: Kern, ABT 100-5 M, United States of America). Samples, whether exposed or covered, underwent 50 iterations of the identical procedure. For measuring the weight change, the scale that formed on the base when it became hot and plummeted into the boat was also utilized.

Simultaneously, after each cycle, the alteration in color, luster, oxide scale, and spallation tendency of both exposed and covered specimens were assessed.

An oxidation test was performed on both coated and uncoated samples at a temperature of 900°C using the tube furnace illustrated in Figure 5.1(a) for reference. In order to ensure uniformity and minimize reading error, coating was applied to all six facets of the substrate.

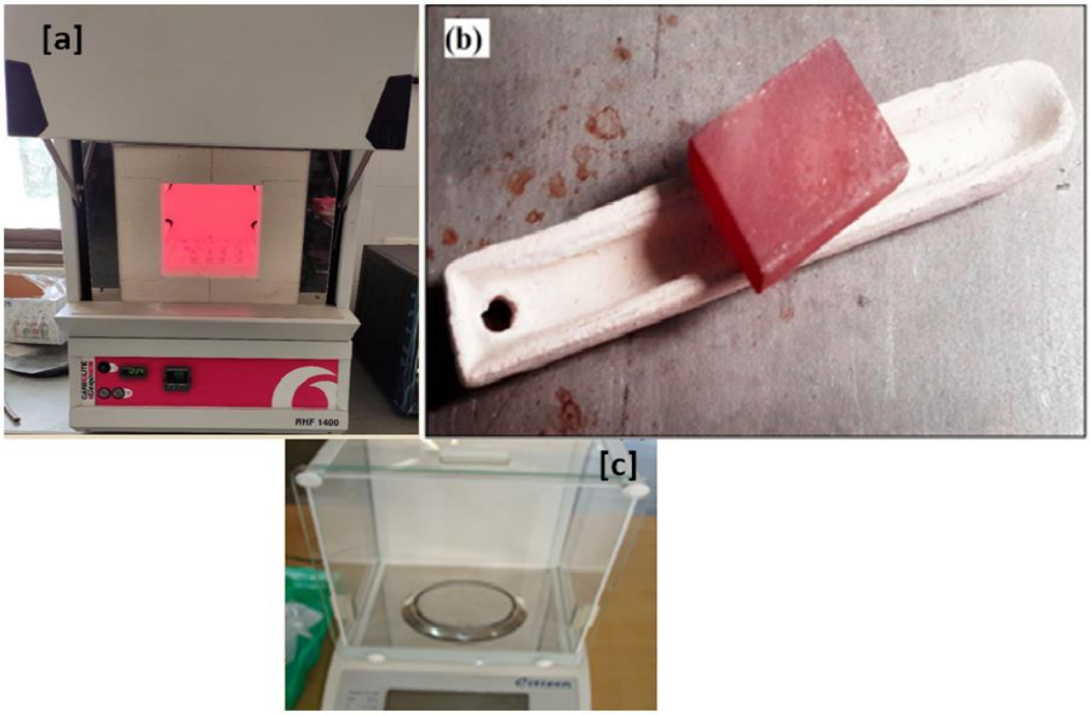

Fig.5.1 (a) A schematic of the tube furnace; (b) A sample of oxidized alumina in a boat; and (c) A weight balance.

By employing a high-temperature furnace, the oxidation behavior of both uncoated and coated specimens at elevated temperatures was determined. Fifty cycles comprised the duration of the investigations. Specimens were exposed to an isothermal temperature of 900°C for one hour during each cycle, after which they were cooled to room temperature in ambient air for twenty minutes. In order to determine the corrosion rate for both uncoated and coated specimens, a thermogravimetric study was performed using the parabolic rate constant of the corroded specimens. Various characterization methodologies were utilized to examine the coatings' properties prior to and following high-temperature oxidation

tests. The findings indicated that the weight gain was considerably diminished by the Al_2O_3-40%TiO_2 ceramic coating in comparison to the untreated substrates.

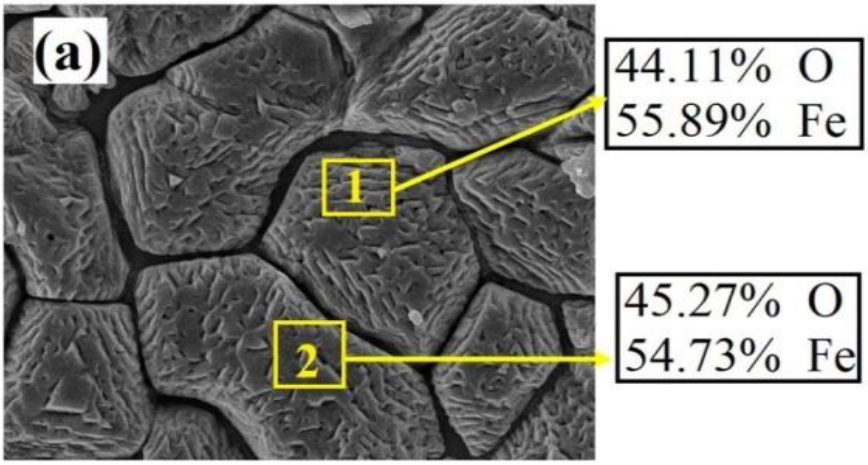

Fig.5.2 EDAX spectrum and SEM micrographs of oxidized: a) substrate uncoated.

Fig.5.2 illustrates the SEM/EDAX analysis of bare ASTM-SA210 GrA1 boiler steel specimens that underwent cyclic air oxidation investigations at 900ºC for a duration of 50 hours. The SEM analysis of the uncoated boiler steel demonstrates the presence of a granulated scale, and the EDAX examination verifies that this scale is composed entirely of Fe and O. This provides robust evidence in support of the potential formation of a feeble Fe_2O_3 phase, which is consistent with the results obtained from XRD analysis.

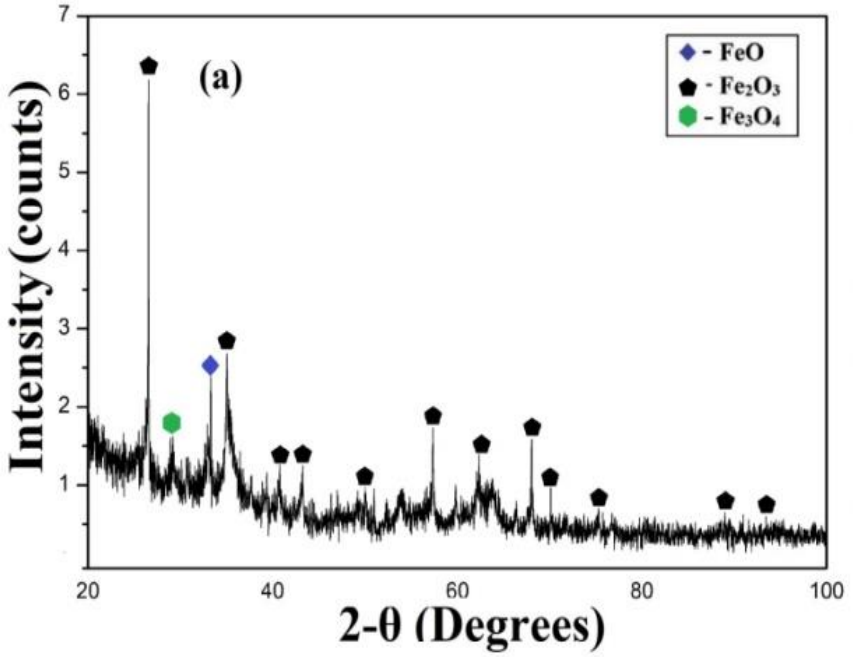

Fig.5.3 Analysis by XRD of the uncoated substrate.

Figure 5.3 displays the XRD analysis results for the oxidized boiler steel ASTM-SA210 GrA1. The XRD analysis of oxidized samples reveals that the dominant phase of the oxide scale observed on the surface of bare ASTM-SA210 GrA1 boiler steel is Fe_2O_3 (hematite). The oxidized scale XRD pattern of hematite (Fe_2O_3) formation in ASTM-SA210 GrA1 boiler steel indicates that Fe reacts with O_2, which is significant because Fe is the primary constituent of ASTM-SA210 GrA1 boiler steel.

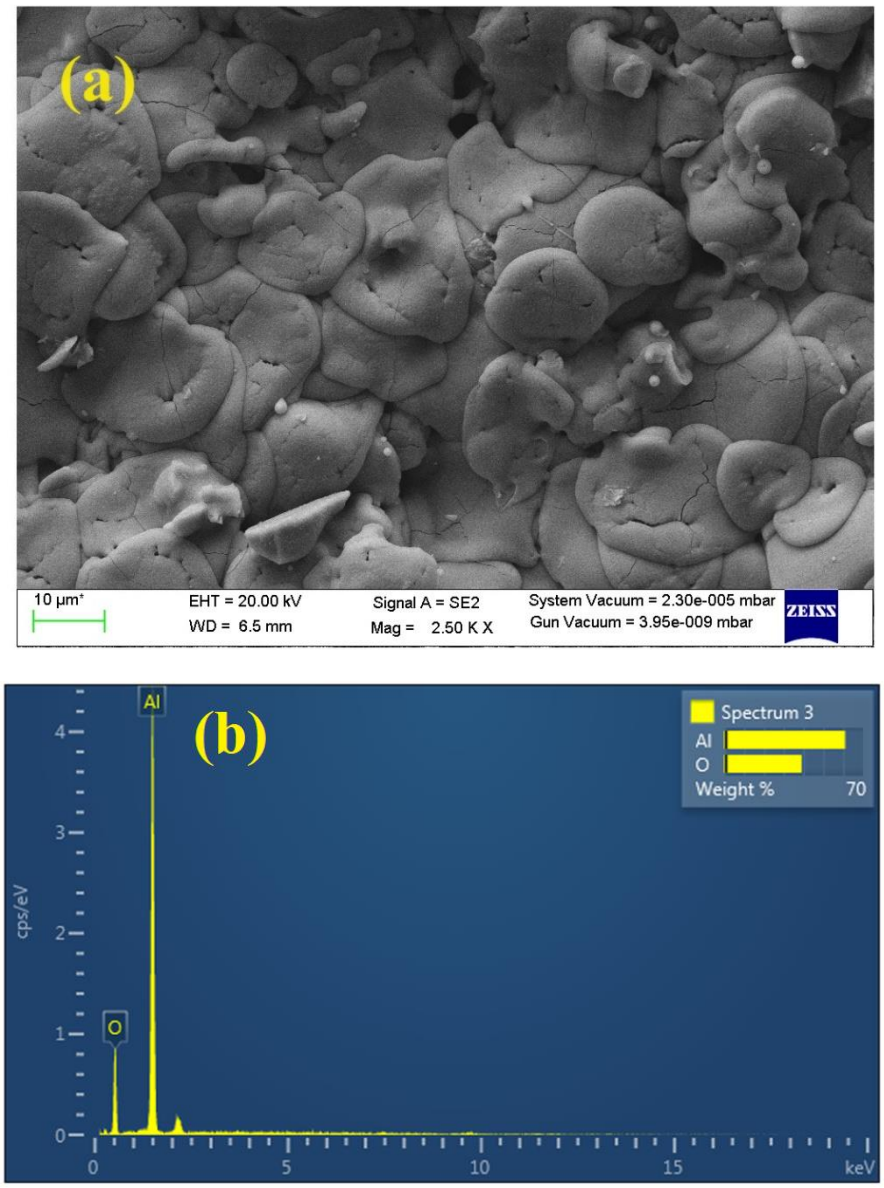

Fig.5.4 (a) The SEM micrograph of the oxidized sample, while (b) illustrates the EDS corresponding to the rectangle in 5.4 (a)

The oxidized surfaces of the coatings that were developed are illustrated in Figures 5.4, 5.5, and 5.6. The initial coating (Figure 5.4) exhibits a few unmelted particles on its surface; these were primarily powder particles that, due to the high melting point

of Al_2O_3 (2072°C), remained unmelted throughout the coating process. These particulates are a contributor to the surface's open porosity, which provides oxygen with access to the subsurface via open sites. The Al_2O_3 coating exhibited the greatest porosity of all coatings at 3.5%. As shown in Fig.5.5, the EDS mapping of the oxidized AL coating is displayed. The presence of Al and O on the surface provides surface resistance, which the XRD results presented in this study attribute to the matter (Stokes and Looney, 2001). The XRD patterns indicate the formation of Al_2O_3 phases, specifically θ-Alumina and α-calumina.

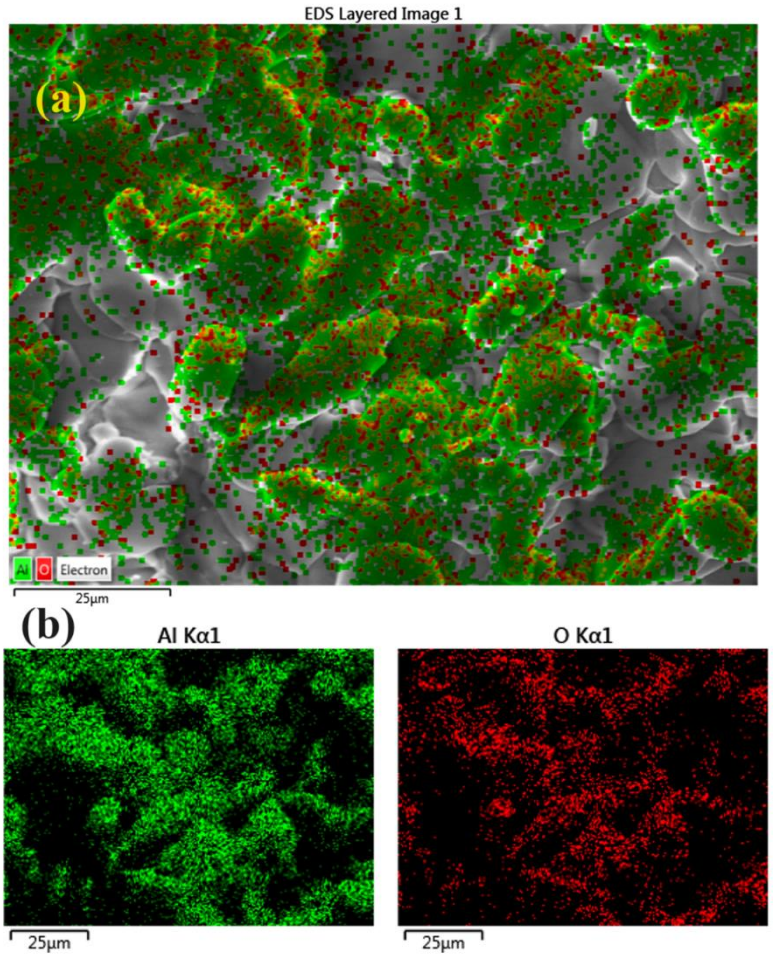

Fig.5.5 (a) SEM micrograph of oxidized AL coating sprayed with a flame; (b) EDS mapping of the aforementioned coating sprayed with a flame.

Fig.5.6 illustrates the XRD pattern of the oxidized AL coatings. The pattern illustrates the remarkable stability of α-alumina, which is a phase composed of aluminum oxide, even when subjected to elevated temperatures. This specific variant of alumina is the

predominant variety of alumina commonly seen in thermal spray coatings. The crystal exhibits a hexagonal configuration.

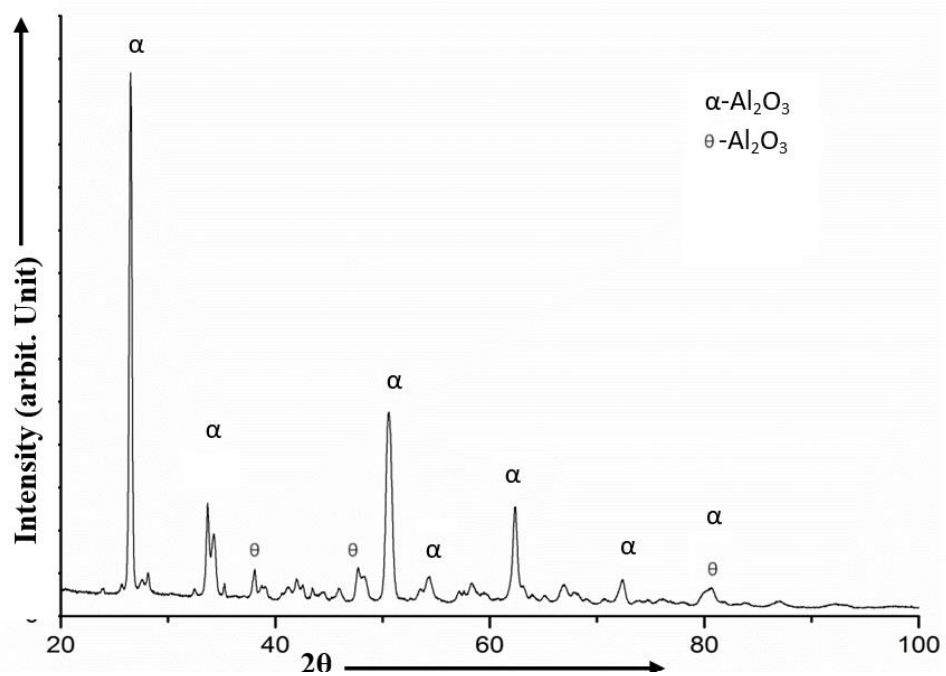

Fig.5.6. The XRD pattern of the oxidised AL coatings at 900ºC.

The θ-Alumina is a metastable type of alumina that can be synthesized by controlling temperature and pressure conditions. It has a unique crystal structure that is different from α-alumina. This specific phase of alumina is in a metastable state and can form under high temperature conditions. It has a unique crystal structure, unlike α-alumina and θ-alumina. In the flame spraying process, the formation of these phases depends on various factors such as the specific temperature, the speed of cooling, and the prevailing conditions. Understanding phase transformations is crucial for tailoring the coating to specific applications, since the resulting phase composition can significantly impact its characteristics and performance. The high temperature oxidation behaviour of the coated SA 210 steel substrate was visually examined after 50 cycles of heating at 900˚C. After 1st cycle the colour of the SA 210 steel changes from grayish-blue to yellowish white. Till 6th cycle no signs of formation of cracks have been observed. But after 7th cycle a crack in the coating was observed this is due to thermal shock while cooling. After 8th cycle the coating peeled off from the surface and fell down in the ceramic boat. This peeling off continued till the 50th cycle but the rate of formation of crack was very slow.

It has been observed that disintegration started after 8th cycle in case of coated SA

210 steel where as in uncoated steel it started from the 3rd cycle. This shows that coating has protected the material for a short period of time. Fig.5.7. shows the SEM micrograph of oxidized sample of AL coating and 5.7b represents the corresponding EDS. The flame spray process involves rapid heating and cooling of the coating material. The Al_2O_3 particles are heated to a molten or semi-molten state and then rapidly solidified upon impacting the substrate. This process can induce thermal stresses due to the significant temperature gradients, leading to the formation of cracks on the coating surface as shown in Fig.4.7. It is common for Al_2O_3 coatings to contain secondary oxide phases, such as spinels or alumina polymorphs (e.g., α-Al_2O_3), leads to the crack formation at the surface as shown in Fig. 5.7a.

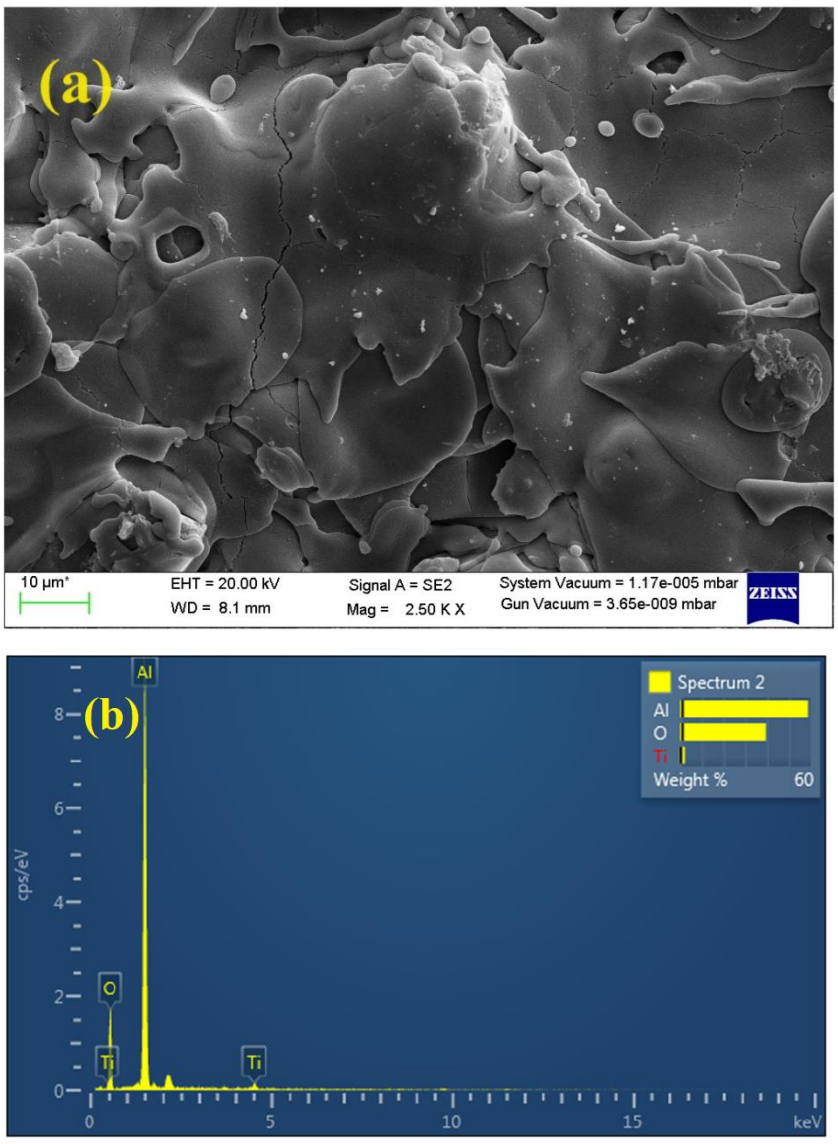

Fig.5.7. (a) SEM micrograph of oxidized sample of AL coating, (b) EDS corresponding to 5.7 (a).

Fig.5.8 presents the EDS mapping of the previously mentioned oxidized AL13TI coating. The presence of Al, O and Ti on the surface can be observed, indicating surface resistance. This observation aligns with the XRD data given in the current literature. The X-ray diffraction patterns indicate the presence of Al_2O_3, TiO_2 and $Al_2Ti_7O_{15}$ phases, and specifically α-alumina.

When TiO_2 is added to Al_2O_3 coatings, at elevated temperatures, a new phase can form between the two oxides: $Al_2Ti_7O_{15}$. This compound is one of several aluminum titanate phases that can emerge in these systems. The formation of $Al_2Ti_7O_{15}$ occurs due to the interaction between aluminum oxide (Al_2O_3) and titanium oxide (TiO_2), particularly at high temperatures, which is common in boiler applications. The reaction leading to the formation of $Al_2Ti_7O_{15}$ is part of the solid-state reactions between alumina and titania under thermal conditions. At high temperatures (typically above 1000°C), Al_2O_3 and TiO_2 start to react to form various aluminum titanate phases, and $Al_2Ti_7O_{15}$ is one such phase. The overall reaction can be expressed as:

$$2\ Al_2O_3 + 7\ TiO_2 \rightarrow Al_2Ti_7O_{15}$$

The XRD pattern of AL13TI coatings is presented in Fig. 5.9. When exposed to a temperature of 900 degrees Celsius, the Al_2O_3-TiO_2 flame spraying coating undergoes oxidation, resulting in the creation of multiple distinct phases. Several phases that may arise include: Rutile TiO_2: At elevated temperatures, TiO_2 has a tendency to undergo a phase transition into the rutile phase, characterized by a denser structure in comparison to the anatase phase. Second phase is Al_2O_3, is the principal component of the coating.

It has the ability to withstand high temperatures and undergo oxidation while maintaining its structure. Additionally, it can also convert into other metastable phases.

Ti-Al-O compounds such as $Al_2Ti_7O_{15}$ has been formed through the interaction of Al_2O_3 and TiO_2 components under certain compositions and circumstances, resulting in the formation of distinct crystalline structures.

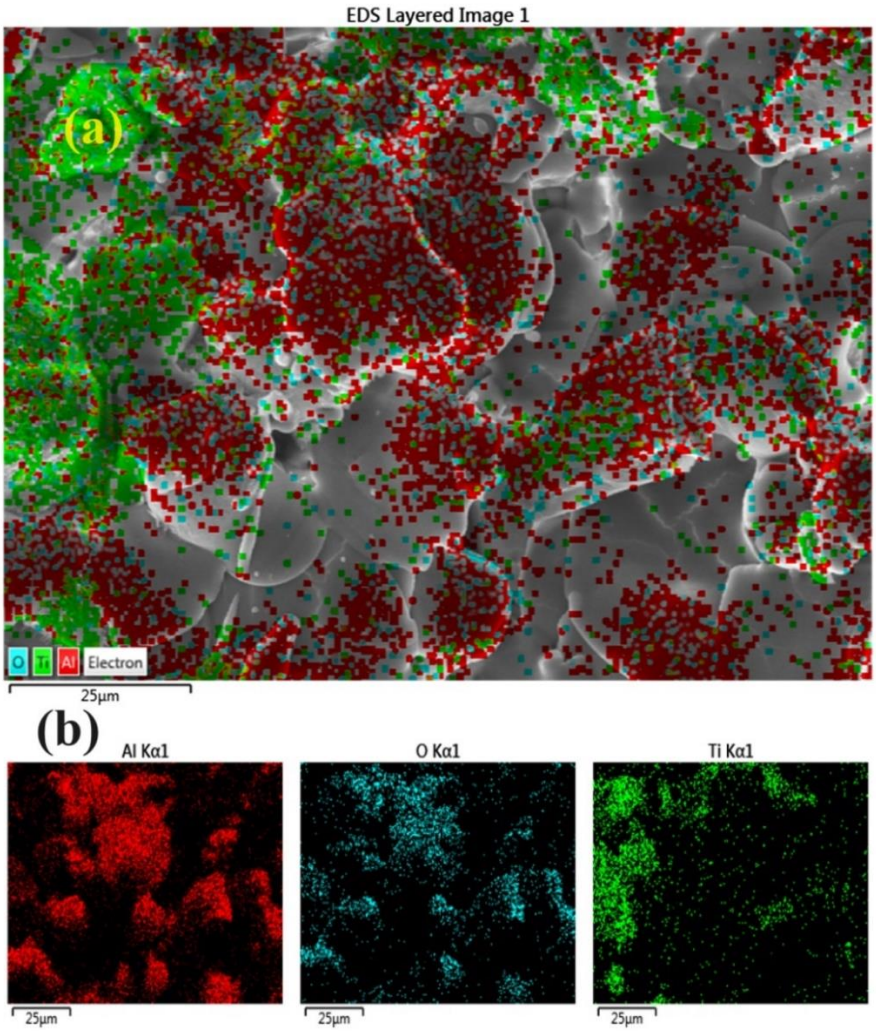

Fig.5.8. (a) SEM micrograph of flame sprayed oxidized AL13TI coating, (b) EDS mapping of flame sprayed oxidized AL coating.

Additional transitional stages: Depending on the precise composition of the coating and the conditions under which it is processed, intermediate phases may emerge that involve the interaction between Al_2O_3 and TiO_2. These phases contribute to the overall intricacy of the oxidation process.

The specific characteristics and makeup of the phases that develop during oxidation at a temperature of 900 degrees Celsius will be influenced by factors such as the original composition of the coating, the presence of impurities, and the material's thermal history. It is crucial to characterize these phases in order to comprehend the behaviour and performance of the coating when exposed to high temperatures. The XRD pattern of the oxidised AL13TI coatings at 900ºC is shown in Fig.5.9.

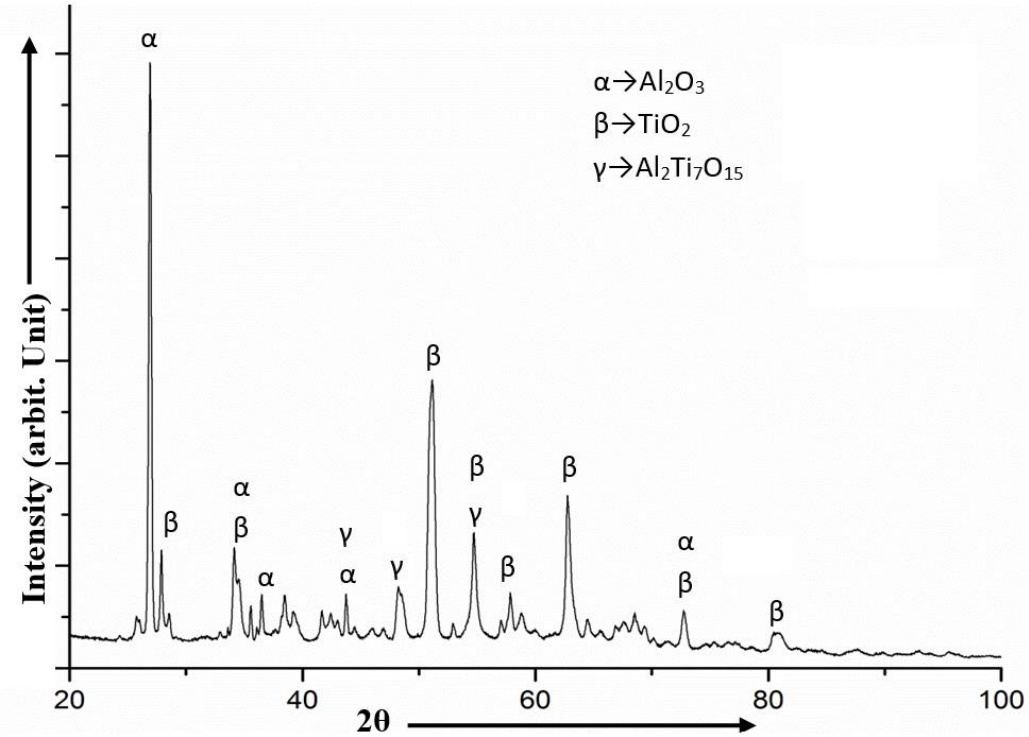

Fig.5.9. The XRD pattern of the oxidised AL13TI coatings at 900ºC.

The same trend has shown by the Al_2O_3+40%TiO_2 coating presented in Fig.5.10. This coating has shown the maximum oxidation resistance as compared to Al_2O_3 and Al_2O_3+40%TiO_2 coatings with a minimum porosity level of around 1.5%.

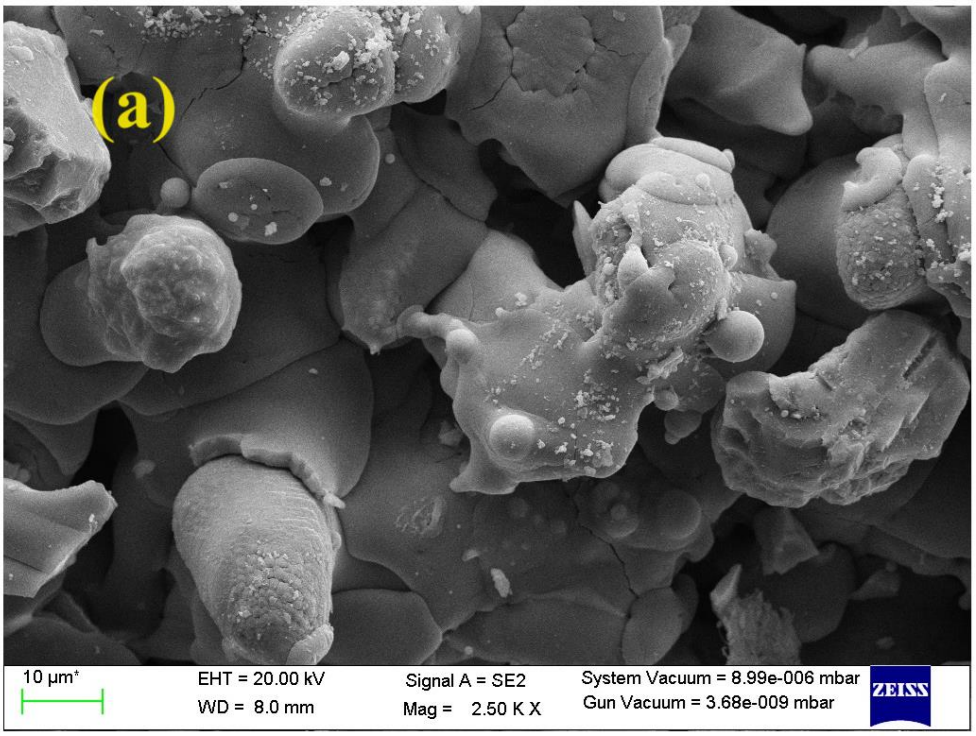

Cont'd next page..

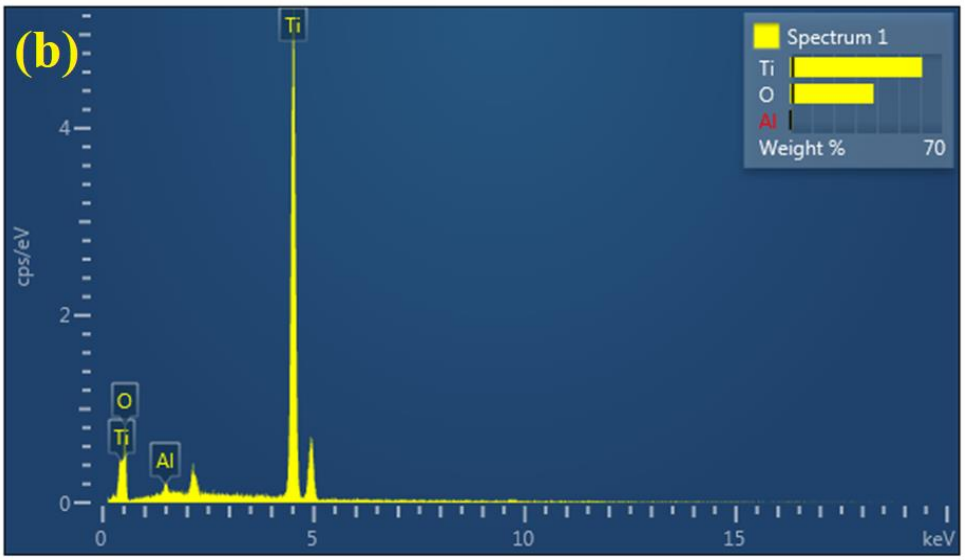

Fig.5.10. (a) SEM micrograph of oxidized sample, (b) EDS corresponding to rectangle in 5.10 (a).

Fig.5.11. Illustrates the EDS mapping of the oxidized AL40TI coating that was mentioned earlier that was mentioned. In this coating, significant presence of Ti can be observed on the surface in green colour as presented in Fig.5.11. The Ti has increased due to 40 wt.% of TiO_2 in the composition of this coating and the difference between concentration can be observed easily between this coating and previous two coatings. The presence of aluminium, oxygen, and titanium on the surface can be used to infer the surface resistance of the material. There is a correlation between this observation and the XRD data that is presented in the existing research. The X-ray diffraction patterns provide evidence that Al_2O_3, TiO_2, and $Al_2Ti_7O_{15}$ phases are present, with α-alumina being the most prominent of these phases.

The XRD pattern of the oxidised AL40TI coatings at 900ºC is shown in Fig.5.12. The oxidation of an Al_2O_3-40wt% TiO_2 flame spraying coating at a temperature of 900 degrees Celsius leads to the formation of several phases. Studies suggest that coatings made of TiO_2 and Al_2O_3-TiO_2, with a composition of 40% by weight, undergo distinct phase shifts due to microstructural changes. The application of these coatings was achieved by the processes of plasma spraying and laser engraving. Despite their chemical composition, these coatings have been found to consist of rutile and α-Al_2O_3 phases.

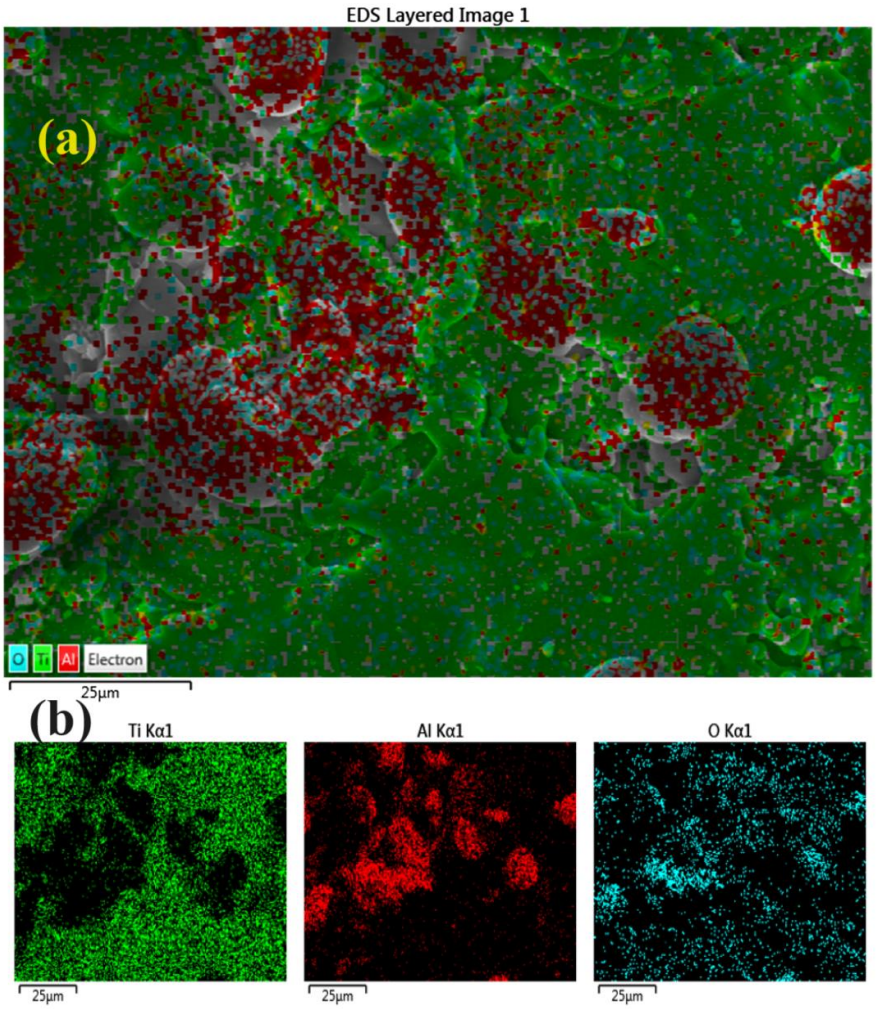

Fig.5.11. (a) SEM micrograph of flame sprayed oxidized AL40TI coating, (b) EDS mapping of flame sprayed oxidized AL coating.

Furthermore, the influence of the crystalline phase on the performance of TiO_2 coatings implies that the phase content significantly affects the photocatalytic activity. The search results do not precisely specify the specific phases created during the oxidation process of the Al_2O_3-40wt.% TiO_2 flame spraying coating at 900 degrees Celsius. It is imperative to remember this key element. The study focuses on the examination of the phases that commonly develop in different compositions, within the framework of changes in microstructure and the effectiveness of photocatalytic processes.

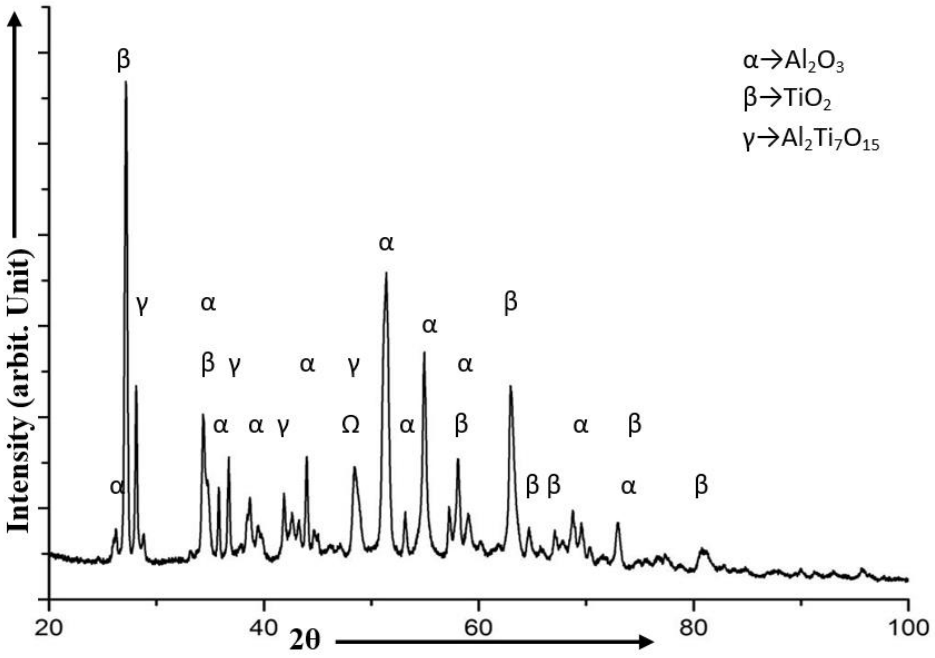

Fig.5.12. The XRD pattern of the oxidised AL40TI coatings at 900ºC.

5.2 ANALYSIS OF MICROWAVE POST-PROCESSED COATINGS

The oxidation analysis of the post-treated coating was performed at 900ºC for 50 cycles. The post-treated coatings were analysed with SEM-EDS analysis. The microwave post-treated coatings have shown the smooth surface, which shows the melting of the coating material takes place during microwave processing of the coatings. The oxidized AL coating is shown in Fig.5.13. The SEM micrograph shows the flattened surface with melted zones as shown in Fig.5.13 (a). The lower porosity of the coatings leads to the increased oxidation resistance. The less porosity cites were seen on the surface of the coating (Singh et al., 2019). However, the oxidation took place due to the phase change of α-Al_2O_3 phases. The increased oxygen content has been observed on the surface as shown in Fig.5.13 (b).

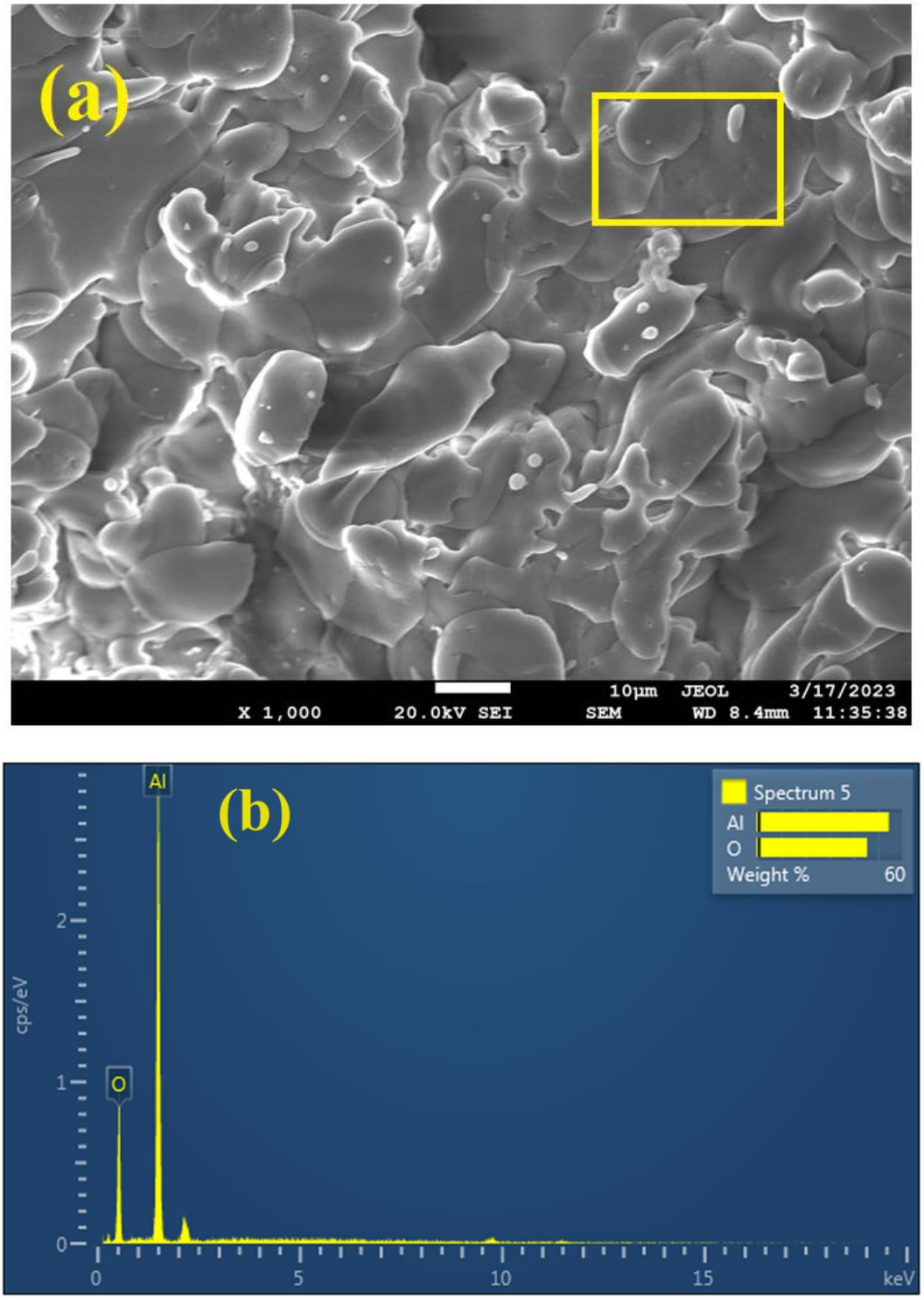

Fig.5.13. (a) SEM micrograph of flame sprayed oxidized PT-AL coating, (b) EDS map of flame sprayed oxidized PT-AL coating exposed to high temperature oxidation at 900ºC.

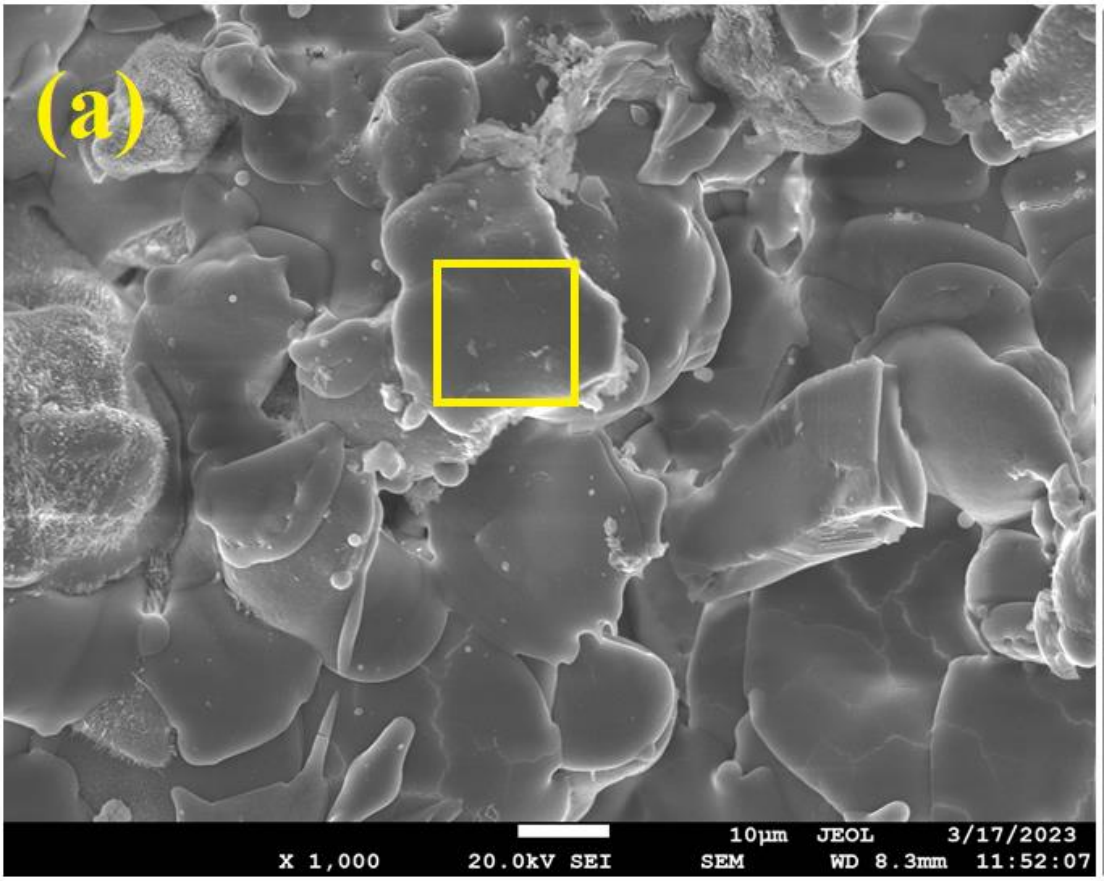

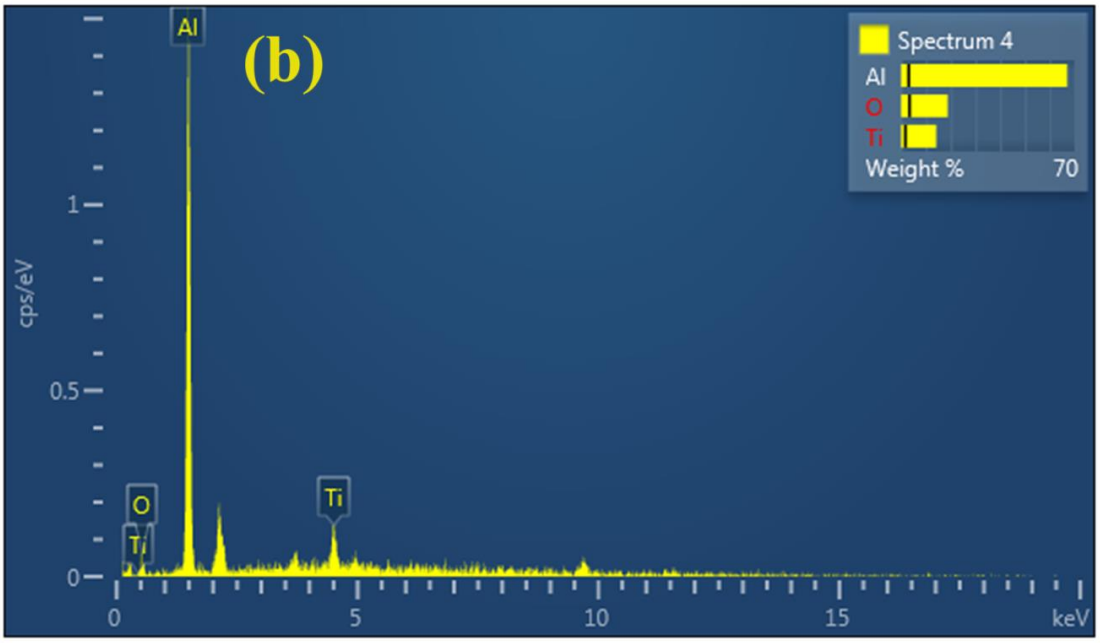

Fig.5.14. (a) SEM micrograph of flame sprayed oxidized PT-AL13TI coating, (b) EDS map of flame sprayed oxidized PT-AL13TI coating exposed to high temperature oxidation at 900ºC.

The application of microwaves as a post-treatment method for coatings has resulted in a smooth surface, indicating that the coating material undergoes melting during the microwave processing due to the melting point of the TiO_2 and Al_2O_3.

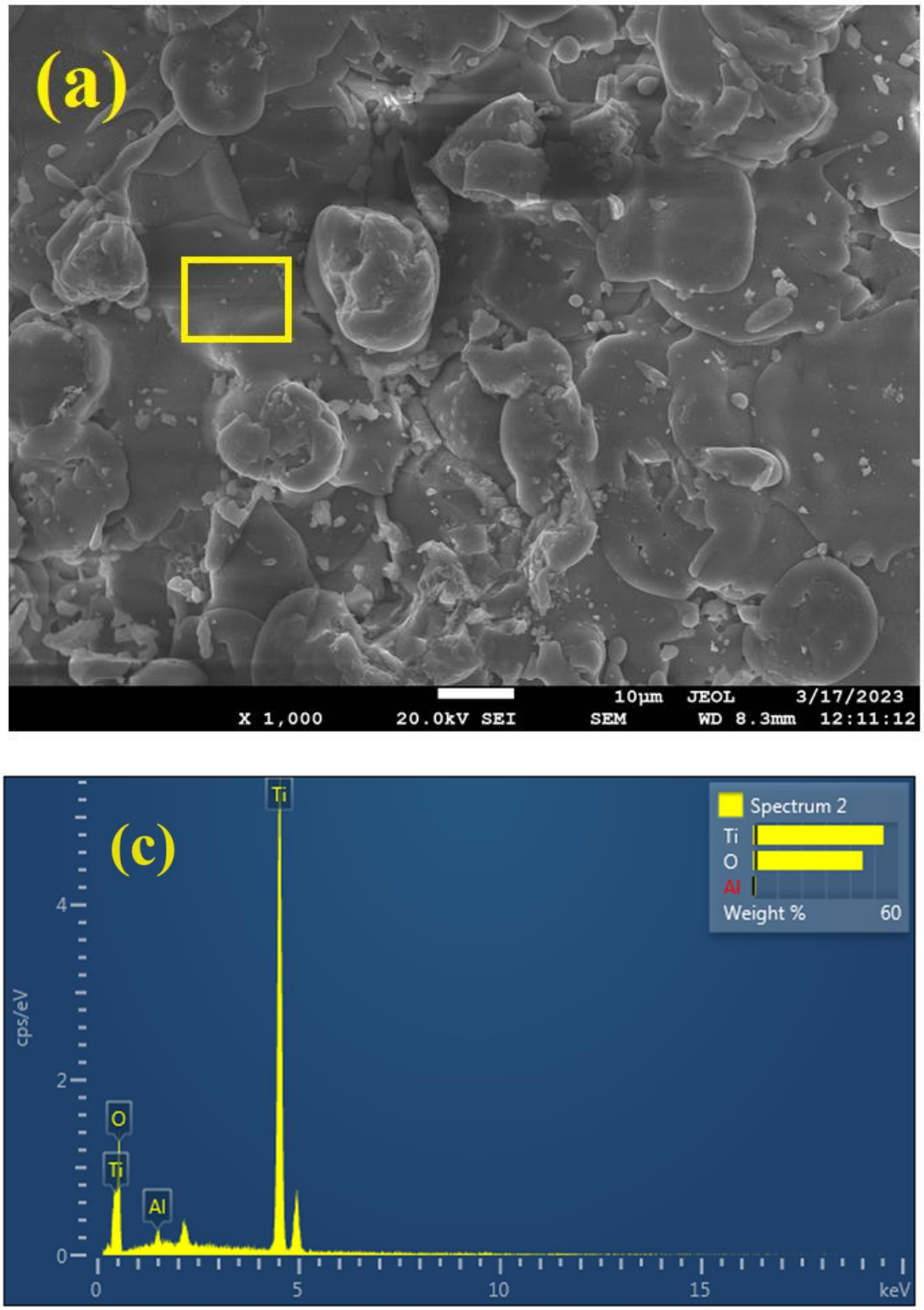

Fig.5.15. (a) SEM micrograph of flame sprayed oxidized PT-AL40TI coating, (b) EDS map of flame sprayed oxidized PT-AL40TI coating exposed to high temperature oxidation at 900ºC

The melting point of TiO_2 is lower than Al_2O_3, which has resulted in the less porosity of PT-AL13TI coating as compared to PT-AL coating. Fig.5.14 illustrates the oxidized PT-AL13TI coating. The surface in Fig.5.14 (a) exhibits both flattened areas and melted zones, as shown in the SEM image. The enhanced resistance to oxidation of the coatings is a direct consequence of the reduced porosity of the coatings. The coating's surface exhibited a reduced porosity compared to its inner. Fig.5.14 (b) clearly demonstrates that the surface exhibits a higher oxygen concentration.

The increase in the content of TiO_2 in AL40TI and further its microwave post-processing has resulted in the highest oxidation resistance amongst all deposited and post-treated coatings. The smooth surface achieved by using microwaves as a post-treatment method for coatings suggests that the coating material melts during the processing, perhaps because of the high melting points of the TiO_2 and Al_2O_3. Since TiO_2 has a lower melting point than Al_2O_3, the PT-AL40TI coating is less porous than the PT-AL and PT-AL13TI coating because of this. The oxidized PT-AL40TI coating is shown in Fig.5.15. The SEM scan shows that the surface in Fig.5.15 (a) has both flattened portions and melted zones. The decreased porosity of the coatings is the direct cause of their improved oxidation resistance. The porosity of the coating was lower on the outside than on the inside. A larger concentration of oxygen is plainly visible on the surface, as shown in Fig.5.15 (b).

5.3 XRD ANAYSIS OF POST-TREATED COATINGS

Fig.5.16 displays the XRD spectra of the coatings after undergoing microwave post processing. The XRD patterns of oxidized patterns shows retaining of phases present in the coating. Fig.5.16 demonstrates that the treated coatings exhibit significantly reduced prominence and altered positioning of the main phase peaks, in comparison to the directly sprayed coatings. The porous as-sprayed deposits undergo densification due to lattice straining, as evidenced by the minimal peak shift observed in the post-processed coatings. The coatings subjected to microwave treatment also exhibited marginal compressive stress, known as compressive stress. The mechanical properties of the post-processed SA210 Grade A1 coatings are improved. Previous studies have also demonstrated comparable results.

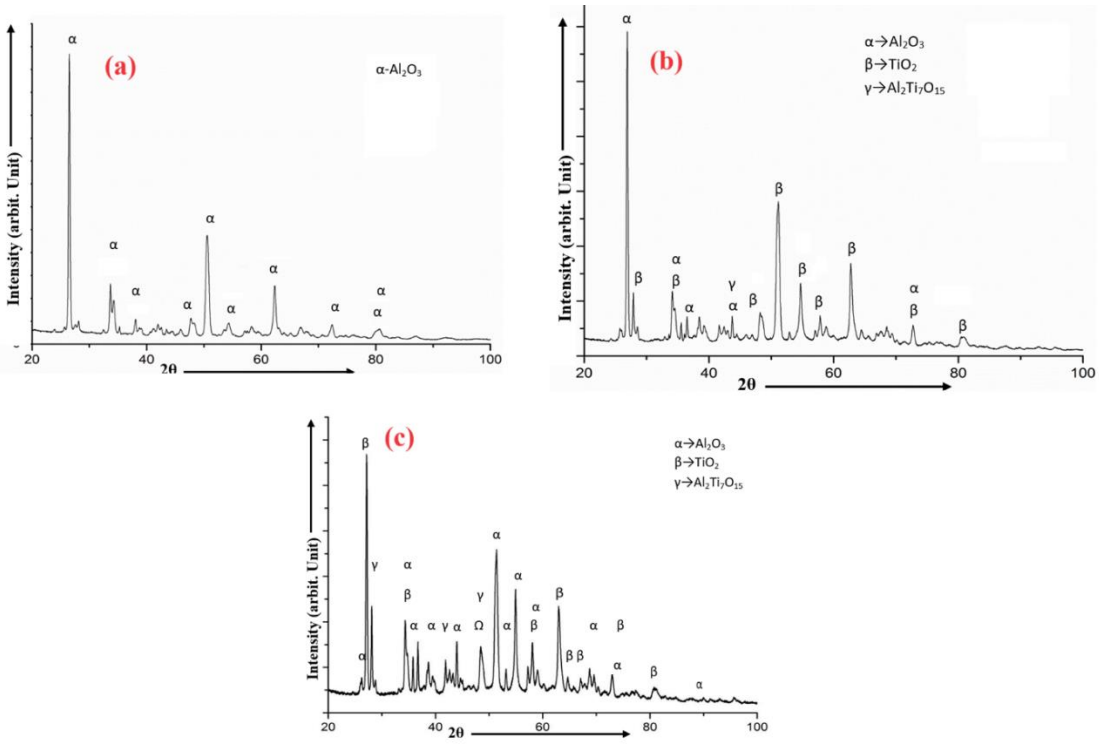

Fig.5.16. The XRD pattern of (a) PT-AL, (b) PT-AL40TI and, (c) PT-AL40TI coatings the oxidised at 900ºC.

The weight gain of the substrate showed the maximum weight gain as shown in the Table 5.1. The weight gain was minimum in case of as sprayed AL40TI and post-treated PT-AL40TI coatings owing to its composition and microstructural characteristics.

Table 5.1 Weight gain of coated and un-coated samples

Coating Composition	**Wt. gain (mg/cm^2)**	**Kp (**x 10^{-10} gm^2/cm^4 s^{-1})
SA 210	120.4	983.638
AL	22.5	18.972
AL13TI	15.6	13.458
AL40TI	11.6	11.235
PT-AL	18.9	15.684
PT-AL13TI	13.4	11.354
PT-AL40TI	7.63	08.545

5.4 SUMMARY

A comprehensive examination of the oxidation characteristics of samples that underwent a 50-cycle isothermal oxidation experiment at 900°C is detailed in Chapter 5. The research encompasses both uncoated and coated specimens, and this synopsis will analyse the experimental configuration, methodologies, findings, and ramifications elaborated upon in the chapter. The chapter initiates with an elaborate exposition of the experimental configuration. A silicon-carbide box furnace operating at 900°C was employed to analyze the isothermal oxidation of uncoated and coated samples over the course of 50 cycles. Cyclic loading was applied to the coated samples, which were composed of Al_2O_3-40%TiO_2 ceramic coatings, in order to closely replicate actual boiler conditions.

The experimental protocol demanded that the specimens be subjected to a tube furnace operating at 900°C for an hour, followed by a 20-minute chilling period at ambient temperature. Untreated samples were polished to a mirror finish, cleansed, and their surface area was measured prior to the oxidation study. After each cycle, the weight variation, color variation, luster, oxide scale, and tendency for spallation of uncoated and coated samples were assessed. In addition, uncoated samples were subjected to SEM/EDAX and XRD analyses to determine their oxide scale composition, which consisted primarily of Fe_2O_3. In comparison to substrates, the coated samples, specifically the Al_2O_3-40%TiO_2 ceramic coating, exhibited considerable potential in diminishing weight gain. For the purpose of illustrative purposes, the chapter incorporates SEM micrographs and EDS mapping to depict the oxidized surfaces. The identification of phases such as α-alumina and θ-alumina demonstrated the complex characteristics of the coatings when subjected to elevated temperatures. The SA 210 steel substrate that was coated demonstrated resistance to oxidation for a restricted period of time; fractures manifested themselves subsequent to the seventh cycle, indicating that the protective effect gradually declines.

Additionally, Chapter 5 explores the topic of microwave post-processing of coatings. The finer surfaces of the microwave-treated coatings were suggestive of material melting that occurred during the processing stage. The composition of TiO_2 and Al_2O_3 was found to be significantly influential, as increased TiO_2 content led to diminished porosity and enhanced resistance to oxidation. EDS mapping and SEM micrographs of

post-treated coatings served as visual indicators of the alterations on the surface. The introduction of marginal compressive stress during microwave post-processing significantly enhanced the mechanical properties of the SA210 Grade A1 coatings. Post-treatment of coatings resulted in modified peak positions, diminished prominence of principal phase peaks, and lattice straining as observed in their XRD spectra. The densification of the porous as-sprayed deposits caused by microwave post-processing contributed to improved mechanical properties. The weight increase of the coated samples differed, with the Al_2O_3+40%TiO2 coating experiencing the least amount of weight increase, which highlights its exceptional resistance to oxidation. The results emphasize the antioxidant properties of specific coatings in relation to oxidation, with the Al_2O_3+40%TiO2 coating demonstrating exceptional efficacy. Microwave post-processing presents an unprecedented aspect, showcasing its capacity to augment mechanical properties and resistance to oxidation.

CHAPTER 6
HOT COROSSION STUDIES

6.1 HOT CORROSION ANALYSIS

The high temperature oxidation behaviour of uncoated SA 210 in aggressive environment of molten salt Na_2SO_4-60wt% V_2O_5 was visually examined at 900˚C for 50 cycles. After applying the salt on the sample, the colour of the sample becomes yellowish. After 1st cycle of heating the colour of the sample changes to black. After 2^{nd} cycle of heating the oxidation layer starts forming. Disintegration of oxidation layer started by peeling off a thin layer in the form of small pieces. Shiny silvery layer is also observed on the surface. This shinny layer changes in to dull grey colour after 30^{th} cycle. The deterioration of the sample and disintegration of oxidation layer by peeling off in the form of small pieces continued till 50^{th} cycle.

The high temperature behaviour of AL coating inaggressive environment of molten salt Na_2SO_4-60%V_2O_5 was visually examined at 900˚C for 50 cycles. After 5^{th} cycle the coating cracked during cooling. The crack in coating may be due to different rate of cooling of the base material and the coatingand thus due to thermal shock the crack occurred. The colour of the sample becomes yellow. The cracks were then intensified in further cycles of heating. The deterioration of the sample continued till 50^{th} cycle. It can be observed that the uncoated SA 210 was not able to withstand the saltat 900˚C after 2^{nd} cycle of heating because scales begin to form after 1^{st} cycle of heating and after 2^{nd} cycle the oxidation layer formed cracked and chipped off from the surface in the form of small pieces. Where as in case of AL coating cracked after 5^{th} cycle which may be due to thermal shock. So, this shows that the coating was successful in protecting the substrate for a short period of time.

The high temperature oxidation behavior of coated AL13TI coating in aggressive environment of Na_2SO_4-60%V_2O_5 molten salt at 900˚C for 50 cycles was visually examined. After 1^{st} cycle the colour becomes yellow. After 6^{th} cycle the coating cracked from the edges during cooling process. The crack formed may be due to the different rates of cooling associated with coating and the sample steel as a result of this thermal shock occurs and coating cracked. After that deterioration of the sample

continued till 50th cycle but at a very slow rate. The similar trend was observed in AL40TI coating except the deterioration has not taken place even after the 50th cycle.

6.2 SEM/EDAX ANALYSIS

The SEM micrograph and EDAX analysis at selected points for uncoated substrate is shown in fig. W. EDAX analysis of uncoated SA 210 after corrosion in Na_2SO_4-60% V_2O_5 showed the major amount of Fe_2O_3, Cr_2O_3 and NiO_2 in its scale along with small amount of SiO_2, MnO_2, etc. Cr_2O_3 and NiO_2 present in the scale may have protected the substrate from further corrosion. Some craters were observed on the surface of the uncoated substrate.

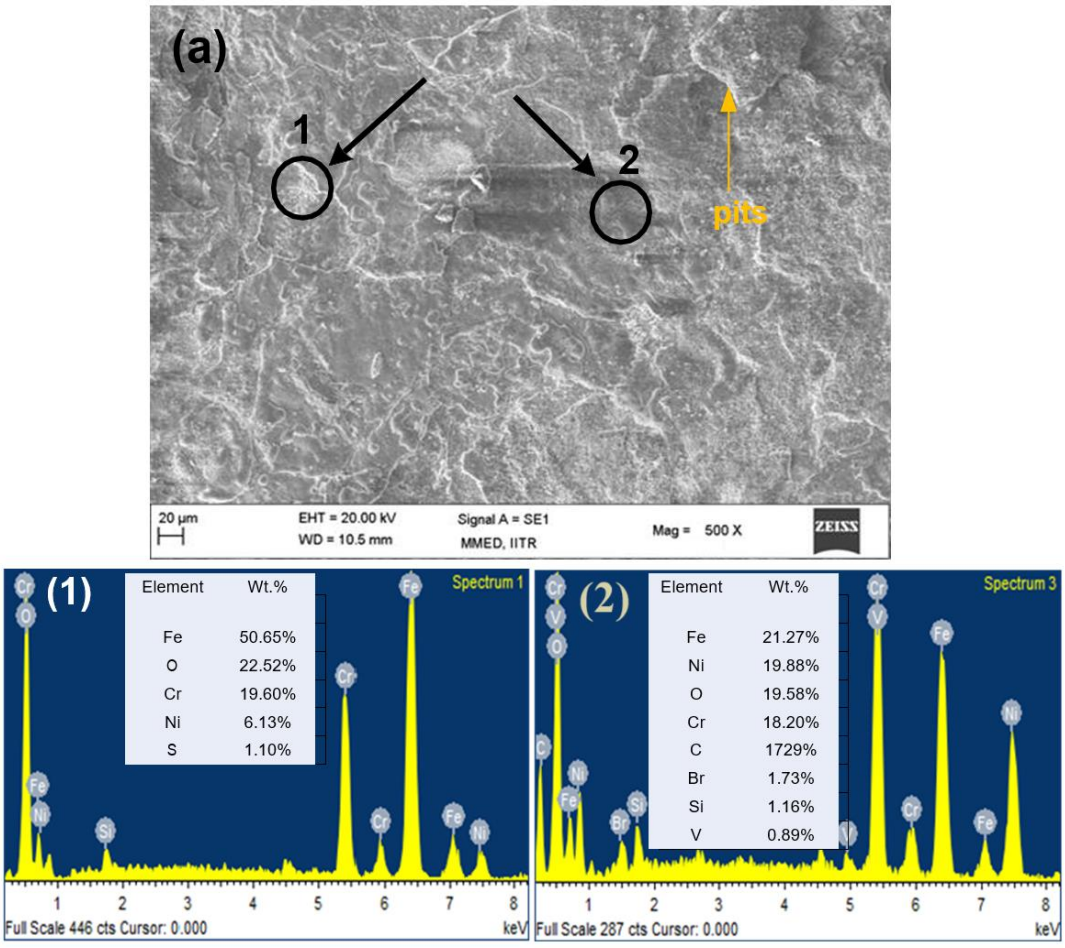

Fig. 6.1 SEM micrograph and EDAX analysis for uncoated SA 210 aftercorrosion in Na_2SO_4-60% V_2O_5 at 900˚C for 50 cycles, 500X

The result shows that the major phase formed during oxidation were Fe_2O_3, NiO_2, Cr_2O_3, Al_2O_3 and TiO_2. Due to the presence of NiO_2, Cr_2O_3, Al_2O_3 and TiO_2 hot corrosion has been reduced because these oxides protected the substrate from further

corrosion. Some peaks of $Al_2Ti_7O_{15}$, V_2O_3 and $NiCr_2O_4$ were also found in case of coated SA 210 boiler steel.

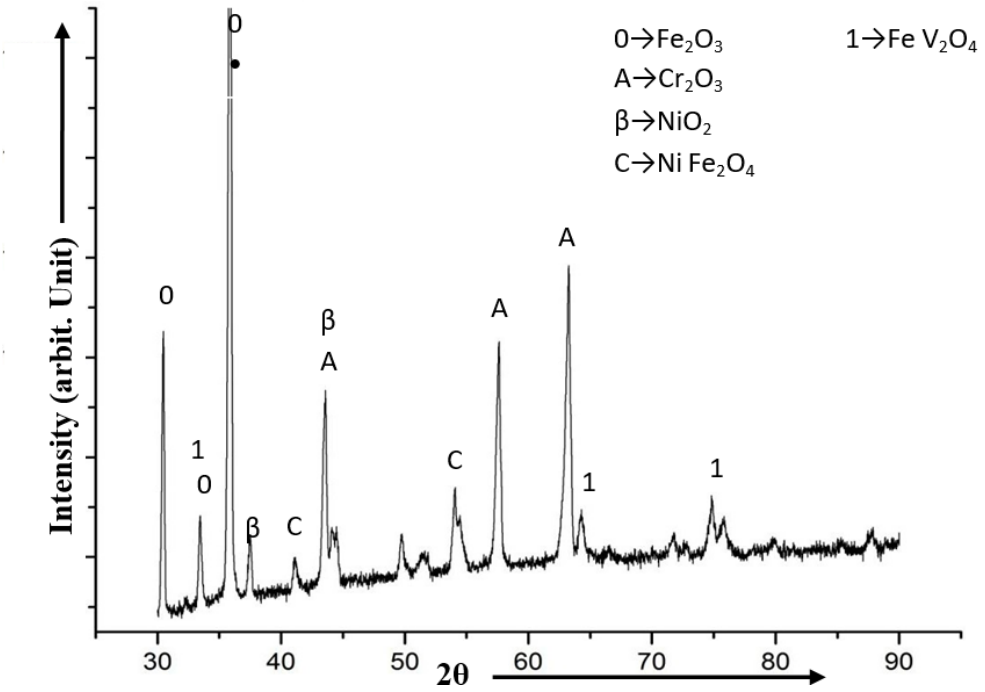

Fig. 6.2. XRD for uncoated SA 210 after corrosion in Na_2SO_4-60% V_2O_5 at 900˚C for 50 cycles, 500X

In the SEM micrograph of hot-corroded AL coating, the salty products can be clearly seen in the form of needles, which are corresponding to the salts present on the surface due to salt attack as shown in Fig.6.1. Cracks were also observed in the coating during corrosion test as shown in the Fig.6.1. The salt products are present on the surface of the corroded coatings. In order to offer a thorough depiction of the SEM micrograph of the thermally sprayed Al_2O_3 coating's hot corroded surface, it is imperative to analyze the particular SEM micrograph under consideration. By analyzing the properties of the corroded surface and the attributes of the Al_2O_3 thermal sprayed coating, it can deduce specific details from the SEM micrograph. Considering the vulnerability of the hot corroded surface to intergranular attack, sulfide particles, and chemical reactions with impurities like salts, chlorides, sulfides, and vanadate's, the SEM micrograph of the hot corroded Al_2O_3 thermal sprayed coating can display specific regions affected by intergranular attack, potential presence of sulfide particles, and the effects of chemical reactions on the coating's surface.

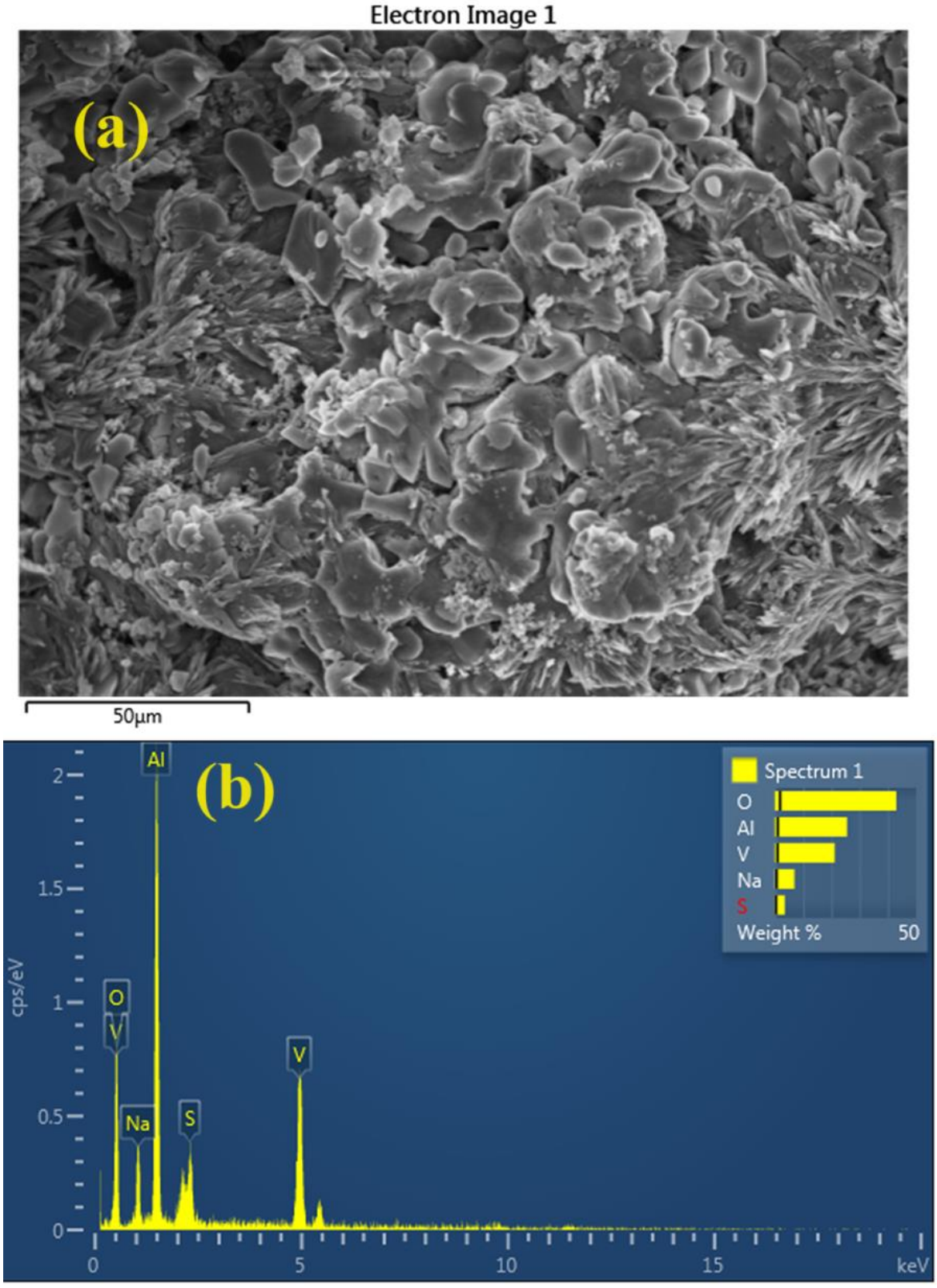

Fig.6.3 (a) SEM micrograph and (b) EDAX analysis for coated AL coating after corrosion in Na_2SO_4-60% V_2O_5 at 900˚C for 50 cycles

In addition, the SEM micrograph can display the degree of denuded zone formation and any surface pitting or material degradation caused by the hot corrosion process. The Al_2O_3 thermal sprayed coating possesses favorable mechanical properties,

exceptional resistance to abrasive wear, hard surface wear, and high-temperature erosion (Sidhu et al., 2007). The presence of elements over the corroded surface is presented in the elemental distribution as shown in Fig.6. Fig.6(a) shows the mixed elements SEM micrographs and the individual elements are presented in Fig.6(b). The presence of Al and V is most significant which shows the presence of coating elements and salt products on the surface. The salt products have led to the degradation of the coating, where the main reason is the high porosity of the AL coating. Fig. 6.2. presents XRD for uncoated SA 210 after corrosion in Na_2SO_4-60% V_2O_5 at 900˚C for 50 cycles.

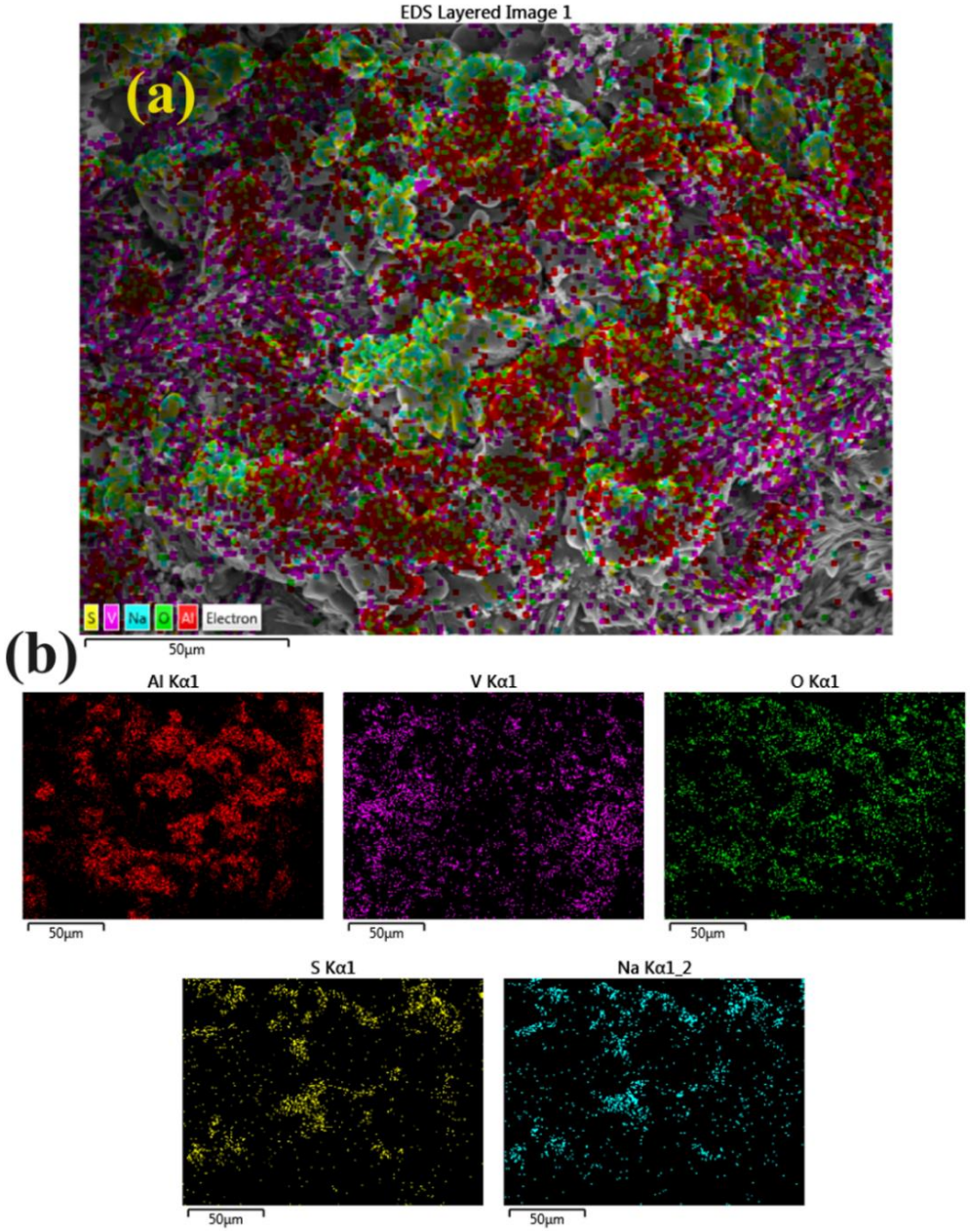

Fig.6.4 (a) SEM micrograph and (b) EDS mapping of coated AL coating after corrosion in Na_2SO_4-60% V_2O_5 at 900˚C for 50 cycles

The XRD result of corroded AL coating shows the major phases formed during oxidation as Al_2O_3, Fe_2O_3, and V_2O_3. As shown in Fig.6.3 the Al_2O_3 itself is a coating material and presence of Fe_2O_3, and V_2O_3 depicts the peeling off of the coating and salts attack on the surface during hot-corrosion test.

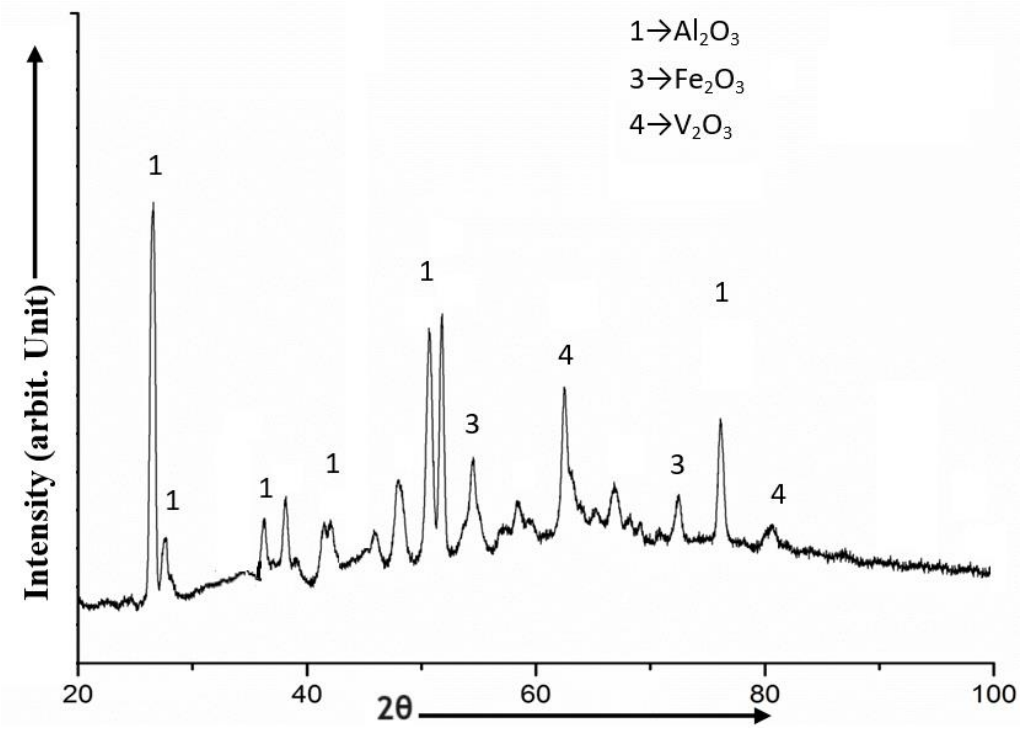

Fig.6.5 XRD of AL coating after corrosion in Na_2SO_4-60% V_2O_5 at 900˚C for 50 cycles.

Hot corrosion can have a substantial influence on the microstructure of a material. Hot corrosion of materials occurs when a salt film deposit at high temperatures causes accelerated oxidation, resulting in alterations to the microstructure. These changes may encompass the creation of novel phases, erosion of grain boundaries, and the emergence of empty spaces and fractures within the microstructure. Hot corrosion can significantly degrade the material's performance and structural integrity by inducing adverse alterations to its microstructure. However in case of AL13TI coated SA 210 substrate Al_2O_3 and TiO_2 were present in major phases with considerable amount in the scale. Which acted as a barrier to the harsh salt environment. Moreover, the addition of TiO_2 leads to the decreased porosity levels and is responsible for the restricted hot-corrosion. The Fig.6.4 shows the surface, where the needles like structure present due to the salt attack has been reduced. The porosity is also low as

compared to the AL coating, the EDS shows the presence of Al, Ti, O, Na, S and V can be observed as shown in Fig.6.4 (b). Fig.6.5 presents the XRD of AL coating after corrosion in Na_2SO_4-60% V_2O_5 at 900˚C for 50 cycles.

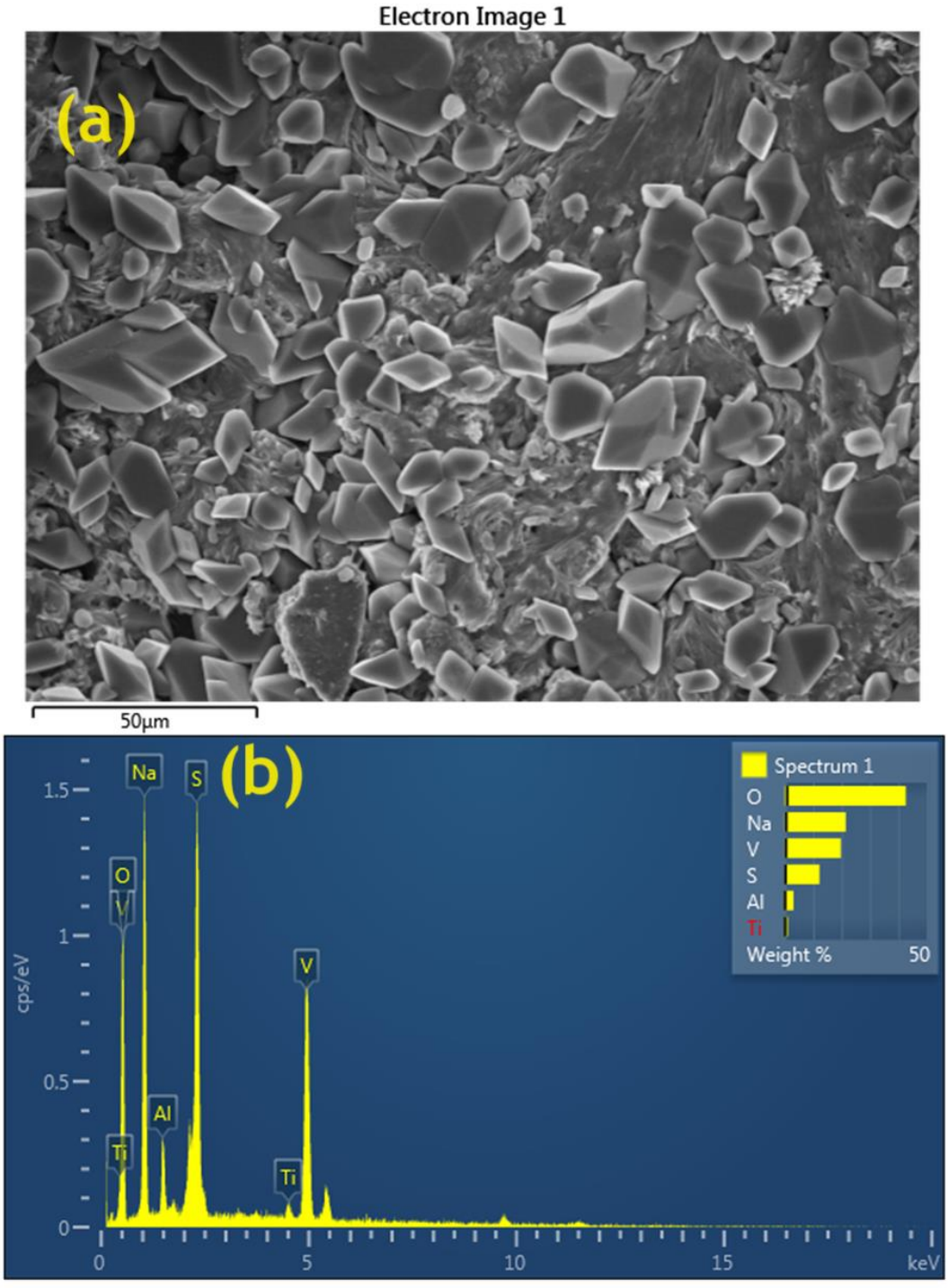

Fig.6.6 (a) SEM micrograph and (b) EDAX analysis for coated AL13TI coating after corrosion in Na_2SO_4-60% V_2O_5 at 900˚C for 50 cycles

As illustrated in Fig.6.6, the elemental distribution reveals the existence of elements

on the corroded surface. Fig.6.6 (a) illustrates the SEM micrographs of the combined elements, while Fig.6.6 (b) depicts the individual elements. The most significant presences of Al, Ti and O indicate that salt compounds and coating elements are present on the surface. The low porosity of the AL13TI coating is the primary factor contributing to the better oxidation resistance.

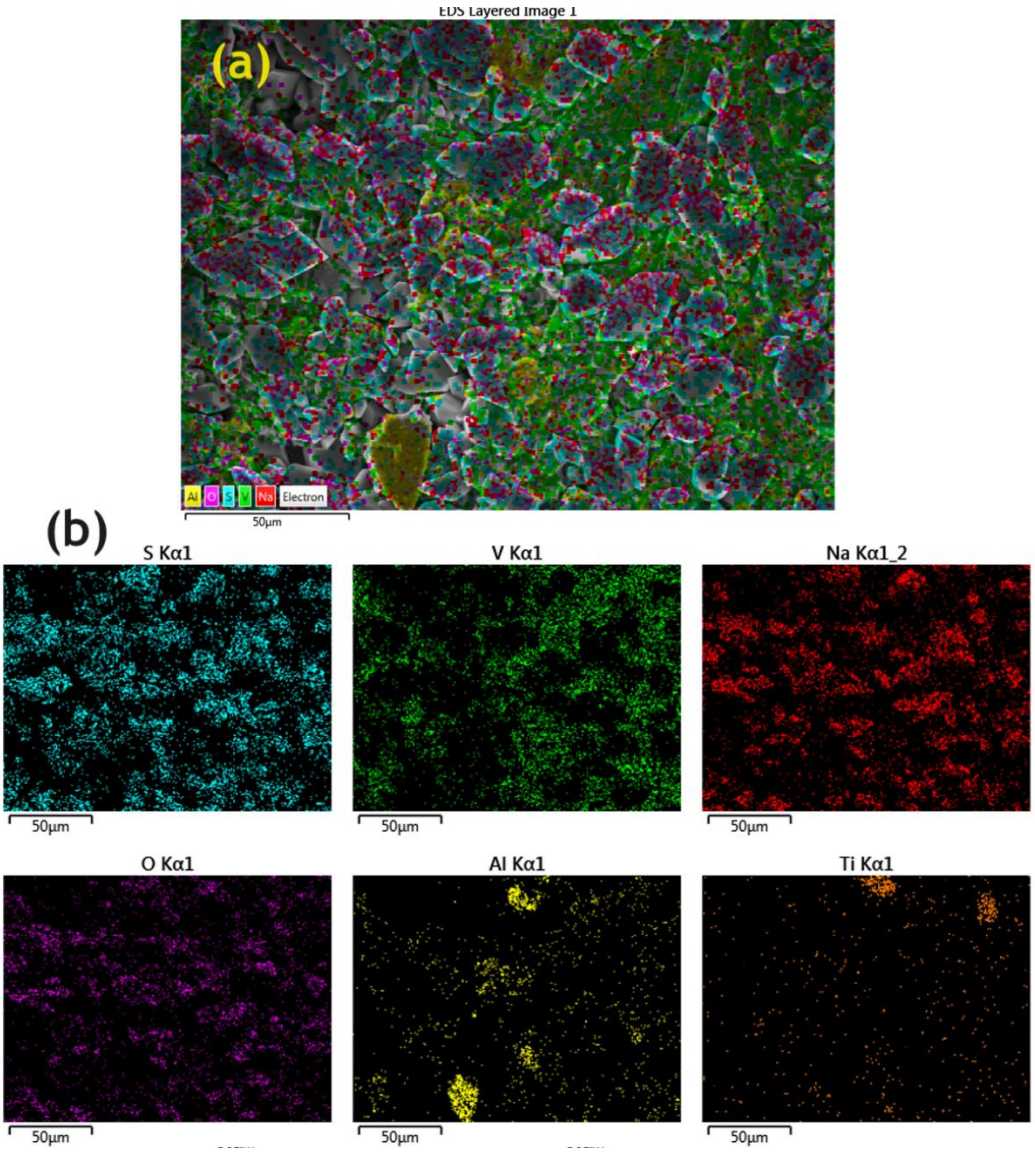

Fig.6.7 (a) SEM micrograph and (b) EDS mapping of coated AL13TI coating after corrosion in Na_2SO_4-60% V_2O_5 at 900˚C for 50 cycles.

The XRD result of corroded AL13TI coating shows the major phases formed during oxidation as Al_2O_3, Fe_2O_3, TiO_2, $NiCr_2O_4$, $Al_2Ti_7O_{15}$ and V_2O_3. As shown in Fig.6.7. The Al_2O_3 and TiO_2 itself are a coating materials and presence of Fe_2O_3, and V_2O_3 depicts the peeling off of the coating and salts attack on the surface during hot-

corrosion test. $Al_2Ti_7O_{15}$ has also formed during the hot corrosion of AL13TI coating. Fig.6.8 presents the XRD of AL13TI coating after corrosion in Na_2SO_4-60% V_2O_5 at 900˚C for 50 cycles.

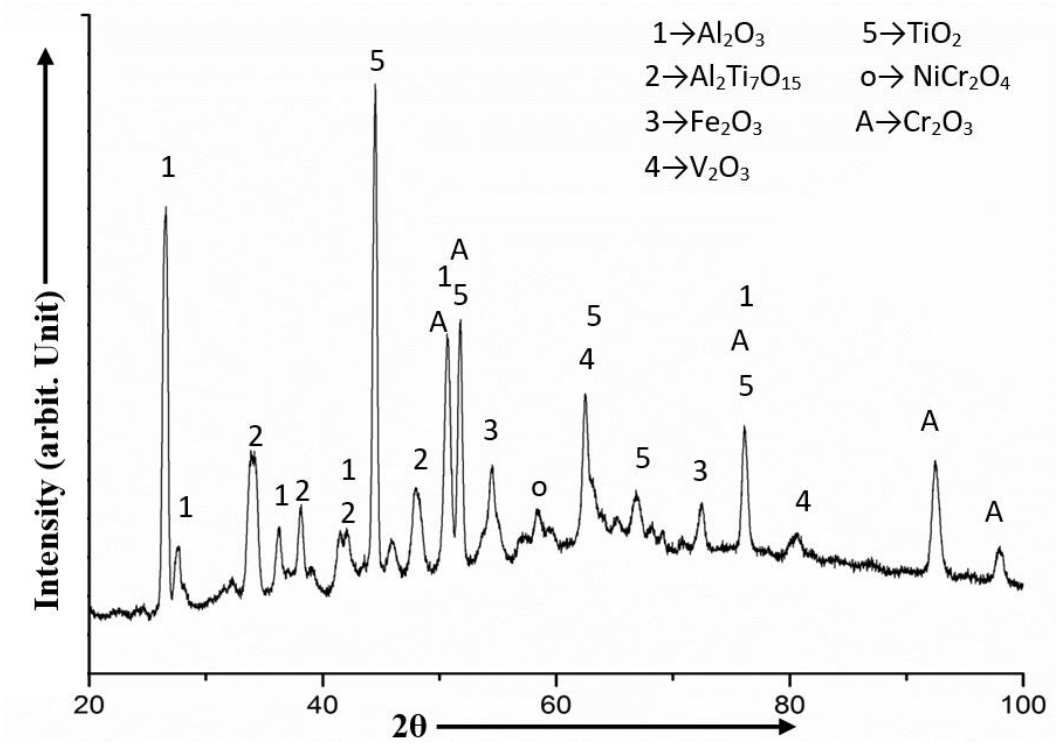

Fig.6.8 XRD of AL13TI coating after corrosion in Na_2SO_4-60% V_2O_5 at 900˚C for 50 cycles.

Fig.6.9 shows the SEM micrograph of AL40TI coating corroded at 900˚C for 50 cycles with Na_2SO_4-60% V_2O_5 salts. The SEM micrograph shows the surface with most melted zones, which is due to addition of TiO_2 in more proportion as compared to AL13TI coating. The melting point difference results in melted zones and leads to the low porosity. When the SA 210 substrate was coated with AL40TI, the primary phases observed in the scale were Al_2O_3 and TiO_2, with a significant proportion present. Which served as an impediment to the severe saline environment. Furthermore, the inclusion of TiO_2 results in reduced levels of porosity and is accountable for the limited occurrence of hot-corrosion (Simms et al., 2004). Fig.6.9 depicts a surface with a diminished presence of needle-like structures caused by salt attack. Compared to the AL coating, the porosity is significantly lower.

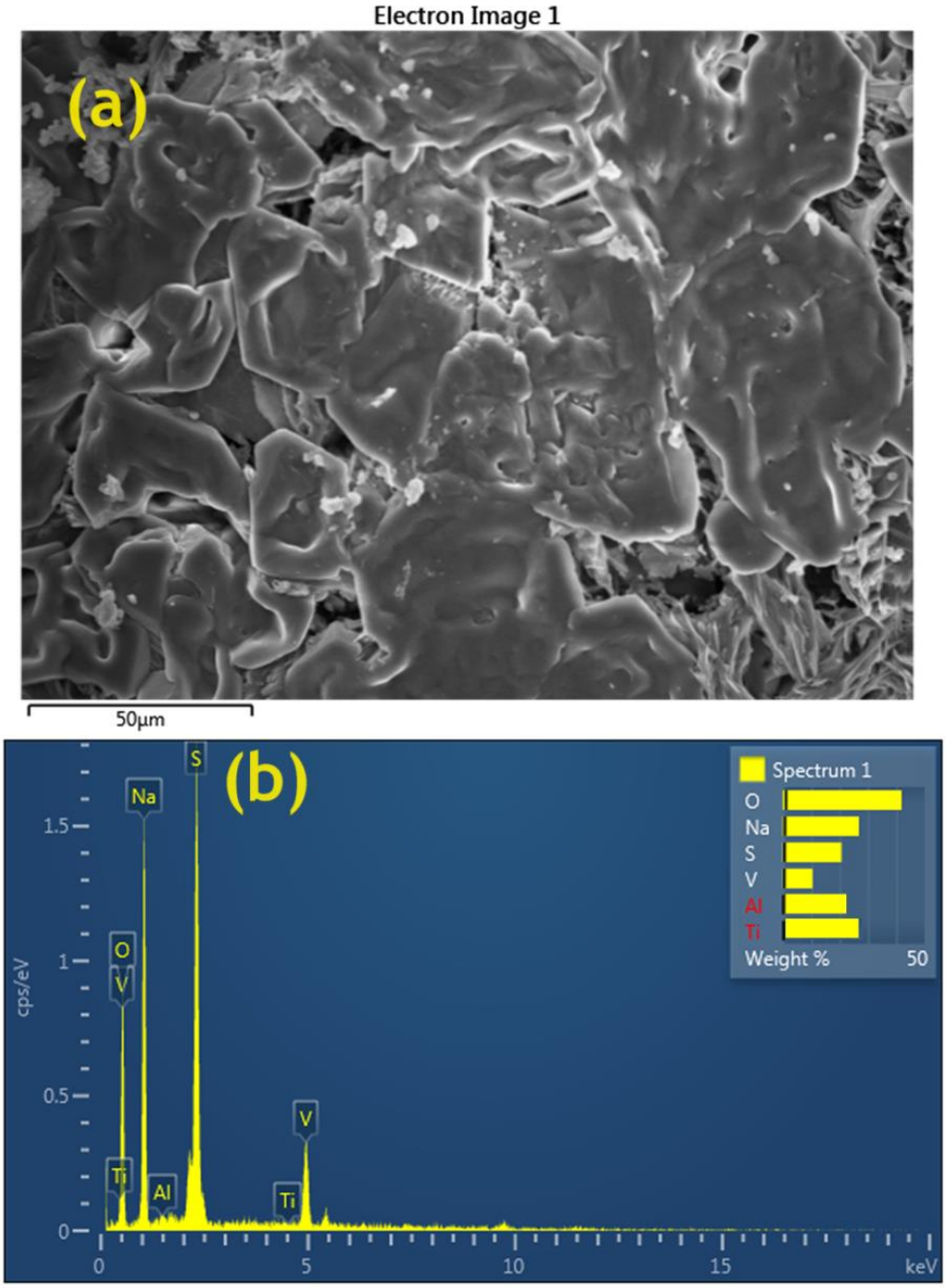

Fig.6.9 (a) SEM micrograph and (b) EDAX analysis for coated AL40TI coating after corrosion in Na_2SO_4-60% V_2O_5 at 900˚C for 50 cycles

The EDS analysis reveals the presence of Al, Ti, O, Na, S, and V, as depicted in Fig.6.9 (b). Fig.6.10 demonstrates that the elemental distribution indicates the presence of elements on the corroded surface. Fig.6.10 (a) displays the SEM micrographs of the combined parts, whereas Fig.6.10 (b) shows the individual elements (Kamal et al., 2010b). The prominent presence of Al, Ti, and O suggests the existence of salt compounds and coating components on the surface. The key aspect that enhances the resistance to oxidation is the AL13TI coating's low porosity.

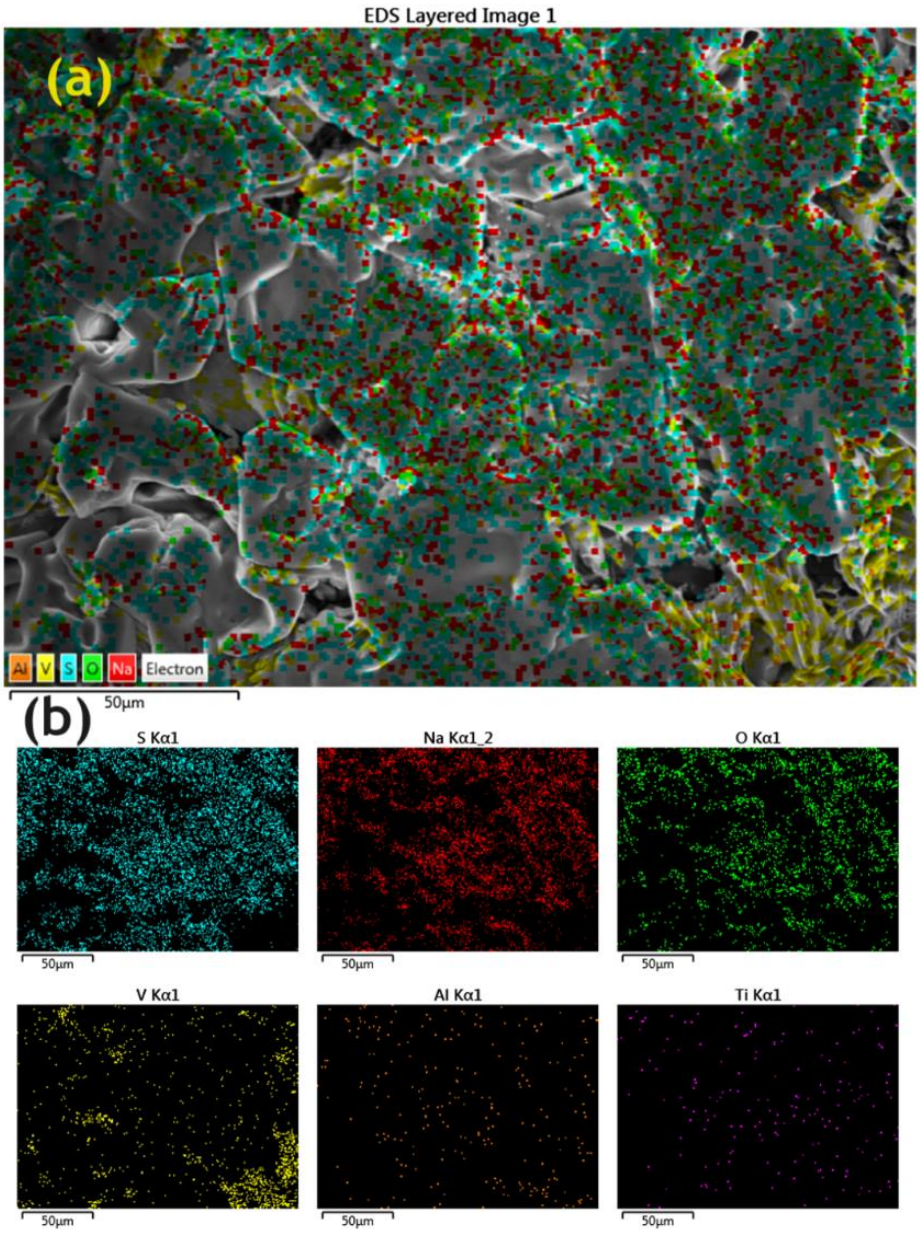

Fig.6.10 (a) SEM micrograph and (b) EDS mapping of coated AL40TI coating after corrosion in Na_2SO_4-60% V_2O_5 at 900˚C for 50 cycles.

Al_2O_3, Fe_2O_3, TiO_2, $NiCr_2O_4$, $Al_2Ti_7O_{15}$, and V_2O_3 are described as the primary phases that were generated throughout the oxidation process, according to the XRD analysis of the corroded AL40TI coating (Kamal et al., 2008; Kaur et al., 2009). In addition, $Al_2Ti_7O_{15}$ has been produced as a result of the hot corrosion of the AL40TI coating. As can be seen in Fig.6.11. During the hot-corrosion test, the presence of Fe2O3 and V_2O_3 illustrates the peeling off of the coating and salts assault on the surface. Al_2O_3 and TiO_2 are both materials that are used as coatings.

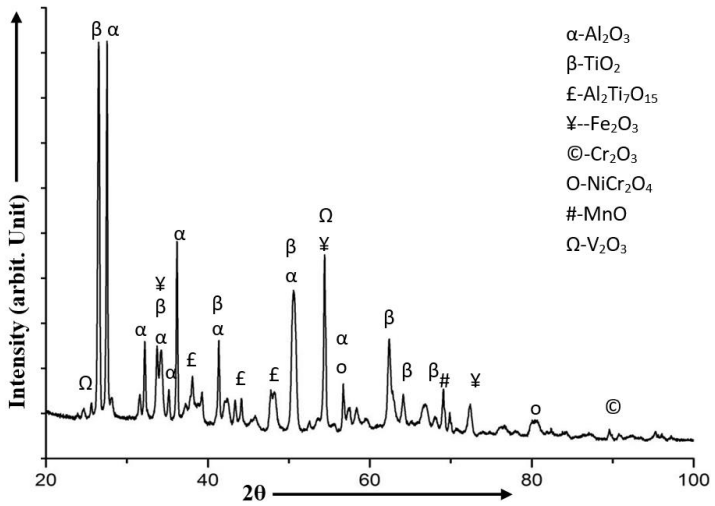

Fig.6.11 XRD of AL40TI coating after corrosion in Na_2SO_4-60% V_2O_5 at 900˚C for 50 cycles

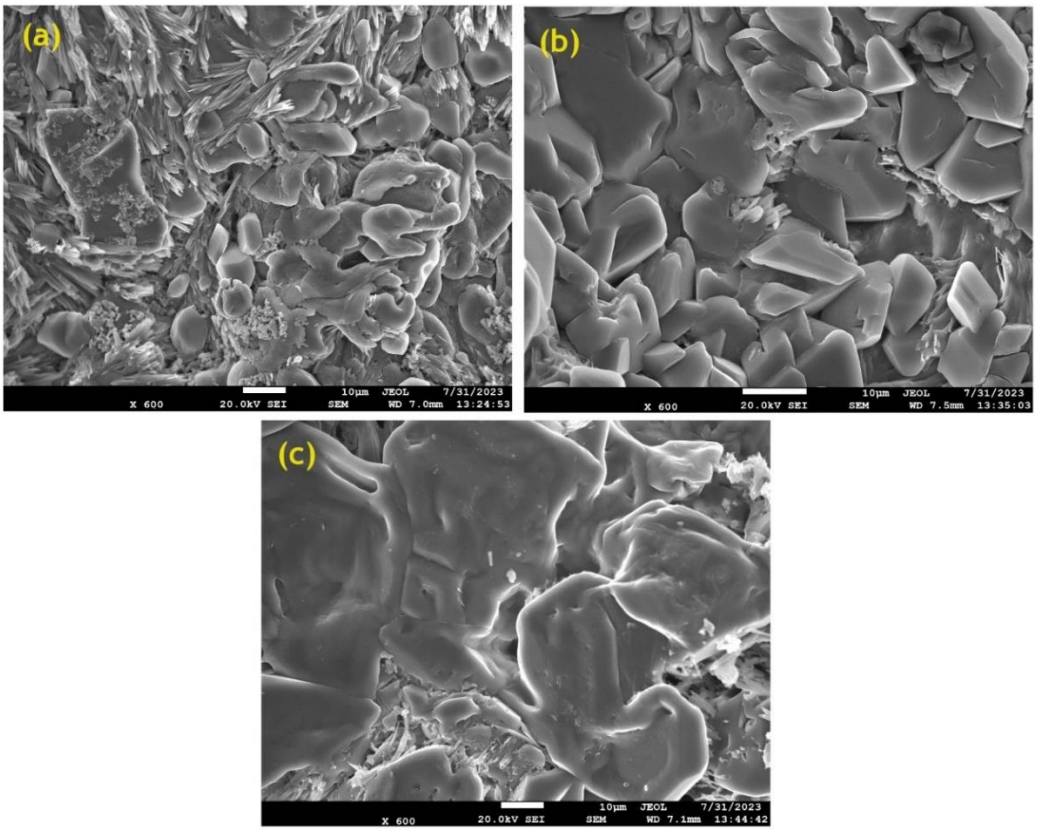

Fig.6.12. SEM micrographs of the microwave heat-treated (a) PT-AL, (b) PT-AL13TI and (c) PT-AL40TI coatings.

As compared to the flame-sprayed coatings, the microwave heat-treated AL, AL13TI and AL40TI coatings have shown better corrosion resistance. The micrographs of the microwave heat-treated hot-corroded coatings can be seen in Fig.6.12. The PT-AL surface still shows the needle like structure present on the corroded surface as shown

in Fig.6.12 (a). The PT-AL13TI and PT-AL40TI coatings have shown smoothened surface as compared to PT-AL. The healing has taken place during the microwave processing has resulted in the better corrosion resistance (Kaur et al., 2012; Kaushal et al., 2014). The open porosity acts as a path for the diffusion of the oxygen and salts products to enter into the surface and further leads to the sub-surface of the coatings. The open porosity cites are minimum in PT-AL40TI coatings as shown in Fig.6.12 (c).

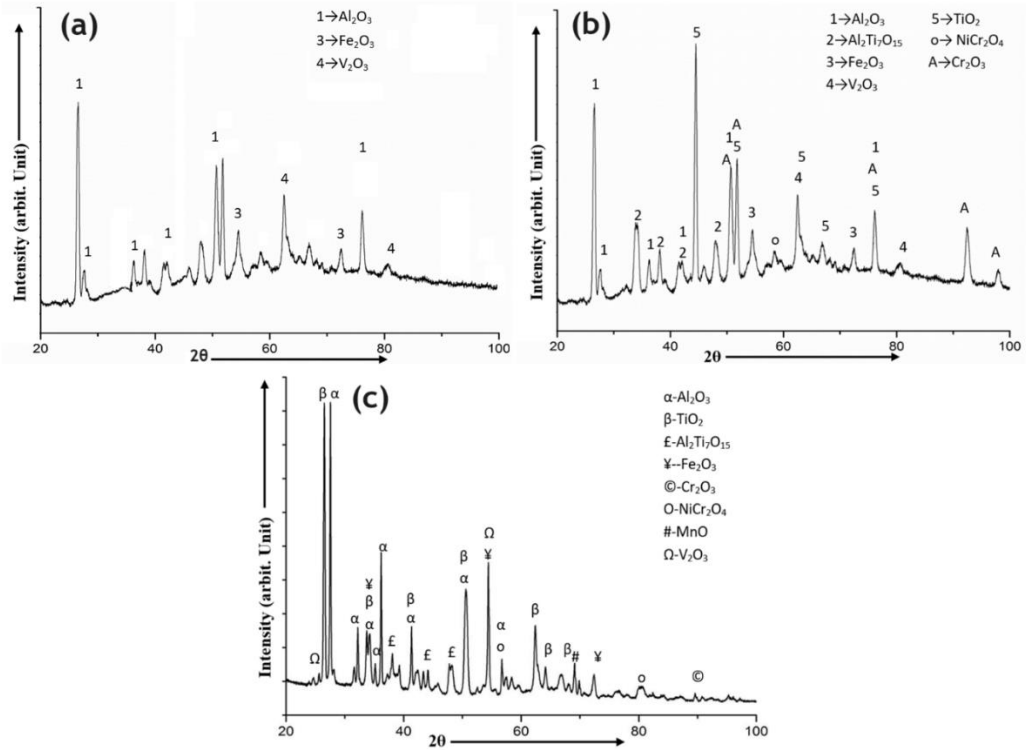

Fig.6.13. XRD patterns of of the microwave heat-treated (a) PT-AL, (b) PT-AL13TI and (c) PT-AL40TI coatings.

Fig.6.13 presents the XRD spectra of the coatings following microwave post processing. The XRD patterns of the hot-corroded samples demonstrate the preservation of the phases found in the coating. Fig.6.13 illustrates the noticeable differences in the appearance and placement of the main phase peaks between the treated coatings and the directly sprayed coatings. The as-sprayed deposits undergo densification through lattice straining, as indicated by the minimal peak shift observed in the post-processed coatings (Kaushal et al., 2012; Kaushal et al., 2010). The coatings treated with microwave technology also showed a slight compressive stress, commonly referred to as compressive stress..

6.3 THERMOGRAVIMETRIC STUDY

The corrosion kinetics of the coated as well as uncoated SA 210 in molten salt environment at 900˚C was studied (Kaushal et al., 2011; Khoi et al., 1975). The weight gain of the substrate showed the maximum weight gain as shown in the Table 6.1. The weight gain was minimum in case of as sprayed AL40TI and post-treated PT-AL40TI coatings owing to its composition and microstructural characteristics.

Table 6.1 Weight gain of coated and un-coated samples under hot-corrosion

Coating Composition	**Wt. gain (mg/cm^2)**	**Kp (** x 10^{-10} $gm^2/cm^4\ s^{-1}$)
SA 210	136.9	1156.894
AL	26.5	23.646
AL13TI	21.8	17.458
AL40TI	15.6	15.679
PT-AL	23.6	21.425
PT-AL13TI	17.6	14.569
PT-AL40TI	11.3	12.364

6.4 SUMMARY

A comprehensive examination of the hot corrosion characteristics of both uncoated and coated SA 210 in a demanding molten salt setting is presented in Chapter 6. The results emphasize the efficacy of coatings, specifically AL13TI and AL40TI, in reducing the rate of corrosion and improving the longevity of the materials. The corrosion products' composition can be discerned through the utilization of SEM/EDAX analyses, which highlight the protective function of oxides that are found in coated samples. The thermogravimetric analysis provides quantitative support for these results, as coated samples demonstrate decreased weight gains and kinetic parameters that suggest decreased corrosion rates. The implementation of microwave post-processing illustrates a potentially fruitful pathway towards enhancing the resistance of coated materials to corrosion (Khor and Cheang, 1994). In its entirety, the chapter provides significant contributions to the fields of materials science, corrosion mitigation, and prospective high-temperature applications.

The authors visually inspect the oxidation behavior of uncoated SA 210 and coated specimens (AL and AL13TI) under high temperatures. A significant observation is the transformation of the uncoated SA 210 sample's color to yellow subsequent to the application of salt. The formation of oxidation layers, cracking, and disintegration result from subsequent cycles (Koivuluoto and Vuoristo, 2009; Koivuluoto and Chukalovskaya, 1997). After five cycles, the AL coating fractures, indicating a restricted protective period. AL13TI coating fractures following the sixth cycle, but degradation is gradual until the fifty-first cycle. In contrast, AL40TI coating remains undamaged even after 50 cycles, indicating an increase in durability. The uncoated SA 210 and coated specimens undergoing heated corrosion are subjected to energy-dispersive X-ray spectroscopy (EDAX) and scanning electron microscopy (SEM) analysis. EDAX analyses and SEM micrographs reveal the composition and surface alterations (Krzyzanowski et al., 2010). Significant quantities of Fe_2O_3, Cr_2O_3, and NiO_2 are present in the scale of uncoated SA 210, which may prevent further corrosion of the substrate. On the other hand, coated SA 210 exhibits oxides such as TiO_2, Al_2O_3, Al_2O_3, $NiCr_2O_4$, and V_2O_3, all of which aid in the mitigation of heated corrosion (Kumar and Sapra, 2016). The AL coating demonstrates the presence of fractures as well as Al, O, Na, and V. The reduced porosity of AL13TI and AL40TI coatings increases their resistance to heated corrosion.

Thermogravimetric Investigation comprises the application of thermogravimetric analysis to examine the kinetics of corrosion. Weight gain assessments are performed on SA 210 samples, including uncoated and coated specimens (AL, AL13TI, and AL40TI), while subjected to heated corrosion conditions. The outcomes suggest that the uncoated SA 210 undergoes the most substantial increase in weight (136.9 mg/cm2), whereas the coated samples demonstrate considerably reduced weight gains. This provides further support for the protective function of coatings. The concept that the coated samples experience reduced corrosion rates is further supported by the kinetic parameter (Kp). Finally, a microwave post-processing method is described in the chapter and applied to AL, AL13TI, and AL40TI coatings. The superior corrosion resistance of the microwave-treated coatings is demonstrated by their smoother surfaces in comparison to the untreated coatings. The post-processed coatings' lattice strain and preservation of coating phases are confirmed by X-ray diffraction (XRD) patterns. The improved hot corrosion performance of pure Al_2O_3 and Al_2O_3 with 13% and 40% TiO_2 coatings, after microwave hybrid heat

treatment, is primarily due to enhanced microstructural densification and reduced porosity. The microwave heating process results in better sintering and grain boundary diffusion, which closes voids and limits pathways for corrosive species to penetrate. The presence of TiO_2 also contributes to the formation of stable aluminum titanate phases ($Al_2Ti_7O_{15}$), which provide additional protection against corrosive agents at high temperatures. These factors reduce the ingress of molten salts and gases, improving the overall corrosion resistance of the coatings.

CHAPTER 7

CONCLUSIONS AND FUTURE SCOPE

7.1 CONCLUSIONS

The following conclusions were obtained on the basis of experimental results obtained and their analysis in the current work.

1. Flame-sprayed Al_20_3-based coatings with different proportions of TIO_2 content have successfully been deposited on SA 210 substrate. The deposited coatings showed homogenous, dense, crack-free, and uniform microstructure.
2. The EDS spectra of different coatings confirm the presence of major elements of feedstock powder used which improved the oxidation and hot-corrosion resistance. EDS maps of all coatings showed the proper distribution of Al_2O_3 and TiO_2 in the deposited coatings.
3. The as-deposited coatings showed Al_2O_3, Fe_2O_3, TiO_2, $NiCr_2O_4$, $Al_2Ti_7O_{15}$ and V_2O_3 phases. The $Al_2Ti_7O_{15}$ new phase was formed, as shown in the coating's XRD pattern. The post-treated coatings have shown the same phases and the distinct disparities in the visual characteristics and positioning of the primary phase peaks between the treated coatings and the coatings that were sprayed directly. The deposits that are sprayed undergo densification by lattice straining, as seen by the minor change in peaks detected in the coatings after processing.
4. The porosity level decreased with an increase in TiO_2 content in the coatings. Maximum porosity in order of 2.5% was observed in AL coating while the lowest porosity was found in the case of AL40TI and PT-AL40TI coatings on order of 1.5 and 1.1, respectively.
5. The micro-hardness analysis showed a trend of increased hardness without TiO_2. A higher hardness of 995 HV was found for AL coating which is approximately 5.8 times higher than the hardness of uncoated SA 210 (225±10 HV). On the other hand, in the case of post-treated coatings, the maximum average micro-hardness value of 1110 HV was obtained for the PT-AL, which is about 3.56 times the hardness of the substrate.

6. The PT-AL40TI coated SA 210 showed the maximum oxidation resistance with approximately 4.7 times better performance as compared to uncoated SA 210. It was found that the increased Tio2 content played a significant role in enhanced oxidation resistance.
7. With the increase in TiO_2 content in AL, the oxidation resistance significantly increased and the microstructural features such as pores has reduced to resist the entry of oxides in the surface and sub-surface of the coatings.
8. Based on the oxidation results, the oxidation resistanace for the uncoated and coated have been arranged in in the following sequence:

   As-sprayed: AL40TI > AL13TI > AL> SA 210 boiler steel

   Post-treated: PT-AL40TI > PT-AL13TI > PT-AL
9. The hot-corrosion for PT-AL40TI was reduced by 3.2 times and 2.8 from the substrate and as-deposited coatings. Whereas in the case of the AL40TI specimen, it is reduced by 2.1, and 1.8 times compared with the substrate. The minimum hot-corrosion in the PT-AL40TI treated samples was due to the fact that after heat treatment, the refinement of the microstructure restricts the salt attacks on the surface thereby decreasing the degradation. The hot-corrosion resistance has been observed in the following sequence:

   As-sprayed: AL40TI > AL13TI > AL> SA 210 boiler steel

   Post-treated: PT-AL40TI > PT-AL13TI > PT-AL

Table 7.1. Table representing the changes and observation noted during the complete research work.

Material / Properties/Features	**Substrate**	**Powder**			**As-sprayed coatings**			**Post-treated coatings**		
	SA 210	Al_2O_3	Al_2O_3-13TiO_2	Al_2O_3-13TiO_2	(Al_2O_3) AL	(Al_2O_3-13TiO_2) AL13TI	(Al_2O_3-13TiO_2) AL40TI	(Al_2O_3) PT-AL	(Al_2O_3-13TiO_2) PT-AL13TI	(Al_2O_3-13TiO_2) PT-AL40TI
SEM analysis for Particle Shape and Size		Blocky/Irregular APS- 40-50µm	Blocky/Irregular APS- 40-50µm	Blocky/Irregular APS- 40-50µm	-	-	-	-	-	-
SEM analysis for topographical analysis		-	-	-	Melted/in-melted and partially melted surface	Melted/in-melted and partially melted surface	Melted/in-melted and partially melted surface	Increased melted zone has been observed	Increased melted zone has been obserevd	Increased melted zone has been obserevd
Porosity Analysis (%age)	-	-	-	-	2.5	2.1	1.5	2.1	1.7	1.1
Micro-hardness ($HV_{0.2}$)	230	-	-	-	995	790	650	1110	825	720
Oxidation analysis **Wt. gain (mg/cm^2)**	120.4	-	-	-	22.5	15.6	11.6	18.9	13.4	7.63
Microstructural and Phase analysis	The intense degradation of surface observed in SEM / Development of Fe_2O_3 phase and its variants	-	-	-	Presence of pores on the surface as observed on /Presence of, α-Al_2O_3.	Somewhat less pores are present on the surface as observed on /Presence of Al_2O_3, TiO_2 and $Al_2Ti_7O_{15}$	Presence of least no of pores on the surface as observed on /Presence of Al_2O_3, TiO_2 and $Al_2Ti_7O_{15}$	Healed surface (Less porosity) /Presence of, α-Al_2O_3 with slight peak shift.	Healed surface with flat melted zones/Presence of Al_2O_3, TiO_2 and $Al_2Ti_7O_{15}$ phases, and α-Al_2O_3 with slight peak shift.	Healed surface with flat melted zones (Least porosity) /Presence of Al_2O_3, TiO_2 and $Al_2Ti_7O_{15}$

						phases, and α-Al_2O_3.	phases, and α-Al_2O_3.			phases, and α-Al_2O_3 with slight peak shift.
Hot-corrosion analysis **Wt. gain (mg/cm^2)**	136.9	-	-	-	26.5	21.8	15.6	23.6	17.6	11.3
Microstructural and Phase analysis	Intense pits formation on surface /Fe_2O_3, NiO_2, Cr_2O_3, Al_2O_3 and TiO_2. Some peaks of $Al_2Ti_7O_{15}$, V_2O_3 and $NiCr_2O_4$ were also found.	-	-	-	Formation of Al_2O_3, Fe_2O_3, and V_2O_3 phases due to hot corrosion products.	EDS shows the presence of Al, Ti, O, Na, S and V/ Phases present are Al_2O_3, Fe_2O_3, TiO_2, $NiCr_2O_4$, $Al_2Ti_7O_{15}$ and V_2O_3	(Least pits among all coatings) EDS shows the presence of Al, Ti, O, Na, S and V/ Phases present are Al_2O_3, Fe_2O_3, TiO_2, $NiCr_2O_4$, $Al_2Ti_7O_{15}$ and V_2O_3	Melted region have nee observed /Formation of Al_2O_3, Fe_2O_3, and V_2O_3 phases due to hot corrosion products.	Melted region have nee observed /EDS shows the presence of Al, Ti, O, Na, S and V/ Phases present are Al_2O_3, Fe_2O_3, TiO_2, $NiCr_2O_4$, $Al_2Ti_7O_{15}$ and V_2O_3	Melted region have been observed /EDS shows the presence of Al, Ti, O, Na, S and V/ Phases present are Al_2O_3, Fe_2O_3, TiO_2, $NiCr_2O_4$, $Al_2Ti_7O_{15}$ and V_2O_3

7.2 FUTURE SCOPE

1. Erosion behaviour of the coating can be investigated.
2. Erosion and corrosion behaviour of these coated substrate can be evaluated inactual boiler condition.
3. Coated surface can be improved by glazing process and then hot corrosion canbe investigated.
4. Different types of coating can be studied to evaluate the corrosion resistance of these coating on the substrate.
5. Different coating technique can be used other than plasma to evaluate the performance of the coating in hot corrosion.

References

1. Abbasi, S., et al. (2019), *Journal of Mechanical Behavior of Biomedical Materials*, 90, 575–586. [DOI: 10.1016/j.jmbbm.2018.10.022]
2. Afzal, M., Ajmal, M., Khan, A. N., Hussain, A., & Akhter, R. (2014). Surface modification of air plasma spraying WC–12% Co cermet coating by laser melting technique. *Optics & Laser Technology*, *56*, 202-206.
3. Ansari, M. S., Bansal, A., Chawla, V., & Aggarwal, V. (2021). Comparative study of hot corrosion behavior of bare and plasma sprayed Al2O3-40% TiO2 coated T-91, A-1 boiler steel and Superfer800H superalloy in Na2SO4-60% V2O5 salt environment. Surface Topography: Metrology and Properties, 9(2), 025029.
4. Ansari, M. S., Chawla, V., Bansal, A., & Aggarwal, V. (2022). Comparative Study of High-Temperature Oxidation Behavior of Bare and Plasma Sprayed Al2O3-40% TiO2 Coated T-91, A-1 Boiler Steel and Superfer800H Superalloy in Air. Journal of Materials Engineering and Performance, 31(1), 753-768.
5. Bai, C. Y., Luo, Y. J., & Koo, C. H. (2004). Improvement of high temperature oxidation and corrosion resistance of superalloy IN-738LC by pack cementation. *Surface and Coatings Technology*, *183*(1), 74-88.
6. Bala, N., Singh, H. and Prakash, S., 2017. Performance of cold sprayed Ni based coatings in actual boiler environment. *Surface and Coatings Technology*, *318*, pp.50-61.
7. Barbooti, M. M., Al-Madfai, S. H., & Nassouri, H. J. (1988). Thermochemical studies on hot ash corrosion of stainless steel 304 and inhibition by magnesium sulphate. *Thermochimica acta*, *126*, 43-49.
8. Beltran**,** A.M. and Shores, D.A. (1972), "Ch. 11 : Hot Corrosion," in The Superalloys, John Wiley and Sons, N.Y.
9. Bhatia, R., Sidhu, H. S., & Sidhu, B. S. (2015). High temperature behavior of Cr 3 C 2-NiCr coatings in the actual coal-fired boiler environment. *Metallurgical and Materials Transactions E*, *2*, 70-86.
10. Bhushan, B., & Gupta, B. K. (1991). Handbook of tribology: materials, coatings, and surface treatments.

11. Birks, N., Meier, G.H. and Pettit, F.S., 2006. *Introduction to the high temperature oxidation of metals*. Cambridge university press.
12. Brar, S. S., Brar, G. S., & Chawla, V. (2017). HIGH TEMPERATURE CORROSION AND ROLE OF PLASMA SPRAY COATINGS-A REVIEW. *technology*, *4*, 5.
13. Budinski, K. G., (1998), "Engineering Materials, Properties and Selection," Pub. Prentice-Hall of India, New Delhi, India.
14. Burakowski, T., & Wierzchon, T. (1998). *Surface engineering of metals: principles, equipment, technologies*. CRC press.
15. Česánek, Z., Houdková, Š., & Lukáč, F. (2018). High-temperature corrosion behavior of selected thermally sprayed coatings in corrosive aggressive environment. *Materials Research Express*, *6*(1), 016426.
16. Chatha, S. S., Sidhu, H. S., & Sidhu, B. S. (2012). High temperature hot corrosion behaviour of NiCr and Cr3C2–NiCr coatings on T91 boiler steel in an aggressive environment at 750 C. *Surface and Coatings Technology*, *206*(19-20), 3839-3850.
17. Chatha, S. S., Sidhu, H. S., & Sidhu, B. S. (2012). High temperature hot corrosion behaviour of NiCr and Cr3C2–NiCr coatings on T91 boiler steel in an aggressive environment at 750 C. *Surface and Coatings Technology*, *206*(19-20), 3839-3850.
18. Chatha, S. S., Sidhu, H. S., & Sidhu, B. S. (2013). High-temperature behavior of a NiCr-coated T91 boiler steel in the platen superheater of coal-fired boiler. *Journal of thermal spray technology*, *22*, 838-847.
19. Chatha, S. S., Sidhu, H. S., & Sidhu, B. S. (2016). Performance of 75Cr3C2-25NiCr coating produced by HVOF process in a coal-fired thermal power plant. *Advanced Materials Research*, *1137*, 88-100.
20. Chatterjee, U.K., Bose, S.K. and Roy, S.K., 2001. *Environmental degradation of metals: corrosion technology series/14*. CRC Press.
21. Chawla, V., Prakash, S., Puri, D., & Sidhu, B. (2006, December). Plasma sprayed coatings for protection against hot corrosion in energy generation and coal gasification systems: a review. In *Proceedings of International Conference on Advances in Mechanical Engineering, BBSBEC, Fatehgarh Sahib (Punjab)*.

22. Cheng, J., et al. (2019). "Hot corrosion behavior and mechanism of high-velocity arc-sprayed Ni-Cr alloy coatings." *Journal of Thermal Spray Technology*, 28, 1263-1276. DOI: 10.1007/s11666-019-00890-0.

23. Cunha, C. A. D., Correa, O. V., Sayeg, I. J., & Ramanathan, L. V. (2017). High temperature erosion-oxidation resistance of thermally sprayed nanostructured Cr 3 C 2-25 (Ni-20Cr) coatings. *Materials Research*, *20*, 994-1002.

24. Daram, P., & Banjongprasert, C. (2020). The influence of post treatments on the microstructure and corrosion behavior of thermally sprayed NiCrMoAl alloy coating. *Surface and Coatings Technology*, *384*, 125166.

25. Deb, D., Iyer, S.R. and Radhakrishnan, V.M., 1996. A comparative study of oxidation and hot corrosion of a cast nickel base superalloy in different corrosive environments. *Materials Letters*, *29*(1-3), pp.19-23.

26. **Dent,** A.H., Horlock A. J., Harris S.J. (2000), "Microstructure formation in HVOF thermally sprayed Ni-Cr-Mo-B alloys," Material Science Engineering A283, pp.242-250.

27. Duran, A., et al. (2020). "Effect of TiO2 Addition on the Properties of Al2O3 Coatings Deposited by Plasma Spraying." *Surface and Coatings Technology*, 387, 125592. DOI: 10.1016/j.surfcoat.2020.125592.

28. Dzhurinskiy, D., Babu, A., Pathak, P., Elkin, A., Dautov, S. and Shornikov, P., 2021. Microstructure and wear properties of atmospheric plasma-sprayed Cr3C2-NiCr composite coatings. *Surface and Coatings Technology*, *428*, p.127904.

29. Eklund, J., et al. (2019). "High-temperature corrosion of HVAF-sprayed Ni-based coatings for boiler applications." *Oxidation of Metals*, 91(5), 729-747. DOI: 10.1007/s11085-019-09992-5.

30. Eliaz, N., Shemesh, G., & Latanision, R. M. (2002). Hot corrosion in gas turbine components. *Engineering failure analysis*, *9*(1), 31-43.

31. Feng, J., et al. (2018). "Effects of Al2O3 and TiO2 on the Microstructure and Properties of Thermal Barrier Coatings." *Materials Science and Engineering: A*, 731, 234-240. DOI: 10.1016/j.msea.2018.06.035.

32. Fryburg, G. C., Kohl, F. J., & Stearns, C. A. (1984). Chemical reactions involved in the initiation of hot corrosion of IN-738. *Journal of the electrochemical society*, *131*(12), 2985.
33. G. Kaushal, H. Singh, S. Prakash, Oxidation of Metals 76, 169-191 (2011).
34. Goh, C.Y., et al. (2019), *Journal of Materials Science*, 54(4), 3403–3420. [DOI: 10.1007/s10853-018-3087-5].
35. Gond, D., Chawla, V., Puri, D., & Prakash, S. (2010). High temperature corrosion behaviour of T-91 and T-22 bare steel in 75wt.% Na 2 SO 4+ 25wt.% NaCl molten salt environment at 900 C. *Journal of Minerals and Materials Characterization and Engineering*, *9*(07), 593.
36. Goyal, L., et al. (2017). "Elevated temperature corrosion studies of AlCrN and TiAlN coatings by PAPVD on T91 boiler steel." *Journal of Materials Engineering and Performance*, 26(4), 5481-5492. DOI: 10.1007/s11665-017-2972-4.
37. Goyal, R., Sidhu, B. S., & Chawla, V. (2018). Improving the high-temperature oxidation resistance of ASME-SA213-T11 boiler tube steel by plasma spraying with CNT-reinforced alumina coatings. *Anti-Corrosion Methods and Materials*, *65*(2), 217-223.
38. Goyala, M., Chawlab, V., & Sidhuc, B. S. (2016). Degradation of Boiler Tube Material at High Temperature Corrosion and Preventive Measures-A Review. *AFTMME'16*, 82.
39. Guney, M., Avcu, Y.Y., Avcu, E. (2020). Advances in Surface Engineering and Biocompatible Coatings for Biomedical Applications. *Coatings* Special Issue. MDPI. [DOI: 10.3390/coatings10030294].
40. Hancock, P. (1987). Vanadic and chloride attack of superalloys. *Materials Science and Technology*, *3*(7), 536-544.
41. Harsha, S., Dwivedi, D. K., & Agarwal, A. (2008). Influence of CrC addition in Ni-
42. He, J. L., Chen, K. C., Chen, C. C., Leyland, A., & Matthews, A. (2001). Cyclic oxidation resistance of Ni–Al alloy coatings deposited on steel by a cathodic arc plasma process. *Surface and Coatings Technology*, *135*(2-3), 158-165.

43. Heath, G. R., Heimgartner, P., Irons, G., Miller, R. D., & Gustafsson, S. (1997, October). An assessment of thermal spray coating technologies for high temperature corrosion protection. In *Materials science forum* (Vol. 251, pp. 809-816). Trans Tech Publications Ltd.
44. Houdková, Š., Česánek, Z., Smazalová, E., & Lukáč, F. (2018). The high-temperature wear and oxidation behavior of CrC-based HVOF coatings. *Journal of Thermal Spray Technology*, *27*, 179-195.
45. https://feedwater.co.uk/boiler-corrosion-prevention-to-stop-deposit-formation/
46. https://www.asbindustries.com/coating-processes/flame-spray-technologies (Flame Spray)
47. https://www.bodycote.com/services/surface-technology/flame-spraying/ (Flame Spray)
48. https://www.metallisation.com/how-does-flame-spray-work/ (Flame Spray)
49. https://www.researchgate.net/figure/Water-tube-boilers_fig2_263878729
50. https://www.sulzermetco.com/
51. https://www.usgs.gov/special-topics/water-science-school/science/a-coal-fired-thermoelectric-power-plant
52. https://www.watertechusa.com/boiler-blowdown
53. Husain, A. and Habib, K., 2005. Investigation of tubing failure of super-heater boiler from Kuwait Desalination Electrical Power Plant. *Desalination*, *183*(1-3), pp.203-208.
54. Jia, S. K., Yong, Z. O. U., Xu, J. Y., Jing, W. A. N. G., & Lei, Y. U. (2015). Effect of TiO2 content on properties of Al2O3 thermal barrier coatings by plasma spraying. Transactions of Nonferrous Metals Society of China, 25(1), 175-183.
55. Kamal, S., Jayaganthan, R. and Prakash, S., 2010a. Hot corrosion behaviour of D-gun sprayed NiCoCrAlYTa coated superalloys at 900° C in molten salt environment. *Surface engineering*, *26*(6), pp.453-462.
56. Kamal, S., Jayaganthan, R. and Prakash, S., 2010b. High temperature cyclic oxidation and hot corrosion behaviours of superalloys at 900 C. *Bulletin of Materials Science*, *33*(3), pp.299-306.
57. Kamal, S., Jayaganthan, R., Prakash, S. and Kumar, S., 2008. Hot corrosion behavior of detonation gun sprayed Cr3C2–NiCr coatings on Ni and Fe-based

superalloys in Na2SO4–60% V2O5 environment at 900° C. *Journal of alloys and compounds*, *463*(1-2), pp.358-372.

58. Kaur, M., Singh, H. and Prakash, S., 2009. High-temperature corrosion studies of HVOF-sprayed Cr3C2-NiCr coating on SAE-347H boiler steel. *Journal of thermal spray technology*, *18*(4), pp.619-632.
59. Kaur, M., Singh, H. and Prakash, S., 2012. High-temperature behavior of a high-velocity oxy-fuel sprayed Cr3C2-NiCr coating. *Metallurgical and Materials Transactions A*, *43*(8), pp.2979-2993.
60. Kaushal, G., Bala, N., Kaur, N., Singh, H. and Prakash, S., 2014. Comparative high-temperature corrosion behavior of Ni-20Cr coatings on T22 boiler steel produced by HVOF, D-Gun, and cold spraying. *Metallurgical and Materials Transactions A*, *45*(1), pp.395-410.
61. Kaushal, G., Kaur, N., Singh, H. and Prakash, S., 2012. Oxidation behaviour of D-Gun spray Ni-20Cr coated ASTM A213 347H steel at 900 C. *Int. J. Surf. Eng. Mater.Technol*, *2*(1), pp.33-38.
62. Kaushal, G., Saheet, H.S. and Prakash, S., 2010. Cyclic Oxidation Behavior of Detonation Gun Sprayed Ni-20 Cr Coating on a Boiler Steel at 900. *Minerals, Metals and Materials Society/AIME, 420 Commonwealth Dr., P. O. Box 430 Warrendale PA15086 USA.[np]. 14-18 Feb*
63. Kaushal, G., Singh, H. and Prakash, S., 2011. Comparative high temperature analysis of HVOF-sprayed and detonation gun sprayed Ni–20Cr coating in laboratory and actual boiler environments. *Oxidation of metals*, *76*(3), pp.169-191.
64. Kaushal, G., Singh, H., & Prakash, S. (2011). High temperature corrosion behaviour of HVOF-sprayed Ni-20Cr coating on boiler steel in molten salt environment at 900° C. *International Journal of Surface Science and Engineering*, *5*(5-6), 415-433.
65. Khanna, A. S. (2002). *Introduction to high temperature oxidation and corrosion*. ASM international.
66. Khanna, A. S., & Jha, S. K. (1998). Degradation of materials under hot corrosion conditions.
67. Khoi, N.N., Smeltzer, W.W. and Embury, J.D., 1975. Growth and structure of nickel oxide on nickel crystal faces. *Journal of the Electrochemical Society*, *122*(11), p.1495.

68. Khor, K.A. and Cheang, P., 1994. Laser post treatment of thermally sprayed hydroxyapatite coatings, in: C.C. Berndt, S. Sampath (Eds.), Thermal Spray Industrial Applications, *Proceedings of NTSC'94,* ASM International, Materials Park, OH, USA, (pp. 153–157).

69. Kim, K., et al. (2020). "Thermal Properties of Al2O3-TiO2 Composite Coatings for Thermal Barrier Applications." *Journal of Thermal Spray Technology*, 29(3), 469-479. DOI: 10.1007/s11666-020-01009-3.

70. Kofstad, P., (1966), "High Temperature Oxidation of Metals," John Wiley and Sons, New York

71. Koivuluoto, H. and Vuoristo, P., 2009. Effect of ceramic particles on properties of cold-sprayed Ni-20Cr+ Al2O3 coatings. *Journal of Thermal Spray Technology*, *18*(4), pp.555-562.

72. Kolta, G. A., Hewaidy, I. F., & Felix, N. S. (1972). Reactions between sodium sulphate and vanadium pentoxide. *Thermochimica Acta*, *4*(2), 151-164.

73. Konyashin, I.Y. and Chukalovskaya, T.V., 1997. A technique for measurement of porosity in protective coatings. *Surface and Coatings Technology*, *88*(1-3), pp.5-11.

74. Krishnan, A., & Gupta, A. (2020). "Role of Additives in Enhancing the Properties of Al2O3-TiO2 Nanocomposites." *Journal of Alloys and Compounds*, 835, 155167. DOI: 10.1016/j.jallcom.2020.155167.

75. Krzyzanowski, M., Beynon, J.H. and Farrugia, D.C., 2010. *Oxide scale behavior in high temperature metal processing*. John Wiley & Sons.

76. Kumar, A. and Sapra, P.K., 2016. Tribological characterisation of SA210 Gr A1 boiler steels for different temperature applications. *International Journal of Surface Science and Engineering*, *10*(4), pp.375-388.

77. Kumar, M., Singh, H. and Singh, N., 2013. Study of Ni-20Cr coatings for high temperature applications-a review. *Archives of Metallurgy and Materials*, *58*.

78. Kumar, S., Kumar, M., & Handa, A. (2018). Combating hot corrosion of boiler tubes–A study. *Engineering failure analysis*, *94*, 379-395.

79. Kumar, S., Kumar, M., & Handa, A. (2020). Erosion corrosion behaviour and mechanical properties of wire arc sprayed Ni-Cr and Ni-Al coating on boiler

steels in a real boiler environment. *Materials at High Temperatures*, *37*(6), 370-384.

80. Liu, L., Xu, H., Xiao, J., Wei, X., Zhang, G. and Zhang, C., 2017. Effect of heat treatment on structure and property evolutions of atmospheric plasma sprayed NiCrBSi coatings. *Surface and Coatings Technology*, *325*, pp.548-554.
81. Liu, Y., Liu, W., Ma, Y., Meng, S., Liu, C., Long, L. and Tang, S., 2017. A comparative study on wear and corrosion behaviour of HVOF-and HVAF-sprayed WC–10Co–4Cr coatings. *Surface Engineering*, *33*(1), pp.63-71.
82. Longa-Nava, Y., Zhang, Y.S., Takemoto, M. and Rapp, R.A., 1996. Hot corrosion of nickel-chromium and nickel-chromium-aluminum thermal-spray coatings by sodium sulfate-sodium metavanadate salt. *Corrosion*, *52*(09).
83. Mahesh, R. A., Jayaganthan, R., & Prakash, S. (2008). Evaluation of hot corrosion behaviour of HVOF sprayed NiCrAl coating on superalloys at 900 C. *Materials Chemistry and Physics*, *111*(2-3), 524-533.
84. Mahesh, R.A., Jayaganthan, R. and Prakash, S., 2008. A study on hot corrosion behaviour of Ni–5Al coatings on Ni-and Fe-based superalloys in an aggressive environment at 900° C. *Journal of alloys and compounds*, *460*(1-2), pp.220-231.
85. Mangla, A. K., Chawla, V., & Singh, G. (2017). Review paper on high temperature corrosion and its control in coal fired boilers. *International Journal of Latest Trends in Engineering and Technology (Special Issue-AFTMME)*, 088-092.
86. Mangla, A., Chawla, V., & Singh, G. (2017). Comparative study of hot corrosion behavior of HVOF and plasma sprayed Ni20Cr coating on SA213 (T22) boiler steel in Na2SO4-60% V2O5 environment. *International Journal of Engineering Sciences & Research Technology*, *4*(11), 2348-8034.
87. Manikandan, D. W. M. (2018). High-temperature corrosion behaviour of HVOF sprayed Cr3C2-25NiCr coated on alloy X22CrMoV12-1 at 600° C. *Journal of Thermal Spray and Engineering*, *1*(1), 7-12.
88. Matthews, S., James, B. and Hyland, M., 2009. High temperature erosion of Cr3C2-NiCr thermal spray coatings—The role of phase microstructure. *Surface and Coatings Technology*, *203*(9), pp.1144-1153.

89. Meier, G.H., 1989. A review of advances in high-temperature corrosion. *Materials Science and Engineering: A*, *120*, pp.1-11.
90. **Metals Handbook** (1975), "Failure analysis and prevention" Vol. 10, ASMPublication, Metal Park OH, USA.
91. Michalak, M., Łatka, L., Sokołowski, P., Candidato, R. T., & Ambroziak, A. (2021). Effect of TiO_2 on the microstructure and phase composition of Al_2O_3 and Al_2O_3–TiO_2 APS sprayed coatings. Bulletin of the Polish Academy of Sciences. Technical Sciences, 69(2).
92. Mishra, N. K., & Mishra, S. B. (2015). Hot corrosion performance of LVOF sprayed Al 2 O 3–40% TiO 2 coating on Superni 601 and Superco 605 superalloys at 800 and 900 C. Bulletin of Materials Science, 38, 1679-1685.
93. Mishra, S.B. and Prakash, S., 2015. Erosion–corrosion behaviour of Ni–20Cr plasma coating in actual boiler environment. *Surface Engineering*, *31*(1), pp.29-38.
94. Mishra, S.B., Chandra, K. and Prakash, S., 2013. Erosion–corrosion performance of NiCrAlY coating produced by plasma spray process in a coal-fired thermal power plant. *Surface and Coatings Technology*, *216*, pp.23-34.
95. Mishra, S.B., Chandra, K. and Prakash, S., 2017. Studies on erosion-corrosion behaviour of plasma sprayed Ni3Al coating in a coal-fired thermal power plant environment at 540° C. *Anti-Corrosion Methods and Materials*, *64(5)*, pp.540-549.
96. Mohamed, M., & Zaki, F. (2021). "Characterization and Properties of Al2O3-TiO2 Ceramic Composites: A Review." *Ceramics International*, 47(4), 5009-5020. DOI: 10.1016/j.ceramint.2020.11.052.
97. Mohamed, M.H. and Wilson, V.H., 2015. Analysis of boiler super heater tubes from high flue gas temperature. *Int. J. Innov. Res. Adv. Eng.(IJIRAE)*, *2*, pp.1-4.
98. N. Bala, H. Singh, S. Prakash,, Metallurgical and Materials Transactions A 42A, 3399-3416 (2011).
99. Natesan, K. (1976). Corrosion-erosion behavior of materials in a coal-gasification environment. *Corrosion*, *32*(9), 364-370.

100. Natesan, K. (1993). Applications of coatings in coal-fired energy systems. *Surface and Coatings Technology*, *56*(3), 185-197.

101. Natesan, K. (1997). Corrosion performance of materials in coal-fired power plants. *CORCON-97: Corrosion and Its Control.*, *1*, 24-35.

102. Nelson, H. W., Krause, H. H., Ungar, E. W., Putnam, A. A., Slunder, C. J., Miller, P. D., Hummel, J. D. and Landry, B. A., (1959), "A Review of Available Information on, Corrosion and Deposits in Coal- and Oil-Fired Boilers and Gas Turbines," Report of ASME Research Committee on Corrosion and Deposits from Combustion Gases, Pub. Pergamon Press and ASME, New York, pp 1-197

103. Nicholls, J. R. (2000). Designing oxidation-resistant coatings. *JoM*, *52*, 28-35.

104. Nielsen, H. P., Frandsen, F. J., Dam-Johansen, K., & Baxter, L. L. Implications of chlorine-associated corrosion on the operation of agriwaste-fired boilers. *Progress in Energy and Combustion Science*, *26*, n3.

105. Oksa, M., Auerkari, P., Salonen, J. and Varis, T., 2014. Nickel-based HVOF coatings promoting high temperature corrosion resistance of biomass-fired power plant boilers. *Fuel processing technology*, *125*, pp.236-245.

106. Prakash, S., Singh, S., Sidhu, B. S., & Madeshia, A. (2001, November). Tube failures in coal fired boilers. In *Proceedings of the National Seminar on Advances in Material and Processing* (pp. 245-253).

107. Praveen, A. S., & Arjunan, A. (2019). Effect of nano-Al2O3 addition on the microstructure and erosion wear of HVOF sprayed NiCrSiB coatings. *Materials Research Express*, *7*(1), 015006.

108. Praveen, A.S., Sarangan, J., Suresh, S. and Subramanian, J.S., 2015. Erosion wear behaviour of plasma sprayed NiCrSiB/Al2O3 composite coating. *International Journal of Refractory Metals and Hard Materials*, *52*, pp.209-218.

109. Premkumar, K., & Balasubramanian, K. R. (2018). Investigation of erosion behaviour on nanocrystalline composite thermal spray coating under hot air jet condition. *Jour of Adv Research in Dynamical & Control Systems*, *10*, 04-Special.

110. Price, M. O., Jackson, J. E., & Quets, J. M. (1992). Process for Producing Chromium Carbide--Nickel Base Age Hardenable Alloy Coatings and Coated Articles so Produced. *Patent NumberUS 5137422*.

111. Priyantha, N., Jayaweera, P., Sanjurjo, A., Lau, K., Lu, F., & Krist, K. (2003). Corrosion-resistant metallic coatings for applications in highly aggressive environments. *Surface and Coatings Technology*, *163*, 31-36.

112. Radhakrishnan, P., et al. (2019). "Mechanical and Thermal Properties of Al2O3-TiO2 Ceramic Composite." *Journal of the European Ceramic Society*, 39(2), 429-436. DOI: 10.1016/j.jeurceramsoc.2018.09.003.

113. Rapp, R. A. (1986). Chemistry and electrochemistry of the hot corrosion of metals. *Corrosion (Houston, Tex.)*, *42*(10), 568-577.

114. Rapp, R. A., & Zhang, Y. S. (1994). Hot corrosion of materials: fundamental studies. *Jom*, *46*, 47-55.

115. Rapp, R. A., Devan, J. H., Douglass, D. L., Nordine, P. C., Pettit, F. S., & Whittle, D. P. (1981). High temperature corrosion in energy systems. *Materials Science and Engineering*, *50*(1), 1-17.

116. Rapp, R.A., 1984. High temperature oxidation of metals forming cation-diffusing scales. *Metall. Trans., B;(United States)*, *15*.

117. Reddy, N. C., Koppad, P. G., Reddappa, H. N., Ramesh, M. R., Babu, E. R., & Varol, T. E. M. E. L. (2019). Hot corrosion behaviour of HVOF sprayed Ni3Ti and Ni3Ti+(Cr3C2+ 20NiCr) coatings in presence of Na2SO4-40% V2O5 at 650° C. *Surface Topography: Metrology and Properties*, *7*(2), 025019.

118. Reid, W.T., 1971. External corrosion and deposits: boilers and gas turbines.

119. Roy, M., 2006. Elevated temperature erosive wear of metallic materials. *Journal of Physics D: Applied Physics*, *39*(6), p.R101.

120. Sadeghi, E., Markocsan, N. and Joshi, S., 2019. Advances in corrosion-resistant thermal spray coatings for renewable energy power plants. part I: effect of composition and microstructure. *Journal of Thermal Spray Technology*, *28*(8), pp.1749-1788.

121. Shukla, V.N., Jayaganthan, R. and Tewari, V.K., 2012. Hot corrosion studies of HVOF-sprayed Cr3C2-NiCr coating on 310S stainless steel in an

actual environment of a coal fired boiler. In *Advanced Materials Research* (Vol. 585, pp. 483-487). Trans Tech Publications Ltd.

122. Sidhu, B. S., & Prakash, S. (2006). Erosion-corrosion of plasma as sprayed and laser remelted Stellite-6 coatings in a coal fired boiler. *Wear*, *260*(9-10), 1035-1044.

123. Sidhu, B. S., Puri, D., & Prakash, S. (2005). Mechanical and metallurgical properties of plasma sprayed and laser remelted Ni–20Cr and Stellite-6 coatings. *Journal of Materials Processing Technology*, *159*(3), 347-355.

124. Sidhu, H. S., Sidhu, B. S., & Prakash, S. (2007). Solid particle erosion of HVOF sprayed NiCr and Stellite-6 coatings. *Surface and Coatings Technology*, *202*(2), 232-238.

125. Simms, N. J., Encinas-Oropesa, A., & Nicholls, J. R. (2004, July). Development of hot corrosion on coated single crystal superalloys. In *Materials Science Forum* (Vol. 461, pp. 941-948). Trans Tech Publications Ltd.

126. Singh, G., Bala, N. and Chawla, V., 2017. High temperature oxidation behaviour of HVOF thermally sprayed NiCrAlY Coating on T-91 boiler tube steel. *Materials Today: Proceedings*, *4*(4), pp.5259-5265.

127. Singh, G., Bala, N., & Chawla, V. (2019). High temperature oxidation behaviour and characterization of NiCrAlY-B4C coatings deposited by HVOF. *Materials Research Express*, *6*(8), 086436.

128. Singh, G., et al. (2018). "High temperature oxidation behaviour of HVOF thermally sprayed NiCrAlY coating on T-91 boiler tube steel." *Materials Today: Proceedings*, 4(5), 5259-5264. DOI: 10.1016/j.matpr.2017.05.035.

129. Singh, S., Goyal, K., & Goyal, R. (2016). Performance of Cr3C2-25 (Ni–20Cr) and Ni–20Cr coatings on T22 boiler tube steel in simulated boiler environment. *J Thin Films Coat Sci Technol Appl*, *3*(2), 19-26.

130. Somasundaram, B., Kadoli, R., & Ramesh, M. R. (2015). Hot Corrosion Behaviour of HVOF Sprayed (Cr 3 C 2–35% NiCr)+ 5% Si Coatings in the Presence of Na 2 SO 4–60% V 2 O 5 at 700 C. *Transactions of the Indian Institute of Metals*, *68*, 257-268.

131. Somasundaram, B., Kadoli, R., Ramesh, M. R., & Ramesh, C. S. (2016). High temperature corrosion behaviour of HVOF sprayed WC-CrC-Ni coatings. *International Journal of Surface Science and Engineering*, *10*(4), 400-413.

132. Sreenivasulu, V., & Manikandan, M. (2018). Hot corrosion studies of HVOF sprayed carbide and metallic powder coatings on alloy 80A at 900° C. *Materials Research Express*, *6*(3), 036519.

133. Stokes, J., & Looney, L. (2001). HVOF system definition to maximise the thickness of formed components. *Surface and Coatings Technology*, *148*(1), 18-24.

134. Stringer, J., 1987. High-temperature corrosion of superallo200ys. *Materials Science and Technology*, *3*(7), pp.482-493.

135. Stringer, J., 1995. Practical experience with wastage at elevated temperatures in coal combustion systems. *Wear*, *186*, pp.11-27.

136. Sun, H., Yi, G., Wan, S., Kong, C., Zhu, S., Bai, L. and Yang, J., 2021. Effect of Cr2O3 addition on mechanical and tribological properties of atmospheric plasma-sprayed NiAl-Bi2O3 composite coatings. *Surface and Coatings Technology*, *427*, p.127818.

137. Sundaresan, C., et al. (2021). "Comparative hot corrosion performance of APS and Detonation sprayed CoCrAlY, NiCoCrAlY, and NiCr coatings on T91 boiler steel." *Corrosion Science*, 189, 1-16. DOI: 10.1016/j.corsci.2021.109563.

138. Swaminathan, S., Hong, S.M., Kumar, M., Jung, W.S., Kim, D.I., Singh, H. and Choi, I.S., 2019. Microstructural evolution and high temperature oxidation characteristics of cold sprayed Ni-20Cr nanostructured alloy coating. *Surface and Coatings Technology*, *362*, pp.333-344.

139. Tiwari, S. N., & Prakash, S. (1997). Studies on the hot corrosion behaviour of some superalloys in Na2SO4-V2O5. *Proc. of SOLCEC, Kalpakkam, India*.

140. Vasudev, H., Singh, P., Thakur, L., & Bansal, A. (2020). Mechanical and microstructural characterization of microwave post processed Alloy-718 coating. *Materials Research Express*, *6*(12), 1265f5.

141. Vasudev, H., Thakur, L., Bansal, A., Singh, H., & Zafar, S. (2019). High temperature oxidation and erosion behaviour of HVOF sprayed bi-layer Alloy-718/NiCrAlY coating. *Surface and Coatings Technology*, *362*, 366-380.

142. Wang, B., 1996. Erosion-corrosion of thermal sprayed coatings in FBC boilers. *Wear*, *199*(1), pp.24-32.

143. Yang, J.Z., Fang, M.H., Huang, Z.H., Hu, X.Z., Liu, Y.G., Sun, H.R., Huang, J.T. and Li, X.C., 2012. Solid particle impact erosion of alumina-based refractories at elevated temperatures. *Journal of the European Ceramic Society*, *32*(2), pp.283-289.

144. Zafar, S., & Sharma, A. K. (2017). Microstructure and mechanical properties of microwave post-processed Ni coating. *Journal of Materials Engineering and Performance*, *26*, 1382-1390.

145. Zhang, H., Dong, X. and Chen, S., 2017. Solid particle erosion-wear behaviour of Cr3C2–NiCr coating on Ni-based superalloy. *Advances in Mechanical Engineering*, *9*(3), p.1687814017694580.

146. Zhao, Y., et al. (2022). "Synthesis and Properties of Al2O3-TiO2 Nanocomposites for High-Temperature Applications." *Ceramics International*, 48(3), 3121-3128. DOI: 10.1016/j.ceramint.2021.10.126.

147. Zhou, J. and Bahadur, S., 1995. Erosion characteristics of alumina ceramics at high temperatures. *Wear*, *181*, pp.178-188.

LIST OF PUBLICATIONS

1. Jai Parkash, Harminder Singh Saggu and H. Vasudev (2022). Microstructural Characterization of alumina-based coating deposited on ASTM-SA210 Boiler Steel, 3rd International conference on Functional, Manufacturing and Performances (ICFMMP-2022), Lovely Professional University, Punjab 29-30th July, 2022.
2. Jai Parkash, Harminder Singh Saggu, Hitesh Vasudev, "Materials Today: Proceedings A short review on the performance of high velocity oxy-fuel coatings in boiler steel applications," Materials Today: Proceedings, no. 50 (2022) 1442-1446, 2021 **(Elsevier, Scopus Indexed).**
3. Jai Parkash , Harminder Singh Saggu, Hitesh Vasudev, "Role of numerical modelling and optimization in the manufacturing of boiler steel surfaces with coatings," International Journal on Interactive Design and Manufacturing (IJIDeM) , 2023 **(Springer, Scopus Indexed, ESCI, IF=2.1).**